B

AGARDograph 22

AGARDograph 22

NATO AGARD

BELGIQUE
CANADA
DANMARK
DEUTSCHLAND
ELLÁS
FRANCE
ISLAND
ITALIA
LUXEMBOURG
NEDERLAND
NORGE
PORTUGAL
TÜRKIYE
UNITED KINGDOM
UNITED STATES

AGARDograph

MACH NUMBER MEASUREMENTS IN HIGH-SPEED WIND TUNNELS

by

J. A. F. Hill, J. R. Baron, L. H. Schindel and J. R. Markham

October 1956

NORTH ATLANTIC TREATY ORGANIZATION

ADVISORY GROUP FOR AERONAUTICAL RESEARCH AND DEVELOPMENT

(ORGANISATION DU TRAITE DE L'ATLANTIQUE NORD)

MACH NUMBER MEASUREMENTS IN HIGH-SPEED WIND TUNNELS

By

Jacques A. F. Hill
Judson R. Baron
Leon H. Schindel
and
John R. Markham

Naval Supersonic Laboratory
Massachusetts Institute of Technology

October 1956

This is one of a series of Wind Tunnel AGARDographs concerned with wind tunnel design, operation, and test techniques. Professor Wilbur C. Nelson of the University of Michigan is the editor.

This AGARDograph was prepared with the cooperation of the Air Force Office of Scientific Research of the Air Research and Development Command, United States Air Force. Support was also received from the Massachusetts Institute of Technology under Project DIC 7303-C.

TABLE OF CONTENTS

SUMMARY

Measurements of subsonic and supersonic Mach numbers in air are discussed from the point of view of calibration measurements of an empty wind tunnel, of measurements of *local Mach numbers at points in the flow* field around a model, and of simulating free flight Mach number in the presence of wind tunnel wall interference. Errors in deducing Mach number from particular measurements are discussed and certain measuring procedures recommended.

SOMMAIRE

Les mesures dans l'air des nombres de Mach subsonique et supersonique sont discutées du point de vue des mesures de calibrage d'une soufflerie à vide, des mesures *des nombres de Mach en des points de* l'écoulement situés autour d'un modèle, et de la simulation du nombre de Mach d'un vol libre en présence de l'interférence des parois de la soufflerie. Les erreurs commises en déduisant le nombre de Mach de mesures particulières sont discutées et certains procédés de mesure sont recommandés.

TERMINOLOGY

A	Cross-Sectional Area of Streamtube
A	Van der Waal's Coefficient
A	$\bar{\theta} \exp \bar{\theta}/(\exp \bar{\theta} - 1)$
A_o	$A(\theta_0)$
A_o	Constant in Beattie-Bridgeman Equation
a	Constant in Beattie-Bridgeman Equation
a	Velocity of Sound
$\tilde{a}$	Velocity of Sound in Liquid Vapor Mixture, $\sqrt{1 - g}\ \gamma RT$
$\bar{a}$	$V/\bar{M}$
a_i	i^{th} Virial Coefficient in Density Expansion
B	Van der Waal's Coefficient
B_I	Asymptotic Value of Velocity Perturbation
B_o	Constant in Beattie-Bridgeman Equation
b	Constant in Beattie-Bridgeman Equation
$b(m)$	Coefficient Defined on Page 10
b_i	i^{th} Virial Coefficient in Pressure Expansion
C	Heat Addition Parameter, q/c_pT
C	Velocity Perturbation on the Wall at the Model Location
C_p	Pressure Coefficient, $(p - p^o)/q$.
C_μ	Viscosity Correction Coefficient
c	Wing Chord

TERMINOLOGY
(Continued)

c	Constant in Beattie-Bridgeman Equation
c_p	Specific Heat at Constant Pressure
c_v	Specific Heat at Constant Volume
$c(m)$	Coefficient Defined on Page 10
D	Drag
D	Diameter of Probe
F	Net Force Acting on Fluid in Stream Tube
$F\left(\frac{\sqrt{M_e^2-1}\,r_0}{x}\right)$	Ratio of Rate of Pressure Increase with Respect to Simple Wave Theory, $\frac{dp/d\xi}{(dp/d\xi)_{\text{simple wave}}}$
g	Mass Fraction of Liquid in Liquid-Vapor Mixture
H	Enthalpy
H	Tunnel Height or Diameter
k	Numerical Constant
k_s	Turbulence Factor
L	Length of Nozzle
ℓ	Reference Length for Reynolds Number
ℓ	Length to Pressure Orifice of Cylindrical Portion of Static Pressure Probe
ℓ_f	Length of Nose of Probe
ℓ_s	Distance from Static Pressure Orifice to Beginning of Support
M	Mach Number

TERMINOLOGY
(Continued)

$\tilde{M}$	Mach Number in Liquid-Vapor Mixture, $v/\tilde{a}$
$\bar{M}$	$\left\{1+\left[(\gamma\tilde{M}^2)/(1/p)(dp/d\delta)_{\delta=0}\right]^2\right\}^{1/2}$
M_w	Mach Number Behind an Oblique Shock
m	$(M \sin\beta)^2$
m	Velocity Ratio
P_i	Parameter Related to Mach Number
Pr	Prandtl Number
p	Pressure
p_c	Cone Surface Pressure
p_i	Pitot (impact) Pressure
p_s	Surface Pressure
p_w	Wedge Surface Pressure
p_{i_w}	Pitot Pressure Behind an Oblique Shock
Q	$(1 + \gamma_2 M_2^2) - (T_1/T_2)(1 + \gamma_1 M_1^2)$
Q	Source Strength (mass flow)
q	Dynamic Pressure $\rho V^2/2 = (1/2)\gamma p M^2$
q	$p_i - p^0$
R	Gas Constant for Air
Re	Reynolds Number $\rho V \ell/\mu$
r	Recovery Factor, $(T_r - T^0)/(T_0 - T^0)$
r	Radial Coordinate

TERMINOLOGY
(Continued)

δ	Wedge Semi-Angle (angle through which flow is turned by a wedge)
δ_c	Cone Semi-Angle (angle through which flow is turned by a cone)
δ^*	Boundary-Layer Displacement Thickness
δ_1	Displacement Thickness for Thin Boundary Layer
θ	Inclination of Velocity Vector
θ	Axial Coordinate, $(\pi x/L) - (\pi/2)$
θ	Characteristic Temperature for Molecular Vibration, 3050° K for Air
$\overline{\theta}$	θ/T
Λ	Wing Sweepback Angle
Λ_0	Reduced Sweepback Angle, $\tan^{-1}(\tan\Lambda / \sqrt{1 - M^2})$
λ	Coefficient of Heat Conduction
λ	Velocity Correction Factor for Model Shape
μ	Coefficient of Viscosity
μ	Index of Refraction
ν	Kinematic Viscosity, μ/ρ
ρ	Density
τ	Velocity Correction Factor for Tunnel Dimensions
τ	Relaxation Time
ϕ_0	Velocity Potential of Free-Air Flow about the Model
ϕ_1	Velocity Potential due to Wall Interference
Ω	ecific Humidity, (mass of water vapor/mass of air)

TERMINOLOGY
(Continued)

r_o	Radius of Cylindrical or Conical Probe
S_i	Sensitivity of Parameter P_i to Mach Number, $(P_i/M)(dM/dP_i)$
s	Entropy
T	Temperature
T_r	Recovery Temperature
u	x Component of Velocity in Two-Dimensional Flow
V	Velocity in One-Dimensional Flow
V'	Turbulence Perturbation Velocity
v	y Component of Velocity in Two-Dimensional Flow
v'	Lateral Components of Turbulence
w'	Lateral Components of Turbulence
x	Axial Coordinate
y	Lateral Coordinate
Z	Compressibility Factor, $(p/\rho RT) = 1$ for Perfect Gas
α	Probe Yaw Angle
α	Mach Angle, $\sin^{-1}(1/M)$
β	Shock Wave Angle
β_c	Shock Wave Angle Produced by a Cone
β_W	Shock Wave Angle Produced by a Wedge
γ	Ratio of Specific Heats, c_p/c_v
γ_p	Ratio of Specific Heats for a Calorically Perfect Gas, 1.4 for Air

TERMINOLOGY
(Continued)

SUBSCRIPTS

$(\ )_e$	Condition just outside of Boundary Layer
$(\ )_o$	Isentropic Stagnation Condition
$(\ )_1$	Condition at State (1)
$(\ )_2$	Condition at State (2)
$(\ )_B$	Body
$(\ )_W$	Wing

SUPERSCRIPTS

$(\ )^*$	Condition at M = 1
$(\ )^o$	Static Condition

I. INTRODUCTION

Since Mach number is the fundamental similarity parameter in high-speed flow, a discussion of its measurement is worth some consideration even by experienced researchers. The establishment, at the outset, of the desired accuracy of Mach number determination will provide a criterion for the adequacy of various measuring techniques and will permit an evaluation of the significance of errors.

Many types of tests may be simulated in a high-speed wind tunnel with results which are sensitive in various degrees to errors in Mach number. One standard task certainly is the measurement of aerodynamic forces and moments. At a Mach number of 3, a one percent error in Mach number will result in about 3.5 percent error in the computation of force coefficient. See Fig. I-1.

Wind tunnel model construction and force measuring standards are sufficiently precise to permit measurements of coefficients to within 1 percent; hence Mach number must be known to better than 1/3 percent to maintain such accuracy. Effects of Mach number gradient over the region of the model (investigated by Morris and Winter, Ref.1) also lead to a required accuracy of 1/3 percent in Mach number uniformity. It will be assumed that in order to know the Mach number to within 1/3 percent, calibration measurements should be made to 0.1 percent and errors of this magnitude can not be disregarded.

In this report, the measurement of subsonic and supersonic Mach numbers in air will be discussed from the point of view of calibration measurements of an empty wind tunnel, of measurements of local Mach numbers at points in the flow field around a model, and of simulating free flight Mach number in the presence of wind tunnel wall interference. The sensitivity of various parameters to change in Mach number will be evaluated and instruments for detecting the necessary properties described. Errors in deducing Mach number from particular measurements will be discussed and certain measuring procedures recommended.

No mention will be made of "Mach meters," which are simply analog computing devices. It will be assumed, instead, that the researcher will be able to make the computations (by machine if convenient) if he has a formula and the necessary measured quantities. It will be assumed that the flow is steady, and consequently consideration of time lag and frequency response of the instrumentation is unnecessary.

Laws relating the Mach number to various measurable properties will first be obtained. In deriving these laws, it will be assumed that the air behaves as a perfect gas and undergoes certain prescribed thermodynamic processes. After describing instruments which can measure those properties of air from which Mach number may be computed, estimates will be made of some of the errors which arise in the measurements.

Two types of error will be considered; those arising from departures of the air from the assumed perfect gas relations and thermodynamic processes, and probe errors which may be regarded as occurring because the insertion of the measuring device induces boundary layers and otherwise disturbs the flow field so that the instrument does not measure exactly the quantity that it was designed to measure.

The report, it is hoped, is comprehensive if not exhaustive; however, as new ranges of Mach number, density, and temperature are achieved in wind tunnels, and as new methods and measuring instruments are invented, new techniques may supplant those now recommended.

II. BASIC LAWS RELATING MACH NUMBER TO OTHER MEASURABLE QUANTITIES

(a) Definition of Mach Number

The state of any substance is completely determined when two independent thermodynamic coordinates are specified. Thus every substance has an equation of state, however complicated, relating its pressure, density, and temperature; other thermodynamic properties, such as internal energy, entropy, or velocity of sound, are in turn related to the pressure, density, and temperature.

The Mach number, M, is defined as the ratio of the velocity of the fluid at some point to the local velocity of sound in the medium. Since the velocity of sound can be considered as a thermodynamic property, the Mach number is fixed by the determination of flow velocity plus any two independent thermodynamic coordinates. It is necessary, of course, to be able to relate these coordinates to the velocity of sound, hence it is desirable first to establish the relation between velocity of sound, a, and other thermodynamic properties.

The velocity of sound is the velocity of propagation of a small pressure wave. The first expression for the velocity of sound in air was given by Newton, although in computing the numerical value, he neglected to allow for the increase in "elastic force" which results from the temperature rise associated with the isentropic process undergone by the gas in propagating a pressure pulse. Newton therefore obtained a value for the velocity of sound which would result if the process were isothermal. The velocity of a sound wave (see for example Ref. 2) is in differential form

$$a^2 = \frac{dp}{d\rho} \qquad (1)$$

In a perfect gas with constant specific heats, during an isentropic process the density and pressure are related by

$$\frac{p}{\rho^{\gamma}} = \text{constant} \qquad (2)$$

where γ is the ratio of specific heats.

In this case

$$\frac{dp}{d\rho} = \gamma \frac{p}{\rho} \qquad (3)$$

and hence the velocity of sound is

$$a = \sqrt{\gamma \frac{p}{\rho}} \qquad (4)$$

or, since the equation of state of a perfect gas is

$$\frac{p}{\rho} = RT \qquad (5)$$

$$a = \sqrt{\gamma RT} \qquad (6)$$

R being the gas constant.

Under conditions of extreme temperature or pressure, the perfect gas assumption may no longer be valid. Then it becomes necessary to replace Eq. (5) by a more appropriate equation of state. For example, Van der Waal's equation of state, which is

$$\left(p + A\rho^2\right)\left(\frac{1}{\rho} - B\right) = RT \tag{7}$$

(reducing to the perfect gas equation when the constants A and B are both zero), or the Beattie-Bridgeman equation

$$p = RT\rho^2\left[1 - \frac{C\rho}{T^3}\right]\left[\frac{1}{\rho} + B_0(1 - b\rho)\right] - A_0(1 - a\rho)\rho^2 \tag{8}$$

can be applied in some cases when the perfect gas relation is inadequate. Tsien (Ref. 3) has derived the one-dimensional flow relations for a Van der Waal gas, while Tao (Ref. 4) has written the equations using the Beattie-Bridgeman equation of state.

The equation of state is sometimes written in series form as

$$\frac{p}{\rho RT} = 1 + \sum_{i=1}^{\infty} a_i \rho^i \tag{9}$$

$$\frac{p}{\rho RT} = \sum_{i=0}^{\infty} b_i p^i \tag{10}$$

called, respectively, the density and the pressure virial expansions. The density virial coefficients for air are tabulated in Refs. 5 and 6.

In the remainder of this paper, it will be assumed unless otherwise specified, that the medium consists of dry air and that it is a perfect gas with constant specific heats having the equation of state given as Eq. (5) above. Section IV will contain some remarks on the errors in Mach number measurement introduced by assuming that air is a perfect gas.

Mach number can be found by dividing a measurement of velocity by the velocity of sound determined from either Eq. (4) or (6). It is usually more convenient, however, to find the Mach number by measuring certain properties at two different states when the Mach number is known at one state and the thermodynamic process between the states is also known.

(b) Changes in Mach Number and Other Parameters in Thermodynamic Processes

The steady one-dimensional adiabatic flow of a nonviscous fluid from station (1) to station (2) in a straight duct (or streamtube) is governed by the following equations (Ref. 2):

Continuity Equation (conservation of mass):

$$\rho_1 A_1 V_1 = \rho_2 A_2 V_2 \tag{11}$$

subscripts refer to states (1) and (2).

Energy Equation (conservation of energy):

$$c_p T_0 = \frac{V_1^2}{2} + c_p T_1 = \frac{V_2^2}{2} + c_p T_2 \tag{12}$$

where T_0 is the stagnation temperature and remains constant.

It is sometimes useful to express the invariant $c_p T_0$ in terms of a reference sound speed. Both the stagnation speed of sound a_0 and the critical speed of sound a^* (occurring in the flow where $V^2 = a^2 = \gamma RT$) are used. They are related to $c_p T_0$ by

$$c_p T_0 = \frac{a_0^2}{\gamma - 1} = \frac{\gamma + 1}{2(\gamma - 1)} a^{*2}. \tag{13}$$

Momentum Equation (Newton's Law):

$$F + A_1(p_1+\rho_1V_1^2) = A_2(p_2 + \rho_2V_2^2) \tag{14}$$

where F is the net force exerted on the fluid between stations (1) and (2) by the duct walls (or the resultant of the pressure forces on the boundaries of the streamtube), and is directed along the axis of the duct since the duct is straight.

Before these equations can be solved, it is necessary to specify the nature of the fluid and the nature of the process between stations (1) and (2). Given a specific fluid, the equation of state

$$p = p(\rho, T) \tag{15}$$

and the entropy

$$s = s(p,T) \tag{16}$$

are known.

Finally, it is desirable to express the Mach number of the flow in terms of the quantities in these equations. For the perfect gas with constant specific heats,

$$M = \frac{V}{\sqrt{\gamma RT}}. \tag{17}$$

The number of unknowns in the system of Eqs. (11) to (17) is eight, namely

$$p, \rho, T, s, V, M, A, F \tag{18}$$

and there are six equations. Two more conditions must be imposed to obtain a unique solution at station (2) in terms of given conditions at station (1).

(1) Isentropic Process

One of the most common processes in one-dimensional fluid flow is an isentropic one for which

$$s_2 = s_1 \tag{19}$$

which is assumed known.

In this kind of process, therefore, if any other one of the quantities of the group (18) is specified at station (2), all the others are determined. The commonly used "isentropic flow tables," found for instance in Refs. 7 to 11, are based on this fact. Station (1) is usually taken as either the stagnation condition M = 0 or the sonic flow M = 1. The quantities at station (2), when normalized with respect to the same quantity at station (1), become unique functions of M and are generally so tabulated as in Table I. The properties, normalized with respect to the condition at M = 1, are plotted in Fig. II-1. Any other variable may be considered independent and V and p have sometimes been used. The force F is of little interest in wind tunnel applications (and difficult to normalize) and is usually not calculated, which means that the momentum equation may be ignored.

(2) Constant Area Process
and Normal Shock

If the condition of constant area is imposed on the flow, it follows also that the force F = 0, because the walls of the duct (or streamtube) are parallel to its axis. Now there are six equations for six unknowns and the flow at station (2) should be completely determined without additional conditions. The six equations may be combined to give a single equation for any one of the downstream variables in terms of the initial conditions. The equation so obtained is always quadratic in form, so that in general there is another solution in addition to the trivial case of identical conditions at both stations. The equation for the velocity, for instance, may be obtained in the form

$$V_1 - V_2 = (V_1 - V_2)\left[\frac{\gamma+1}{2\gamma}\,\frac{a^{*2}}{V_1 V_2} + \frac{\gamma-1}{2\gamma}\right] \tag{20}$$

with the nontrivial solution,

$$V_2 = \frac{a^{*2}}{V_1}\ . \tag{21}$$

If state (1) is supersonic, $V_1 > a^*$, then state (2) is subsonic and vice versa. If the entropy change between stations (1) and (2) is calculated, it is found that a transition from a supersonic flow to a subsonic flow is accompanied by an entropy increase while a transition in the other direction requires the entropy to decrease. Therefore, only the first kind of transition can possibly be found in nature.

The fact that the nontrivial solution is unique implies that no intermediate states can occur between states (1) and (2), in other words that the transition must be in the form of a discontinuous jump. The natural phenomenon predicted by this theory is of course the normal shock wave.

Some relations for normal shock transition are given in Table 1. The Mach number M_2 downstream of the shock and the ratios across the shock of other thermodynamic properties are given in terms of the upstream Mach number. They are plotted in Fig. II-2. Normal shock functions are also tabulated numerically in Refs. 7 to 11.

(3) Oblique Shock

The relations between the downstream condition, state (2), and state (1) upstream of a plane oblique shock can be derived geometrically from the normal shock relations by noting that the component of flow normal to the shock changes in accordance with the normal shock formulas, while the component parallel to the shock remains unchanged. The determination of the conditions at an oblique shock, therefore, requires the specification of two parameters, such as the oncoming Mach number and the angle between the flow direction and the plane of the shock. Ratios of thermodynamic properties before and after the oblique shock are plotted or tabulated in terms of these and other pairs of parameters in Refs. 7, 8, 9, and 10.

(4) Constant-Area Heat Addition

Another process, constant-area heat addition, will be useful in analyzing the effects of water condensation. It will be assumed that at some point in the flow sufficient heat is added to raise the stagnation temperature from T_{0_1} at state (1) to T_{0_2} at state (2). Since the area is kept constant, and the force $F = 0$, the continuity equation and momentum equations are the same as for the normal shock case (Eqs. (11) and (14)); but since heat, q, has been added, the energy equation for a perfect gas with constant specific heat will read

$$\frac{V_2^2}{2} + c_p T_2 = q + \frac{V_1^2}{2} + c_p T_1 \tag{22}$$

$$\frac{M_2^2}{M_1^2} = \frac{2\gamma M_1^2 C - \gamma M_1^4 - 1 \pm (1+\gamma M_1^2)\sqrt{(1-M_1^2)^2 - 2(\gamma+1)M_1^2 C}}{2M_1^2\left[\dfrac{\gamma-1}{2} - \gamma M_1^2 - \gamma^2 M_1^2 C\right]} \tag{23}$$

where C is the heat addition parameter

$$C = \frac{q}{c_p T_1}$$

and q is the amount of heat added.

If M_1 is supersonic, this equation has two solutions. The negative value of the square root makes M_2 subsonic and represents the case of heat addition accompanied by a normal shock, while if the positive square root is chosen, then the process involves only the addition of heat with no normal shock. The normal shock functions may therefore be regarded as resulting from the special case of the heat addition relations in which M_1 is supersonic, C is zero (no heat added), and the negative square root is chosen in Eq. (23).

(c) When the Various Processes Apply

(1) Mach Number Regimes

The *isentropic process is a fundamental* one relating two states in the flow. Since a reversible adiabatic process is by definition isentropic, such a definition will fit all except two of the processes discussed in this report. One exception is the heat addition process which accompanies the condensation of water vapor. The other exception is the flow through a normal or oblique shock which is irreversible. It will be noted that heat conduction and viscosity can also cause changes in entropy, but these effects are usually negligible except in boundary layers.

Since at subsonic speeds no shock waves are possible, the isentropic process is usually employed for making flow measurements involving conditions at two states. At transonic velocities, shock waves will be weak, and the flow nearly isentropic. However, since there will generally be supersonic regions in a transonic flow, it is necessary to take account of any existing shock waves. The presence of shock waves in the flow can cause significant errors in computations of Mach number deduced on the assumption that the flow is isentropic. A normal shock at M = 1.1 for example, implies a 0.1 percent loss in stagnation pressure.

In the supersonic region, accelerating flow will generally be isentropic, while deceleration will be accompanied by strong normal or oblique shocks. Generation of known shock conditions is a useful method of obtaining two states at which properties can be measured. On the other hand, stray shock waves can lead to erroneous Mach number measurements if their presence is not accounted for. Fortunately, a weak oblique shock, such as might appear in a wind tunnel due to an irregularity in the nozzle contour, will have only a negligible effect on Mach number measurements. It is therefore easy to measure Mach number in an empty supersonic wind tunnel, but strong shock waves of unknown strength generated by a model, make flow measurements in the vicinity of the model more difficult. However, in supersonic flow, unlike the subsonic case, it is possible to insert a measuring probe which does not disturb the entire flow field by its presence.

The same will be true for hypersonic flow, but in that case, the process between two states may involve such extreme variations of temperature, or may occur so rapidly that corrections may be necessary for nonequilibrium or nonperfect gas effects. Furthermore, in hypersonic flow the boundary layer has important effects on the flow field around a body or probe so that accurate methods of measuring free stream static pressure for example, are difficult to find. An additional difficulty arises because the large reduction in temperature as the air expands in a hypersonic wind tunnel may cause the condensation of air in the nozzle.

(2) Flow Regimes

The thermodynamic relations and equations of flow are derived on the assumption that air is a collection of molecules so numerous that it may be described as a continuum. When the density is so low that the probable behavior of individual molecules must be considered, then these equations may no longer hold. Further, viscous effects become more pronounced as the density decreases. Tsien (Ref. 12) divides the density spectrum into a "free molecule" region for which $M/R_e > 10$; a "slip flow" region where $M/R_e > 1$ for $R_e \leqq 1$ and $M/\sqrt{R_e} > 1$ for $R_e > 1$ and $M/\sqrt{R_e} < 1/100$; and a continuum flow region, where $M/\sqrt{R_e} > 1/100$.

The division is an arbitrary one, but the distinguishing characteristics are that the mean free path is much larger than body dimensions in free molecule flow. In continuum flow, the mean free path is negligibly small while in slip flow, the mean free path is still small but not negligible in comparison with body dimensions. Some consequences of very low density regimes are discussed in Ref. 13.

(3) Imperfect Gas Effects

The perfect gas equation of state for air, $p = \rho RT$, has been assumed in deriving the one-dimensional flow equations. The further assumption has been made that the specific heats c_p and c_v are constant with the ratio

$$\gamma = \frac{c_p}{c_v} = 1.4 .$$

Departure from the assumption of constant specific heats (called "caloric imperfections") will usually be of far greater consequence in wind tunnel testing than will deviation from the equation of state of a perfect gas ("thermal imperfections"). The ratio of specific heats, γ, as a function of both pressure and temperature is tabulated in Refs. 5 and 14. At room temperature and pressure, γ is approximately 1.40. Increasing temperature causes γ to decrease; while γ increases with rising pressure.

Mach number calibration of a wind tunnel with a heated air supply will require some corrections for caloric imperfections. The ratio of specific heats will then differ from 1.4 and moreover will change during the expansion process through the nozzle. Besides the change with temperature and pressure, γ will be a function of rate of expansion (or compression) since a "relaxation time" is required for the air to assume its equilibrium state.

Thermal imperfections are deviations from the ideal gas equation of state. The compressibility factor, Z, is defined by

$$Z = \frac{p}{\rho RT}$$

and is unity for a perfect gas.

Compressiblity factors for air are given in Refs. 5 and 6. At low temperature, the factor will be less than 1. Generally, however, when the temperature is high enough for significant effects of departures from the perfect gas equation of state, the variations in specific heat will cause even larger changes in Mach number and other flow properties.

Some attempt may be made to evaluate the effects of departures from the perfect gas equation of state by deriving the isentropic flow and constant-area flow equations using Van der Waal's, the Beattie-Bridgeman, or the virial equation of state.

III. METHODS OF MEASURING MACH NUMBER

(a) Measurable Properties

Well-developed techniques are available for measuring pressure, density, velocity, temperature, mass flow, or shock-wave geometry.

The equations given in Table I will generally relate Mach number to suitable combinations of these properties. The choice of which properties to measure and of which instrument to use depends on a number of factors such as:

(1) The reading accuracy with which the property can be measured.

(2) Its sensitivity to Mach number change.

(3) Errors in making the measurements and in computing Mach number from them.

(4) Convenience and simplicity of instrumentation.

(5) The regimes of temperature and density.

The purpose of this chapter will be to compare the sensitivities of various measurable parameters to increments in Mach number. A brief description will also be given of the instruments which may be used to make the measurements. In relating a parameter to Mach number and computing its sensitivity, it is assumed that the one-dimensional flow relations given in Table I may be applied, that the instrument correctly measures the required property, and that this measurement may be read with infinite precision. Violations of the flow relations and inherent errors in the measuring devices will be discussed in Section IV.

(b) Sensitivity

A parameter, P_i, will be defined as a particular combination of measurable quantities from which the Mach number may be deduced. Then the sensitivity, S_i, is defined as the fractional change in Mach number which results for a unit fractional change in this measured parameter.

For small increments, the effect of sensitivity may be written in the differential form

$$\frac{dM}{M} = S_i \frac{dP_i}{P_i} \ . \tag{24}$$

A parameter which is sensitive to Mach number, and hence provides a good basis for measurement, will have a small value for S_i. It must be remembered that the practical measuring and reading accuracies of different parameters must be taken into account since Eq. (24) indicates that the smallest measurable fractional increment in Mach number, dM/M, is the product of the sensitivity and the smallest measurable fractional increment in the parameter.

(c) Methods

(1) Pressure

Mach number is most commonly deduced from pressure measurements. Various types of pressure probes will first be described. More detailed information can be found in Ref. 15, for example.

a. Stagnation Pressure, p_0

When a fluid is brought isentropically to rest, it is said to be in a stagnation condition. The pressure measured at this state is the stagnation pressure. Since a supersonic stream generally can not be decelerated isentropically, the stagnation pressure can be measured directly only in subsonic flow.

Fig. III-1 shows a typical stagnation pressure probe. It contains a small orifice in the front of a spherical nose. The axis of the probe should be aligned with the stream with the hole on the axis. Although such a probe shape will be relatively insensitive to small deviations in flow direction, it can not be considered reliable in a flow field having a large velocity gradient (such as in a boundary layer).

b. Static Pressure, p°

The static pressure would be that acting on a body which is moving with the velocity of the stream. To measure static pressure, in principle all that is required is a pressure tap in the side of a probe so arranged as not to disturb the flow. In practice it is impossible to insert any kind of measuring probe into the stream without disturbing the flow, and in particular, the growth of the boundary layer will displace the flow around the probe.

Four static pressure probes are illustrated in Fig. III-2. The first is a blunt-nosed probe used in subsonic flow where, if the pressure tap is placed well back from the nose and at the proper distance forward of the tube support, it will indicate the static pressure. To minimize errors due to flow angularity, the pressure orifice is usually ring-shaped encircling the probe.

Stagnation pressure can be measured with the same probe by including an orifice in the nose, but due to the necessity of having the static orifice so many probe diameters behind the nose, it is not possible to measure stagnation and static pressure at the same point. Such a probe may also be used in supersonic flow, but a sharper nose such as the one in Fig. III-2b will reduce the nose-shock disturbance to the flow.

Another type of supersonic probe is shown in Fig. III-2c where the static pressure is measured on the surface of a flat plate, so placed that the flow over the measuring surface is not disturbed by the nose shock. Such an instrument is sensitive to flow angle, however.

A long tube with static pressure orifices may be used for calibration on the centerline of either subsonic or supersonic nozzles. The front of the tube is supported upstream of nozzle as shown in Fig. III-2d so that nose effects are eliminated. If the tube occupies a significant percentage of the cross-sectional area of a supersonic nozzle, it may be contoured so that it does not affect the Mach number of the flow.

c. Wedge Static Pressure, p_w

The static pressure on a wedge (illustrated in Fig. III-3) can be used to infer Mach number in supersonic flow through use of the oblique shock formulas discussed in Section II.

d. Cone Static Pressure, p_c

Cone static pressure can also be used to infer supersonic Mach numbers since exact solutions are known for conical supersonic flow and given in Refs. 8, 9, 11, and 16. A conical probe is shown in Fig. III-4. Four pressure holes placed around the cone give an average pressure which is not sensitive to small flow angles. A fifth hole in the front of the probe can be used to measure pitot pressure (as defined in the next paragraph). Since its dimensions can be kept quite small, this five-hole probe makes a good instrument for deducing Mach number from measurements of only local properties. It is necessary, however, to put the surface-pressure taps sufficiently far back as to be unaffected by the finite size of the apex of the cone (a distance of 25 times the outside diameter of the tip at the forward hole is found satisfactory in Ref. 17, but probably about 10 tip diameters would be sufficient).

e. Pitot Pressure, p_i

Pitot pressure is the stagnation pressure behind a normal shock. A good pitot tube is illustrated in Fig. III-5. The front should be cut off square in order to produce a normal shock in front of the pressure orifice which is of much smaller diameter than the probe. In subsonic flow where there is no normal shock, the pitot tube will indicate stagnation pressure.

f. Pitot Pressure Behind an Oblique Shock, p_{i_w}

In order to obtain a ratio of two different pressures (from which the Mach number can be computed) without resorting to a static pressure or a stagnation pressure measurement at a large distance from the point at which the Mach number is desired, the pitot pressure can be measured ahead of and behind an oblique shock.

The oblique shock is generated by a wedge as shown in Fig. III-6. Since the shock angle must be known in order to apply the oblique shock formulas, the wedge angle is so selected that the computed Mach number is insensitive to small errors in measurement of shock angle (see Ref. 18).

The optimum shock angle β is given by the solution of

$$\frac{\partial p_{i\,w}}{\partial \beta} = 0$$

In terms of Mach numbers (for $\gamma = 1.4$)

$$M^2 + b(m)\,M + c(m) = 0 \tag{25}$$

where M is the Mach number to be measured (presumably known approximately), and $m = M^2 \sin^2 \beta$.

The coefficients are

$$b(m) = -\frac{13m^3 + 207m^2 - 21m - 55}{72m}$$

$$c(m) = \frac{3m^3\,(14m + 143) - 5(9m^2 + 57m - 15)}{216m}$$

The optimum shock angle and the wedge angle which will produce it are plotted in Fig. III-7. The Mach number may be computed from various pressure ratios designated as parameters, P_j. Some useful combinations are tabulated in Table II.

Only the first two parameters are useful in subsonic flow (they are then identical). Mach numbers based on local properties only may be deduced from parameters P_2, P_4, P_5, P_8, P_9, P_{10}, P_{11}. The others assume that the flow is isentropic from some known upstream reference condition on the streamline leading to the probe.

The sensitivities for each method are tabulated in Table III and are plotted as functions of Mach number in Figs. III-8, 9, 10, and 11. A similar analysis including plots of sensitivities appears in Ref. 19. Barry, in Ref. 20 has also plotted sensitivity functions defined in a slightly different manner.

(2) Density

Density measurements are, of course, limited to compressible gas flows and principally make use of optical or radiation techniques. The required apparatus is in general of much greater complexity than that employed in pressure work. However, a radiation field does not in itself interfere with the airflow process and also does not necessarily impose the presence of probes within the flow field. Further, at extremely low pressure and density (less than 10^{-3} atmospheres), pressure probe measurements are subject to substantial error. For these reasons density measurements are worth consideration in some instances. Descriptions of the techniques can be found in Ref. 21.

a. Stagnation Density, ρ_0

The density of air at rest may be deduced from measurements of stagnation pressure and temperature by means of the equation of state. If the air is approximately at rest, such as upstream of the wind tunnel nozzle, then stagnation pressure and temperature are easily measured, or, in principle, the stagnation density may be found directly by weighing a sample of a known volume of air.

b. Free-stream or Static Density

One method of deducing Mach number from the density is to measure the local density and then compute Mach number from the ratio of ρ^0/ρ_0. The most common instrument for this purpose is the interferometer. In this device, coherent light waves are passed through both a test region and a "standard" reference region and then recombined so as to yield interference arising from resulting phase differences (see Fig. III-12). When the superimposed rays differ in optical path length by an integral number of wavelengths, reinforcement occurs; when they differ by an odd number of half-wavelengths (out of phase), the rays cancel.

The path length changes are a result of the dependence of the gas index of refraction upon density as given by the Dale-Gladstone law which states that $(\mu - 1)$ is proportional to the density where μ = index of refraction. These interferometer bands of alternating brightness and darkness correspond to constant density loci.

In practice, a background band pattern is employed by slightly rotating one of the mirrors in the system so that some interference is inherently present. When density changes occur, the bands are locally shifted by an amount proportional to the density change. The proportionality constant involves the refraction index, the wavelength of light, and the light path length through the flow. Quantitative evaluations (Refs. 21, 22, and 23) are then restricted to two-dimensional or axi-symmetric flows. Even then, only the change in density from some known value can be measured.

The complexity of an interferometer unit may, in principle, be replaced by a "schlieren interferometer." The latter is virtually identical to an ordinary schlieren system (described under "wave geometry") with a coherent light source (Refs. 24 and 25). However, this device requires further development before wide application may be made.

Density may also be determined from the spectral absorption powers of gases. Radiation of known wavelength can be passed through the flowing medium and later received on a detector. From knowledge of the transparency of the gas as a function of density, a point by point survey of the field may be completed. Oxygen absorption phenomena may be employed, or tracer quantities of ozone or mercury may be introduced in the air supply.

Some practical difficulties are encountered in each case. For example, any windows in the system must be transparent for the radiation considered, and all radiation paths aside from the test region must contain a suitable nonabsorbing medium. The major applicability is in those cases where the product of density and path length is so small (less than 10^{-4} gm/cm^2) that the interferometer fails. However, the practical restrictions limit the general use of the absorption technique at present.

An analogous method makes use of X-ray absorption (Refs. 26 and 27). Winkler, in Ref. 21, gives both the absorption and error in density for measurements in airflow as a function of density (10^{-3} to 1 atmospheres) for several wavelengths ranging from 2 to 13 angstroms. For the larger wavelengths, accuracy to about 2 percent is estimated. Since the wavelengths of X-rays are short, there is very little diffraction and therefore the technique may be employed in flow regions closely adjacent to bounding surfaces. In addition, it is possible to adjust the sensitivity for a range of densities and path lengths by means of changes in the wavelength used. Like the absorption method mentioned above, the X-ray technique must be reserved for very special instances in practice.

The density parameter is the ratio of static and stagnation density

$$P_{12} = \frac{\rho_0}{\rho^0} = \left[1 + \frac{\gamma - 1}{2} M^2\right]^{\frac{1}{\gamma-1}}$$

The corresponding sensitivity is

$$S_{12} = \frac{1 + \frac{\gamma - 1}{2} M^2}{M^2}$$

(3) Velocity

Several methods are available (see Ref. 21) for making direct measurements of the air velocity. In most cases the measurement consists of the time interval for a pulse, particle, or ion to traverse a given length. Thus, in general, an average speed is involved which restricts the technique to uniform flow conditions. The interpretation of Mach number requires a temperature in addition, for which the stagnation condition is suitable.

Ion tracers can be produced in a variety of ways: X-rays, electron beams, alpha particles, or by an electric spark. These can be injected into the flow from the boundary or emitted from a probe holder. Rather elaborate apparatus is required to measure the time taken by the particle to travel from the point at which it is emitted to the detecting point (Ref. 21). A synchronizer, pulser, and electrode are needed at the emitting station and a detector and amplifier at the receiver. The particle passes through the flow field and boundary layer around the emitter and hence its velocity will differ from that in the undisturbed stream. Over short paths (about 1 cm) the transit time (Ref. 28) is on the order of 10^{-5} seconds in a supersonic wind tunnel. Nevertheless, measurements within 1 percent to 2 percent in Mach number have been made by this method over a range of $.3 < M < 3.8$ (Ref. 29).

The electrical conductivity of air has also been suggested as a means of determining velocity. An electrical potential across a small gap (order .01 mm) produces a current flow of the Townsend discharge, corona, or glow types. For a given field strength and geometry, the current is a function of velocity. For the Townsend discharge the sensitivity of velocity to current is somewhat greater than one and is much greater in the case of a corona formation. The glow anemometer proves to have a nonlinear calibration. Unfortunately the static pressure is also required to fully define the velocity and a calibration is required for each discharge probe.

The relation between velocity and Mach number can be written

$$P_{13} = \frac{V}{\sqrt{T_0}} = \frac{\sqrt{\gamma R}\, M}{\sqrt{1 + \frac{\gamma - 1}{2} M^2}}$$

for which the sensitivity is

$$S_{13} = 1 + \frac{\gamma - 1}{2} M^2 .$$

The sensitivity is rather poor and increases rapidly with M. Velocity measurements are therefore of most value at relatively low Mach numbers.

(4) Temperature

One of the most elusive thermodynamic properties is the temperature. Where the air is moving slowly, or not at all, it is relatively easy to measure the stagnation temperature; but in a fast moving stream only a so-called "recovery temperature" can be determined directly.

a. Stagnation Temperature, T_0

The stagnation temperature is that of air brought adiabatically to rest. In a slow moving stream, as upstream of a supersonic nozzle, almost any temperature measuring device such as a thermocouple or ordinary thermometer will measure the stagnation temperature since the air comes to rest at the surface of the instrument, although at high temperatures, radiation shielding might be required. The stagnation temperature remains constant throughout an adiabatic flow even though the flow may be irreversible as in the presence of shock waves.

b. Recovery Temperature, T_r

Due to the combined effects of viscosity, thermal conductivity, and radiation, a temperature probe measures some quantity intermediate between free stream static temperature, T^0, and stagnation temperature. The fraction of stagnation-temperature rise "recovered" by the probe is defined by the recovery factor r

$$r = \frac{T_r - T^0}{T_0 - T^0} . \tag{26}$$

If r = 1, then $T_r = T_0$; while if r = 0, then $T_r = T^0$. It may be desirable, if the flow from upstream of the nozzle is not adiabatic, to make a local measurement of T_0. Then every effort is made to manufacture a probe with r = 1. Such a design is shown in Fig. III-13. A measurement of T_0 can be combined with a velocity to give a parameter related to Mach number. This parameter P_{13} is defined in the discussion of velocity measurements. The combinations using mass flow are presented in that section as P_{15} and P_{16}.

The ratio of stagnation to static temperature can be written as a function of M.

$$\frac{T_0}{T^0} = 1 + \frac{\gamma - 1}{2} M^2 .$$

In terms of T_r from Eq. (26), this relation gives for the parameter P_{14}

$$P_{14} = \frac{T_0}{T_r} = \frac{1 + \frac{\gamma - 1}{2} M^2}{1 + \frac{\gamma - 1}{2} M^2 r}$$

with sensitivity

$$S_{14} = \frac{\left(1 + \frac{\gamma - 1}{2} M^2\right)\left(1 + \frac{\gamma - 1}{2} M^2 r\right)}{(\gamma - 1) M^2 (1 - r)}$$

For good sensitivity, it is desirable to make r as small as possible. On a surface aligned with the stream, the recovery factor varies from about .85 to .90 depending on the nature of the boundary layer, so that P_{14} is a poor parameter for Mach number measurement. By expanding the flow before it reaches the temperature element, it is possible to achieve a slightly lower recovery factor. By creating unsteady flow conditions at the temperature probe, recovery factors may be made greater than one, or less than zero. These conditions, however, would require the use of a calibrated probe.

(5) Mass Flow

In supersonic flow, the mass rate of flow may be measured by a so-called mass-flow probe as illustrated in Fig. III-14. The probe has a sharp inlet of known area. Air from the stream passes through the probe into an evacuated tank. The flow through the probe into the tank continues for a measured period of time and is then shut off by a quick-acting valve. The weight of the air in the tank and the time required for its accumulation then give the mass rate of flow into the probe. If the inlet is sufficiently sharp, then all of the flow in front of the inlet area will be captured by the probe as long as the back pressure is low enough to maintain supersonic flow at the inlet.

From the measured mass rate of flow, ρVA and the known area of the probe ρV may be computed. The area A is the area of the captured flow and will be equal to the probe inlet area only if the probe swallows the flow and if the reduction of effective probe area due to shock waves and boundary layer is negligible compared with A or is found by calibration of the probe.

The mass flow may be related to the Mach number through the stagnation pressure and temperature.

$$P_{15} = \frac{\rho V \sqrt{T_0}}{p_0} = \sqrt{\frac{\gamma}{R}}\, M \left[1 + \frac{\gamma-1}{2} M^2\right]^{-\frac{\gamma+1}{2(\gamma-1)}}$$

and

$$S_{15} = \frac{1 + \frac{\gamma-1}{2} M^2}{1 - M^2} .$$

For a local measurement, pitot pressure may be employed in place of stagnation pressure. Then

$$P_{16} = \frac{\rho V \sqrt{T_0}}{p_i} = P_{15} P_3$$

and

$$S_{16} = \frac{S_{15}\, S_3}{S_{15} + S_3} .$$

The sensitivities are plotted in Fig. III-15.

(6) Wave Geometry

In supersonic flow the influence region upstream of an obstacle is bounded by a characteristic shock pattern associated with the obstacle. Either an increase in the Mach number of the oncoming flow or a decrease in the slenderness of the obstacle results in a lessening of the forward influence. Conversely, reducing the Mach number or increasing bluntness eventually cause the shock pattern to originate ahead of the body. Due to geometric similarity the shock pattern and body may be characterized by appropriate angles.

Most commonly the solutions for a wedge or cone are employed for measurement purposes to obtain the Mach number as a function of the nose shock angle and the nose half-angle. In the case of the cone, it is necessary to resort to tabulated results (Refs. 8, 9, and 16). The limiting case of a wedge or cone shock angle is the Mach angle, α, corresponding to an infinitesimal disturbance. In practice, any small projection will yield Mach waves especially at some distance from the object.

The sensitivity to Mach number for each of the three following cases:

a. Mach wave, α

b. Wedge shock angle, β_W

c. Cone shock angle, β_C

is shown in Fig. III-16 as obtained from the following relations:

a. Mach wave

$$P_{17} = \alpha = \sin^{-1}(1/M)$$

$$S_{17} = -\alpha \cot \alpha$$

b. Wedge shock angle

$$P_{18} = \beta_W; \quad \frac{1}{M^2} = \sin^2 \beta_W - \frac{\gamma+1}{2} \cdot \frac{\sin \beta_W \sin \delta}{\cos(\beta_W - \delta)}$$

$$S_{18} = -\frac{M^2 \beta_W}{2} \sin^2 \beta_W - \frac{\gamma+1}{4} \cdot \frac{\sin \delta}{\cos^2(\beta_W - \delta)}$$

c. Cone shock angle

$$P_{19} = \beta_C$$

$$S_{19} = \frac{\beta_C}{M} \left(\frac{dP_{19}}{dM} \right)^{-1}$$

where dP_{19}/dM and β_C are obtained from tabulated results referred to earlier.

Visualization of the above shocks and waves is made possible with the aid of either a schlieren or shadowgraph system (Fig. III-12). Whereas the interferometer mentioned earlier is dependent upon density itself, the schlieren and shadowgraph employ density gradients and rates of change of gradients to yield contrasting bright and dark areas on a viewing screen. A qualitative idea of the flow field may be obtained from either, and in particular the bow shocks of models are easily discernible.

The shadowgraph is the simplest device, requiring only a spark flash and a receiving screen. The schlieren system includes a "knife edge" placed at a focal point after the light rays have passed through the test region. By this means some of the deflected rays are prohibited from reaching the screen and the resulting pattern exhibits intensity variations related to the density gradients under observation.

Some interesting schemes make use of acoustic strength pulses (Ref. 21) which are emitted from the flow boundary by suitable oscillators or a spark. For example, the shock front induced by a spark is spherical and proceeds downstream at the flow velocity. The envelope of a series of these spheres which can be viewed in schlieren or shadowgraph is a Mach line.

Another device emits planar acoustical wavefronts from an oscillating quartz crystal. Using spark photography the waves appear as echeloned bands parallel to the surface. The tangent of the echelon sweepback angle is the Mach number while the velocity may also be obtained as the product of the emission frequency and the "slip" between successive bands. By providing a receiver at an opposite boundary, a variation of this technique eliminates the need for photography.

For all of the above acoustic schemes a point determination of Mach number is unavailable. In addition, the boundary layer must be a relatively small fraction of the flow width through which a wave has traveled. However, for rough measurement purposes in two-dimensional flow, the methods are attractive from the point of view that no probes need be inserted in the stream itself, and that no calibration is required.

IV. ERRORS IN MEASUREMENT AND THEIR CORRECTION

(a) Accuracy Requirements and Limitations

The determination of the Mach number in any flow is an experimental measurement which is necessarily inaccurate. The inaccuracy is the sum of uncertainties and errors. The uncertainties can be reduced to roughly the level of the least count of the measuring instruments by repeated observation; they will not be considered here. The sum of the errors represents the difference between the true Mach number and a suitable average of a number of measurements of Mach number under identical conditions. In other words, the error represents that part of the inaccuracy of a measurement which is systematic and repeatable.

As indicated in the first section of this report, the Mach number should be measured, for calibration purposes to 0.1 percent. The limit set by the measuring instruments can be fairly easily established in the case of pressure measurements, the most common type of measurement in Mach number determination. If only a small number of pressures is being measured, and micromanometers are used, pressures may be read to about one part in 10,000 or

$$\frac{\Delta p}{p} < .0001 .$$

Where many pressures are being read and manometer boards are photographed, the reading inaccuracy is of the order of

$$\frac{\Delta p}{p} < .001 .$$

In Section III it was shown that the sensitivities of most Mach number recovery methods involving pressures are of the order of unity. Consequently the designer's limit on accuracy and the second of the measuring instrument limits are consistent. It will be assumed that the density of any manometer fluid may be determined with similar accuracy. It is then both desirable to consider and possible to measure errors of the order of

$$\frac{\Delta M}{M} = .001 .$$

Assuming that the instruments and their read-outs are perfect, errors will still arise in two ways. First the pressure, density, or other property measured by the instrument may differ physically from the quantity which is used in the formula to deduce the Mach number. For example, a static pressure probe may correctly read the pressure at the orifice; but due to boundary layer or some effect of the presence of the probe on the stream, this may not actually be the free stream static pressure. These errors will be called probe errors.

Other errors may arise because the gas does not actually follow the assumed process between two measured states, or may not obey the perfect gas equations, or the computation of Mach number based on nonviscous laws may be in error due to viscous effects. These errors due to deviations from the assumed thermodynamic relations will be considered first.

(b) Errors Due to Departure from the Assumed Flow Conditions

The formulas for the parameters and their sensitivities given in Section III are derived on the assumptions of a prescribed process in a nonviscous perfect gas. The violation of these assumptions will lead to errors in the calculation of Mach number. The magnitude of such errors will be estimated in this section by using improved models of the actual flow. The first improvement is in the description of an adiabatic process. The condensation of water vapor or air adds heat to the stream, while viscosity and heat conduction modify the assumption of an isentropic process. Weak shock waves from nozzle walls add additional irreversibility.

Several departures from the assumed perfect gas relations are also considered. The change in the specific heats with temperature, called caloric imperfections, form the most significant variation from the assumed ideal gas. Since after a change in temperature, a finite time elapses before the specific heats reach their equilibrium values, the specific heat becomes a function of time as well as temperature.

In some high-speed flow processes (notably the normal shock) this time lag has measureable effect. Air will also depart from the equation of state of an ideal gas, $p = \rho RT$, but in the range of wind tunnel processes, the caloric imperfections will be considerably more important.

(1) Water Vapor Condensation

Water vapor is present in some amount in the air supply of any wind tunnel. As the airstream is cooled in its acceleration to high speeds, this water vapor is also cooled, and very often sufficiently low temperatures are reached for it to condense. The expansion of the air is then nonisentropic, and the flow parameters in the test section are changed from their design values.

To study water vapor condensation effects quantitatively, it is necessary to have a measure of the humidity of the air. For calculations, the specific humidity, or mass of water vapor per unit mass of dry air, is useful. The quantity most easily measured, on the other hand, is the dewpoint from which the specific humidity may be determined in terms of the pressure at which the dewpoint is obtained.

The relation is shown in Fig. IV-1. Typical operating dewpoints for supersonic tunnels in the United States are dewpoint $\sim$ - 35°C; specific humidity $\sim$ .0001. The limits of condensation free flow under these conditions, are shown approximately in Fig. IV-2.

The condensation process seems to be different at subsonic and supersonic speeds. Below M = 1, it is a gradual process extending over an appreciable streamwise distance in the flow. At supersonic speeds condensation takes place very suddenly, forming one or more condensation shock. In either case, there is a large amount of supersaturation at the condensation point; in other words the stream must be cooled well below the saturation temperature for condensation to take place.

Over a wide range of tunnel operating conditions, both at the British National Physical Laboratory (Ref. 30) and at Massachusetts Institute of Technology's Naval Supersonic Laboratory (Ref. 31), an approximately constant 45°C of supercooling has been measured. The influence of the rate of cooling, which varies from nozzle to nozzle, on this result was found to be very small. The supercooling is therefore probably about the same over a wide range of tunnel sizes, both larger and smaller than those involved in these tests (0.1 - 0.3 m² test section).

At the downstream end of a long test section with uniform flow, the supercooling may be less, and the curves of Fig. IV-2 have been drawn for the conservative value of 30° C supercooling.

Since the dewpoint measured in a wind tunnel varies from test to test, two types of error will be introduced by the condensation of water vapor in the stream. First, if the tunnel is calibrated at one dewpoint (with very dry air for example), while a model is later tested at a different dewpoint (in wet air), then the Mach number, and all other measurements will generally be incorrectly interpreted unless allowance is made for the effects of water condensation. Also, if the Mach number is deduced from an upstream measurement within or downstream of a condensation region, then the correct computation of Mach number will require an allowance for condensation effects.

Calculations of water-vapor condensation effects at supersonic speeds are straightforward if it is assumed that the flow is one-dimensional and that condensation occurs in a normal shock with saturated air on the downstream side. For the range of initial humidities of interest, all the effects of condensation may be ascribed to the heat release in the condensation shock. Isentropic flow of dry air may be assumed both upstream and downstream of the shock. A convenient way of calculating the effect of heat addition is through the use of the formulas for one-dimensional, constant-area flow with heat addition found in Table I.

The effects of water vapor condensation depend not only on the humidity of the air supply but also on its stagnation temperature and pressure, so that it would be difficult to present results in a generally applicable form. Qualitatively, condensation at supersonic speeds is always accompanied by a stagnation pressure loss and Mach number decrease at the condensation shock. The flow in the test section experiences the same loss in stagnation pressure and a generally different decrease in Mach number. Orders of magnitude of these effects as a function of initial dewpoint are shown in Figs. IV-3 and IV-4 for a range of operating conditions. There is, of course, also a change in stagnation temperature, corresponding directly to the amount of heat released.

In one-dimensional flow, the effect of water condensation on the flow properties in the test section can be completely specified in terms of the changes in Mach number and stagnation temperature and pressure change. In particular, it is possible to compute the change in static pressure as it might affect the measurement of Mach number. The static pressure change is also most conveniently measured in experimental investigations of condensation effect.

Fig. IV-5 shows experimental results obtained for a range of supply conditions and Mach numbers in the Naval Supersonic Laboratory's tunnel at Massachusetts Institute of Technology and in some of the supersonic tunnels of the United Aircraft Corporation's Research Department. Also shown is a typical theoretical result. From such experiments one may conclude that, although the simple one-dimensional theory predicts most of the trends found in practice, results for specific conditions may easily be in error by as much as 100 percent. It seems unlikely that accurate results could be obtained by substituting an elaborate correction procedure for a good dryer.

Of greater interest from the point of view of Mach number measurements are the effects of water vapor condensation on pitot pressure. They are complicated by the possibility of re-evaporation in or downstream of the normal shock in front of the pitot tube. Because the opposing effects of stagnation pressure loss and Mach number decrease in the test section are roughly equal in magnitude, the net effect on pitot pressure is much more sensitive to Mach number and supply conditions than the effect on static pressure. In fact, in Massachusetts Institute of Technology's Naval Supersonic Laboratory tunnel, the balance is so close that the effect changes sign, condensation decreasing pitot-pressure at low Mach numbers and increasing it at high Mach numbers.

A detailed theoretical and experimental study for this tunnel has been made by J. R. Baron (Ref. 32) using data obtained in the course of a calibration of the M = 3.25 nozzle. The results are shown in Fig. IV-6 where the theory assumes total re-evaporation in the normal shock. The Mach number predicted by the ratio of pitot pressure to stagnation pressure upstream of the nozzle would be relatively independent of dewpoint and would be the actual Mach number for dry-air conditions. The dewpoint requirement for an apparent Mach number error of .001 is 30 degrees less severe than the requirement for a true Mach number error of this size. The implied superiority of pitot pressure measurements for calibration purposes is believed to hold in general, for a wide range of operating conditions in supersonic tunnels, though the margin of 30°C should be regarded as typical rather than universal.

(2) Air Condensation

At sufficiently high Mach numbers, with ordinary supply temperatures, the isentropic cooling of the airstream may become so large that not only the water vapor but also the air itself may begin to condense. This condensation is gradual rather than sudden and not in the form of a condensation shock. The amount of supercooling, below the air saturation temperature, depends quite strongly on the amount of impurities present, especially of carbon dioxide and water vapor.

With normal tunnel air supplies (dried to atmospheric dewpoints as low as -50°C) the National Advisory Committee for Aeronautics (Refs. 33 and 34) found essentially no supercooling. On the other hand at the Guggenheim Aeronautical Laboratory, California Institute of Technology, supercoolings of the order of 12°C have been obtained with the normal air supply in the 5-inch hypersonic tunnel at M = 7.5 (Ref. 35). Intermediate amounts of supercooling have been observed at the Naval Ordnance Laboratory (Ref. 36). Assuming no supercooling at all, the limits of condensation-free flow are as shown in Fig. IV-7.

When some air condensation has taken place, the interpretation of Mach number measurement is much more complicated than in the case of water condensation. The general problem has been discussed, for instance, by Buhler (Ref. 37) on whose work the following brief discussion is based. In the flow of a perfect gas, the Mach number has two fundamental characteristics: it is a direct measure of the ratio of dynamic pressure to static pressure and of angle of propagation (relative to the local velocity vector) of weak waves. In two-phase flow, unless the propagation of a weak wave is isentropic with respect to the vapor phase alone, the Mach number cannot retain both these characteristics.

It can be shown that the speed of sound in a two-phase fluid is given, as in single phase flow, by

$$a = \left(\frac{\partial p}{\partial \rho}\right)_s . \tag{27}$$

To evaluate this speed in terms of other properties, say the temperature, it is necessary to make some assumption about the interaction between the vapor and the droplets during the passage of a sound wave. If it is assumed that there is no heat transfer between the vapor and droplets, and that the latter follow the velocity fluctuations in the fluid, a velocity of sound

$$\tilde{a} = \sqrt{(1-g)\gamma RT} \tag{28}$$

is obtained, where g is the mass fraction of the mixture which is liquid.

This is the sound velocity for which the relation

$$q = \frac{1}{2} \, p \gamma \tilde{M}^2 \tag{29}$$

is maintained, where

$$\tilde{M} = \frac{V}{\tilde{a}} \tag{30}$$

is the pseudo-Mach number.

Other assumptions may of course be made about the droplet-vapor interaction during the passage of a sound wave. Extreme values of the sound speed can be obtained by assuming that:

a. The droplets follow neither the velocity nor the temperature fluctuations of the vapor.

b. The droplets follow both the velocity and temperature fluctuations. It is reasonable to suppose that the actual sound speed falls somewhere in between the two values so obtained. It is not necessarily equal to the value of $\tilde{a}$ given by Eq. (28), however.

Unless a direct method is used, the actual measurement of the velocity of sound in a hypersonic tunnel with two-phase flow requires a theoretical analysis of the condensation process. Here we are not concerned with a nucleation theory which attempts to predict the onset of condensation but rather with a theory which gives the flow equations for the fully developed two-phase flow well downstream of the dewpoint.

A theory of this latter kind has been published by Buhler (Ref. 37) and to some extent verified by experiments in the Guggenheim Aeronautical Laboratory, California Institute of Technology, hypersonic wind tunnels. In this theory it is simply postulated that the expansion downstream of condensation takes place along the saturation curve of the fluid. Air, incidentally is treated as vapor with a single saturation curve, rather than as a mixture of individual gases.

Consider, then, Fig. IV-8. The Rayleigh pressure ratio p°/p_i and the ratio of pitot pressure to stagnation pressure are uniquely related for isentropic flow ($\gamma = 1.4$) as shown. Let S represent the point at which the air is just saturated. Usually, it is assumed that, downstream of this point, the expansion is along the saturation curve instead of the isentrope; the relation of pitot pressure to static pressure can be calculated from Buhler's equations. The curve shown represents the saturated flow for $P_0 = 10.7$ atmospheres.

The experimental results were observed in the Guggenheim Aeronautical Laboratory, California Institute of Technology, 5-inch hypersonic tunnel with the ordinary air supply. They clearly show some degree of supersaturation followed by a gradual onset of condensation and an eventual approach to flow along the saturation line. Sufficiently far downstream of the dewpoint, the saturated expansion theory is valid.

If the validity of the saturated expansion theory is granted, measurements of static and pitot pressure are sufficient to determine most other properties of the fluid. In particular, it turns out that $\tilde{M}$ is very nearly equal to the Mach number obtained from the pressure ratio $p°/p_i$ through the usual Rayleigh pitot-tube equation. The theory cannot, of course, provide any information about the droplet-vapor interaction during the passage of a sound wave and hence cannot give a value for the speed of sound in the flow.

Using the results of the saturated expansion theory, it is possible with one additional measurement, to obtain the sound speed $\bar{a}$ related to the angle of propagation of a wave relative to the velocity vector. Grey (Ref. 38) shows that $\bar{a}$ is related to the rate of change of wedge pressure with wedge angle evaluated at zero flow deflection

$$\bar{M} = \frac{V}{\bar{a}} = \left\{ 1 + \frac{\gamma^2 \tilde{M}^4}{\left(\frac{1}{p} \quad \frac{dp}{d\delta}\right)^2_{\delta=0}} \right\}^{\frac{1}{2}} \tag{31}$$

where $\tilde{M}$ can be obtained for a pitot and static measurement as discussed above.

At the present stage of knowledge concerning two-phase flow, it is necessary to measure two Mach numbers for testing in hypersonic flow downstream of condensation. The similarity parameter is $\bar{M}$ and the dynamic pressure for reducing forces to coefficients must be calculated using $\tilde{M}$. A theory of the condensation process is required to relate these two Mach numbers to measurable quantities such as pressure. The only theory so far advanced postulates a saturated expansion from the saturation temperature; experimental results deviate markedly from its prediction near the beginning of condensation but agree with them further downstream.

Within the region of validity of the theory $\tilde{M}$ can be obtained directly from a pitot-static measurement. $\bar{M}$ must be obtained independently from a complicated measurement. It is conceivable that, based on many tests, an empirical relation between $\bar{a}$ and $\tilde{a}$ (involving, perhaps some other measurable flow parameters) could be developed.

(3) The Effects of Weak Shock Waves Between the Measuring Stations

The assumption that the expansion through a supersonic nozzle is isentropic is also violated if there are shock waves in the flow. Ideally, of course, the walls do not generate any compressions in the flow, but there are inevitably small deviations from the design contour when the nozzles are machined and some expansion waves are bound to be reflected as weak compressions rather than being perfectly canceled. It is conceivable a priori that a number of these compressions could coalesce into weak shocks and lead to a measurable entropy rise.

Estimates of shock strengths likely to arise in practice may be based on experience or on plausible conjectures. Using the first approach, one notes that one of the strongest waves observed during the calibrations of the MIT Naval Supersonic Laboratory nozzles corresponded to a jump of .02 in Mach number in the M = 1.71 nozzle. It was clearly visible in a schlieren photograph.

The entropy rise for a wave of this strength is very small

$$\frac{\Delta s}{R} < .0001$$

and it would take more than one hundred such waves to give a stagnation pressure loss of 0.1 percent.

The other estimate is based on a plausible conjecture about the flow deflection corresponding to the typical wave. For small deflection δ it is known that

$$\frac{\Delta s}{R} \sim \frac{\gamma(\gamma+1)}{12} \frac{M^6}{(M^2-1)^{3/2}} \delta^3 \tag{32}$$

Equating the flow deflection with the estimated maximum error in the slope of the nozzle, a typical value might be $\delta = .002$ giving

$$\frac{\Delta s}{R} \sim 3 \times 10^{-7}$$

for $M \sim 4$.

It would take more than three thousand such waves to give a stagnation pressure loss of 0.1 percent.

(4) Effect of Viscosity

The possible effects of viscosity and thermal conductivity have been ignored in deriving the one-dimensional formulas listed in Table I. If the fluid has coefficient of viscosity μ and coefficient of heat transfer λ, then the change in entropy due to viscous dissipation and heat conduction from neighboring streamlines can be computed (in two-dimensional flow) from the energy equation (Ref. 39).

The time-rate of change of entropy along a streamline is given by

$$\mu \frac{\partial s}{\partial x} + v \frac{\partial s}{\partial y} = \frac{1}{\rho T} \left\{ -\frac{2}{3} \mu \left[\frac{\partial u}{\partial x} + \frac{\partial v}{\partial y} \right]^2 + 2\mu \left[\left(\frac{\partial u}{\partial x} \right)^2 + \left(\frac{\partial v}{\partial y} \right)^2 \right] + \mu \left[\frac{\partial v}{\partial x} + \frac{\partial u}{\partial y} \right]^2 \right\}$$
$$+ \frac{1}{T} \frac{\partial}{\partial x} \left(\lambda \frac{\partial T}{\partial x} \right) + \frac{1}{T} \frac{\partial}{\partial y} \left(\lambda \frac{\partial T}{\partial y} \right) \tag{33}$$

which incidentally expresses the well-known fact that the entropy remains constant along streamlines in the absence of viscosity and heat conduction.

In a real fluid, the entropy will change along a streamline in regions where there are velocity or temperature gradients. From the point of view of Mach number measurements in wind tunnels, the main regions of interest are those in which the flow is accelerated from the stilling section to the test section and in which it is decelerated to rest at the mouth of a pitot tube. The second process has been the subject of many theoretical and experimental investigations and is discussed in another section of this paper. The rapid expansion of a real fluid in a supersonic nozzle will be now be considered.

On the basis that the effects of viscosity and heat condition are very small and produce very small changes in the flow field, the velocity and temperature gradients of the inviscid flow may be inserted in the right hand side of Eq. (33). For any chosen streamline, the rate of change of entropy along it is thus completely determined and the total change between two points can be found by direct integration.

The procedure is especially simple if the chosen streamline is also a line of symmetry of the flow; in particular, along the centerline of a symmetrical nozzle,

$$v = \frac{\partial T}{\partial y} = \frac{\partial s}{\partial y} = \frac{\partial u}{\partial y} = \frac{\partial \rho}{\partial y} = 0 \tag{34}$$

and Eq. (33) immediately simplifies to

$$\rho u T \frac{\partial s}{\partial x} = \frac{4}{3}\mu\left[\left(\frac{\partial u}{\partial x} - \frac{\partial v}{\partial y}\right)^2 + \frac{\partial u}{\partial x}\frac{\partial v}{\partial y}\right] + \frac{\partial}{\partial x}\left(\lambda \frac{\partial T}{\partial x}\right) + \frac{\partial}{\partial x}\left(\lambda \frac{\partial T}{\partial y}\right). \tag{35}$$

All quantities may be related to the centerline velocity distribution by applying the isentropic flow equations. From the continuity equation

$$\frac{\partial(\rho u)}{\partial x} + \frac{\partial(\rho v)}{\partial y} = 0 \tag{36}$$

and in expanded form, since $\partial\rho/\partial y = 0$ on the centerline of a symmetric nozzle,

$$\frac{1}{u}\cdot\frac{\partial v}{\partial y} = -\frac{1}{\rho u}\cdot\frac{\partial(\rho u)}{\partial x} = -\frac{1}{\rho u}\cdot\frac{d(\rho u)}{dx}. \tag{37}$$

The one-dimensional isentropic flow formulas given in Table I may be differentiated to relate $\partial v/\partial y$ to the Mach number distribution by noting that since $\rho u A$ = constant

$$-\frac{1}{\rho u}\frac{d(\rho u)}{dx} = \frac{1}{A}\cdot\frac{dA}{dx} = \frac{1}{u}(M^2-1)\frac{du}{dx}. \tag{38}$$

Hence, combining Eqs. (37) and (38)

$$\frac{\partial v}{\partial y} = (M^2-1)\frac{\partial u}{\partial x}. \tag{39}$$

Since the second derivative $\partial^2 u/\partial y^2$ is also required, it may be found by differentiating the irrotationality condition

$$\frac{\partial u}{\partial y} = \frac{\partial v}{\partial x} \tag{40}$$

giving

$$\frac{\partial^2 u}{\partial y^2} = \frac{\partial}{\partial x}\left(\frac{\partial v}{\partial y}\right) = \frac{\partial(M^2)}{\partial x}\frac{\partial u}{\partial x} + (M^2-1)\frac{\partial^2 u}{\partial x^2}. \tag{41}$$

Again differentiating the formula for u in terms of M it is found that

$$\frac{1}{M^2}\frac{dM^2}{dx} = 2\left(1 + \frac{\gamma-1}{2}M^2\right)\frac{1}{u}\cdot\frac{du}{dx}. \tag{42}$$

Therefore

$$\frac{\partial^2 u}{\partial y^2} = (M^2-1)\frac{\partial^2 u}{\partial x^2} + 2M^2\left(1 + \frac{\gamma-1}{2}M^2\right)\frac{1}{u}\left(\frac{\partial u}{\partial x}\right)^2. \tag{43}$$

From the nonviscous energy equation

$$c_p T + \frac{1}{2}(u^2 + v^2) = \text{constant} \tag{44}$$

Hence on the center streamline, where $v = 0$

$$\frac{dT}{dx} = -\frac{u}{c_p}\cdot\frac{du}{dx}. \tag{45}$$

To obtain $\partial^2 T/\partial y^2$, however, it is necessary to expand the velocities at any point x in a power series about the centerline values ($u = u_0$, $v = 0$). Then

$$u = u_0 + \frac{1}{2}\frac{\partial^2 u}{\partial y^2} y^2 + \ldots$$

$$v = \frac{\partial v}{\partial y} y + \frac{1}{6}\frac{\partial^3 v}{\partial y^3} y^3 + \ldots \tag{46}$$

and

$$u^2 + v^2 = u_0^2 + \left[u_0 \frac{\partial^2 u}{\partial y^2} + \left(\frac{\partial v}{\partial y}\right)^2 \right] y^2 + \ldots \tag{47}$$

Then by differentiating Eq. (44)

$$\frac{\partial^2 T}{\partial y^2} = -\frac{1}{2c_p}\frac{\partial^2}{\partial y^2}(u^2 + v^2) = -\frac{1}{c_p}\left[u\frac{\partial^2 u}{\partial y^2} + \left(\frac{\partial v}{\partial y}\right)^2 \right]. \tag{48}$$

Introducing the expressions for $\partial^2 u/\partial y^2$ and $\partial v/\partial y$ given by Eqs. (43) and (39) gives finally

$$\frac{\partial^2 T}{\partial y^2} = -\frac{1}{c_p}\left[(M^2-1)u\frac{\partial^2 u}{\partial x^2} + (\gamma M^4 + 1)\left(\frac{\partial u}{\partial x}\right)^2 \right]. \tag{49}$$

Now Eq. (35) may be integrated along the center streamline from state (1) to state (2) to obtain the entropy change.

It will be assumed that the air starts from rest at state (1) and increases to a final uniform condition at state (2) so that $\partial T/\partial x = 0$ at both limits. Integrating by parts and normalizing, one obtains

$$s_2 - s_1 = \frac{L^2}{Re^* T_0}\int_0^1 \frac{A}{A^*}\frac{T_0}{T}\frac{\mu}{\mu^*}\left(\frac{\partial u}{\partial x}\right)^2 \left[\frac{4}{3}(M^4 - 3M^2 + 3) - \frac{1}{Pr}(\gamma M^4 - \gamma M^2 + 2) \right] d\left(\frac{x}{L}\right)$$

$$- \frac{L^2}{Re^* T_0}\int_0^1 \frac{A}{A^*}\frac{T_0}{T}\frac{\mu}{\mu^*} u \frac{\partial^2 u}{\partial x^2}\frac{(M^2-1)}{Pr} d\left(\frac{x}{L}\right) \tag{50}$$

letting $x = 0$ at state (1) and $x = L$ at state (2) and substituting the previously determined formulas for the derivatives in terms of the velocity distribution.

Re^* is the Reynolds number $= (\rho^* u^* L)/\mu^*$

Pr is the Prandtl number $= \mu c_p/\lambda$

T_0 is the stagnation temperature

and the * implies conditions at $M = 1$.

To evaluate this integral numerically, it is necessary and sufficient to prescribe the velocity distribution u(x). Different values of the entropy change will be obtained for different nozzle designs, and it is impossible to give a generally applicable value. In most cases the flow starts from a region of uniform very low-speed flow and expands to a region of uniform high-speed flow.

A simple velocity distribution which has zero gradients before and after expansion is

$$u = a_0 \left[1 + \sin\left(\pi \frac{x}{L} - \frac{\pi}{2} \right) \right] \tag{51}$$

where a_0 is the velocity of sound when the fluid is at rest (x = 0); this velocity distribution is shown in Fig. IV-9.

The test section Mach number (at x = L) will be about 4.47. The integration for this distribution becomes

$$s_2 - s_1 = \frac{\pi \gamma R}{Re^*} \int_{-\frac{\pi}{2}}^{\frac{\pi}{2}} \frac{A}{A^*} \frac{T_0}{T} \frac{\mu}{\mu^*} \left[\frac{4}{3} M^4 - 4M^2 + 4 - \frac{1}{Pr} (\gamma M^4 - \gamma M^2 + 2) \right] \cos^2 \theta \, d\tau$$

$$+ \frac{\pi \gamma}{Re^*} R \int_{-\frac{\pi}{2}}^{\frac{\pi}{2}} \frac{A}{A^*} \frac{T_0}{T} \frac{\mu}{\mu^*} \frac{(M^2 - 1)}{Pr} (\sin \theta + \sin^2 \theta) \, d\theta \tag{52}$$

where

$$\theta = \pi \frac{x}{L} - \frac{\pi}{2} \tag{53}$$

and R is the gas constant.

These integrals can easily be evaluated by numerical integration since for any value of θ, Eq. (51) gives the corresponding value of u/a_0, and hence of all other terms in the integrand. In Fig. IV-10, a constant value of 0.7 has been assumed for Pr and μ has been obtained from the NBS-NACA tables of air properties (Ref. 5).

It is interesting to note that the largest value of the integrand occurs near the test section. The area under the curve gives the total entropy change

$$\frac{s_2 - s_1}{R} = \frac{1700}{Re^*} . \tag{54}$$

It is still necessary to determine what the effect this entropy rise has on the flow in the nozzle. For a perfect gas

$$s_2 - s_1 = c_p \ln \frac{T_{o_2}}{T_{o_1}} - R \ln \frac{p_{o_2}}{p_{o_1}} \tag{55}$$

where T_{o_1} and T_{o_2} are stagnation temperatures and p_{o_1} and p_{o_2} are stagnation pressures at states (1) and (2). Having determined $s_2 - s_1$, it is now necessary to find how much of this entropy rise corresponds to a temperature change and how much to a pressure change. The energy equation may be written in terms of the enthalpy on the center streamline of a symmetrical nozzle as

$$\rho u \frac{dH_o}{dx} = \frac{\partial}{\partial x}\left(\lambda \frac{\partial T}{\partial x}\right) + \lambda \frac{\partial^2 T}{\partial y^2} + \frac{4}{3} u \left[\left(\frac{\partial u}{\partial x} - \frac{\partial v}{\partial y}\right)^2 + \frac{\partial u}{\partial x}\frac{\partial v}{\partial y} + u \frac{\partial^2 u}{\partial x^2} + u \frac{\partial^2 u}{\partial y^2}\right] + \frac{2}{3} u \frac{\partial u}{\partial x}\left(2\frac{\partial u}{\partial x} - \frac{\partial v}{\partial y}\right) \tag{56}$$

where $H_o(x)$ is the total enthalpy, that is, the enthalpy which would result if the air were brought isentropically to rest from its condition at point x.

The terms in this equation can be evaluated as done previously for the entropy. In fact most of the terms are of similar form. The final equation then becomes

$$\frac{H_{o_2} - H_{o_1}}{H_{o_1}} = \frac{(\gamma-1)\pi}{Re^*}\int_{-\frac{\pi}{2}}^{\frac{\pi}{2}} (1.1429 + .09524\,M^2 - .1333\,M^4)\,\frac{A}{A^*}\,\frac{\mu}{\mu^*}\,\cos^2\theta\,d\theta$$

$$- \frac{(\gamma-1)\pi}{Re^*}\int_{-\frac{\pi}{2}}^{\frac{\pi}{2}} (1.429 - .09524\,M^2\,\frac{A}{A^*}\,\frac{\mu}{\mu^*}\,(\sin\theta + \sin^2\theta)\,d\theta$$

$$- \frac{(\gamma-1)\pi}{Re^*}\int_{-\frac{\pi}{2}}^{\frac{\pi}{2}} (.8M^2 - .267\,M^4)\frac{A}{A^*})\,\frac{\mu}{\mu^*}\,\frac{T}{\mu}\,\frac{d\mu}{dT}\,\cos^2\theta\,d\theta. \tag{57}$$

This integrand is plotted in Fig. IV-11.

Since $H_o = c_p T_o$, the integration yields directly

$$\frac{T_{o_2} - T_{o_1}}{T_{o_1}} = \frac{6}{Re^*}. \tag{58}$$

Thus practically all of the entropy rise corresponds to a lowering of the total pressure in the test section. In this example, from Eq. (55)

$$\ln \frac{p_{o_2}}{p_{o_1}} \sim \frac{p_{o_2} - p_{o_1}}{p_{o_1}} \sim \frac{c_p}{R}\,\frac{T_{o_2} - T_{o_1}}{T_{o_1}} - \frac{s_2 - s_1}{R} = -\frac{1694}{Re^*}. \tag{59}$$

This change in total pressure will result in an erroneous computation of Mach number if it is based on measurements of stagnation pressure p_0 in the stilling section, and some local pressure such as pitot pressure in the test section, unless of course, allowance is made for viscous effects. In a tunnel with a nozzle one meter long at $T_0 = 45°C$, a 0.1 percent drop in p_0 at the test section would result when p_0 was about 1/10 atmosphere in the above example.

Although it is dangerous to generalize from one example, it may be judged from the nature of the equations that the neglect of viscous effects on the flow process produces a very small error in Mach number measurement except in a low Reynolds number wind tunnel. The entropy rise appears almost wholly as a loss in total pressure with only a very small change in stagnation temperature. The effect would presumably be more pronounced at high Mach numbers so that the computation carried out here for $M = 4.47$ is representative of supersonic, but not hypersonic, speeds.

Finally one note of caution must be applied to the conclusion that viscous effects on entropy are likely to be small. This calculation was carried out for the center streamline because of the simplification introduced by the condition of symmetry. It may be, however, that the terms which do not appear in the centerline calculation cause much larger errors on streamlines off of the line of symmetry.

(c) Real Gas Effects

Air is not an ideal gas and hence does not have constant specific heats. Solutions of the one-dimensional flow equations and tabulated properties for isentropic and normal shock processes, however, are derived on the assumption that $p = \rho RT$ and $\gamma = 7/5$. The properties of the real gas (Ref. 5). are illustrated in Figs. IV-12 and IV-13. Fig. IV-12 shows the compressibility factor $Z = p/\rho RT$ which is one for a perfect gas. The ratio of specific heats γ is shown in Fig. IV-13. Approximate isentropic lines (derived using $Z = 1$ and $\gamma = 1.4$) show the variation in Z and γ as the air expands in a wind tunnel nozzle.

It is apparent from these figures that, especially at very high pressures, air departs somewhat from the ideal gas assumptions as it expands through a nozzle. By examining the effect of various constant values of γ on the Mach number and other flow properties, it is possible to estimate how large a variation from $\gamma = 1.4$ can be considered as negligible.

To estimate the effect of variations in γ and Z properly, however, it is necessary to carry out the one-dimensional flow calculations with variable specific heats and an improved equation of state. It is found, in general, that the change in γ is of greater significance in wind tunnel applications than is the departure from the perfect gas equation of state. Some effects of γ variation, called caloric imperfections, are given in Ref. 8. The one-dimensional flow equations have been solved, moreover, using Van der Waal's equation of state in Ref. 3 and the Beattie-Bridgeman equation in Ref. 4.

The problem is further complicated by the fact that a finite time is required for air suddenly changed from one state to another to regain equilibrium in its new state. The ratio of specific heats is therefore a function of this "relaxation" time as well as temperature and pressure.

(1) Erroneous, Constant, Ratio of Specific Heat

In Ref. 7 one-dimensional flow tables are presented for γ = 9/7, 7/5, and 5/3 which enable one to evaluate grossly the effect of γ errors on Mach number predictions. For the small errors in γ to be expected (~0.2 percent) in practice use may be made of $d\gamma/dM$ for a more precise determination.

In general the Mach number parameters P_i given in Section III contain factors of the form

$$t_j = \left[f(M, \gamma) \right]^{\zeta(\gamma)} \tag{60}$$

Taking note that

$$\frac{1}{t_j} \frac{dt_j}{dM} = \frac{\zeta'}{\zeta} \ln t_j + \zeta \frac{\left(t_j^{\frac{1}{\zeta}}\right)'}{\left(t_j^{\frac{1}{\zeta}}\right)}$$

it is a simple procedure to carry out an analytical reduction of the γ influence. Here $(\ )'$ means $d/dM = \partial/\partial M + (d\gamma/dM)(\partial/\partial\gamma)$.

The parameter P_1 is a function of γ and M. If the parameter has some fixed measured value, then the Mach number which is thereby indicated will depend on the value of γ. For example, if $P_1 = p_0/p^0$ is measured, then the variation of corresponding Mach number with γ is given by

$$\left(\frac{d\gamma}{dM}\right)_1 = \frac{2\gamma(\gamma-1)^2 M}{2\left(1+\frac{\gamma-1}{2}M^2\right)\ln\left(1+\frac{\gamma-1}{2}M^2\right)-\gamma(\gamma-1)M^2} . \tag{62}$$

A somewhat more complicated parameter is $P_2 = p_i/p^0$ which may be expressed as $P_2 = t_1 t_2$. The corresponding γ effect is then given by

$$\left(\frac{d\gamma}{dM}\right)_2 = -\left[\frac{2\gamma(\gamma-1)(1-2M^2)}{M\left[2\gamma M^2-(\gamma-1)\right]}\right]$$

$$\left\{\frac{2(M^2-1)}{(\gamma+1)\left[2\gamma M^2-(\gamma-1)\right]} - \frac{\gamma}{\gamma+1} + \frac{1}{\gamma-1}\ln\left[\frac{(\gamma+1)^2 M^2}{2\left[2\gamma M^2-(\gamma-1)\right]}\right]\right\}^{-1} \tag{63}$$

Lastly, for $P_3 = p_o/p_i$:

$$\left(\frac{d\gamma}{dM}\right)_3 = \frac{4\gamma(\gamma-1)(M^2-1)^2}{M\left[2\gamma M^2-(\gamma-1)\right]\left[(\gamma-1)M^2+2\right]}$$

$$\left\{\frac{\ell n\left[\frac{\left[2\gamma M^2-(\gamma-1)\right]\left[(\gamma-1)M^2+2\right]}{\left[(\gamma+1)M\right]^2}\right]}{(\gamma-1)} - \frac{2(M^2-1)}{(\gamma+1)}\left[\frac{1}{2\gamma M^2-(\gamma-1)} + \frac{\gamma}{(\gamma-1)M^2+2}\right]\right\}^{-1}.$$

The above relations are plotted as functions of M in Fig. IV-14 for γ = 1.4. Similar curves are presented by Barry (Ref. 20) for other measurement parameters.

For the parameters plotted in Fig. IV-14, the Mach number will be computed accurately by assuming γ = 1.4 so long as $\Delta\gamma < .002$ and hence errors of this magnitude may be neglected. The isentropic lines on Fig. IV-13 indicate, moreover, that in a wind tunnel operating at around atmospheric supply conditions, the change in γ through the nozzle will be within this limit. Parameters based on the generation of oblique shock waves by inserting a wedge in the stream will give large errors in Mach number due to γ change at wedge angles near that for shock detachment.

---

(2) Caloric Imperfections

Neglecting deviations from the perfect gas equation and dissociation, the effects of temperature enter into the airflow process through the caloric equation of state which relates the specific heat at constant volume, c_v, and the internal energy, u,

$$c_v = \frac{\partial u}{\partial T}_\rho \tag{65}$$

If the vibrational modes of molecular motion are assumed to be simply harmonic, kinetic theory predicts for the ratio of specific heats (Ref. 8)

$$\gamma = 1 + \frac{\gamma_p - 1}{1 + (\gamma_p - 1)\frac{A^2}{\exp\bar{\theta}}} \tag{66}$$

where

$$A = \bar{\theta}\,\frac{\exp\bar{\theta}}{(\exp\bar{\theta}-1)}$$

$$\bar{\theta} = \frac{\theta}{T}$$

$\gamma_p = \gamma$ for calorically perfect gas and θ is the "characteristic temperature for vibration" from statistical mechanics = 3050°K for air.

The function γ (T) is shown in Fig. IV-13 for various pressures. The one-dimensional flow equations for pressure and Mach number previously given in Table I are then amended according to Refs. 8 and 40 to

$$\frac{p}{p_0} = \left(\frac{\exp \bar{\theta}_0 - 1}{\exp \bar{\theta} - 1}\right)\left(\frac{T}{T_0}\right)^{\frac{\gamma_p}{\gamma_p - 1}} \exp (A - A_0)$$

(isentropic) (67)

and

$$M^2 = \frac{2T_0}{\gamma T}\left[\frac{\gamma_p}{\gamma_p - 1}\left(1 - \frac{T}{T_0}\right) + \bar{\theta}_0\left(\frac{1}{\exp \bar{\theta}_0 - 1} - \frac{1}{\exp \bar{\theta} - 1}\right)\right]$$

(adiabatic) (68)

Some of the consequences of the molecular excitation are shown in Fig. IV-15 for T_0 = 1111°K. The ordinate represents the ratio of the value of the parameter in an imperfect gas flow to the value for constant γ = 1.4 as given in Table I. It has been assumed that θ = 3050°K which is a good approximation for air (Ref. 40). The temperature effect becomes appreciable at fairly low supersonic Mach numbers and is asymptotic beyond approximately a Mach number of 4. At higher stagnation temperatures the asymptotic value is reached at still greater Mach numbers. It is expected that high temperatures will occur only in very high-speed tunnels (i.e. hypersonic) where the figure indicates that the imperfect gas modification is constant. However, the interpretation of accurate measurements will require the inclusion of these effects over the entire Mach number range.

The effect of shocks can be evaluated from

$$M_2^2 = \frac{2T_1}{\gamma_2 T_2}\left[\frac{\gamma_1 M_1^2}{2} + \frac{\gamma_p}{\gamma_p - 1}\left(1 - \frac{T_2}{T_1}\right) + \bar{\theta}_1\left(\frac{1}{\exp \bar{\theta}_1 - 1} - \frac{1}{\exp \bar{\theta}_2 - 1}\right)\right] \tag{69}$$

and

$$\frac{p_1}{p_2} = \frac{1}{2}\left[Q + \sqrt{Q^2 + 4\frac{T_1}{T_2}}\right] \tag{70}$$

$$Q = (1 + \gamma_2 M_2^2) - \frac{T_1}{T_2}(1 + \gamma_1 M_1^2) . \tag{71}$$

The subscripts 1, 2 indicate conditions upstream and downstream of the shock front.

The γ effect is still further complicated for a real gas by the fact that $\gamma = \gamma$ (p,T). The variation of γ with pressure and temperature is given in Ref. 5. Hypersonic tunnels inherently will involve both large temperature and pressure changes. The pressure effect is such as to oppose that for temperature given by Eq. (66) above and decreases with increasing temperature. At 100 atmospheres the value of γ is increased by 0.4 percent at 1250°K and 21 percent at 250°K over the values for 0.01 atmospheres. It is interesting to note that at 40 atmospheres and 500°K, $\gamma \cong 1.40$. Real gas effects should therefore be included when either high temperature or pressure are involved. The time-dependent phenomena of relaxation also is important in measurements directly behind large flow gradients such as shock waves. This question is discussed in the next section.

(3) Effects of Heat-Capacity Lag (Relaxation)

The variation with temperature of the specific heats of air, previously discussed, comes about because the various degrees of freedom of diatomic molecules are not fully excited at all temperatures. At very low temperatures only the translational degrees are active and all diatomic gases behave like a monatomic gas with $\gamma = 1.67$. For the constituents of air, the rotational degrees are the first to become excited with increasing temperature and for the low pressure conditions in most wind tunnel test sections, they may be considered fully excited at temperatures above saturation, so that $\gamma \leq 1.4$.

The decrease of γ to values below 1.4 takes place when the vibrational degrees of freedom begin to be excited and, again for wind tunnel application, this point may be taken as around 350°K to 400°K. It takes a large rise of temperature, up to about 1800°K before the vibrational degrees of freedom are fully excited and γ reaches the value of 1.29. At even higher temperatures ionization and dissociation effects become important accompanied by further decreases in γ, but they will be encountered in shock tubes rather than in wind tunnels.

Now the variation of γ with temperature just described is the one which occurs under equilibrium conditions, in other words, if the temperature changes relatively slowly. Changes in the energy associated with any degree of freedom of the molecule are brought about by collisions with other molecules. In the case of air, it is found that the translational and rotational degrees of freedom adjust very quickly to equilibrium in a process involving one or a few collisions.

The vibrational energy, on the other hand acquires its equilibrium value only after hundreds or thousands of collisions. In a process involving rapid changes of temperature, therefore, that part of the heat capacity of the gas associated with the vibrational degrees of freedom (if the temperatures are such as to excite them at all) will lag behind the equilibrium values. The effects of this heat-capacity lag are also called relaxation effects in the sense that, if a non-equilibrium state is established in the gas, it will subsequently "relax" to equilibrium conditions.

The aerodynamic consequences of heat-capacity lag have been considered by a number of authors, notably by Kantrowitz (Ref. 41) who suggests two ways of evaluating the phenomena. One way is to compute the entropy change associated with the exchange of heat between the vibrational and other degrees of freedom and to use this change in the computation of the end points of a process.

The other way is applicable when the process is very rapid compared with the relaxation time and essentially no internal heat transfer occurs before the final pressure is attained. In this latter case, the gas-dynamic formulas for isentropic flow may be used with a value of γ corresponding to the temperature before the sudden change. The internal heat transfer will have to occur eventually and will still change the entropy but if the boundary conditions are such that the pressure cannot change, this will not matter.

In general, the possibility of heat-capacity lag must be considered whenever the temperatures are such that, under equilibrium conditions, the vibrational degrees of freedom would be appreciably excited. The typical wind tunnel satisfying this condition is the heated hypersonic tunnel. The vibrational heat capacity is excited to equilibrium conditions in the stilling section.

Equilibrium conditions in the test section correspond to zero vibrational energy (unless the wind tunnel is heated far above the temperature required to avoid air condensation). It is possible then, in a short nozzle, that the expansion is not under equilibrium conditions and therefore not isentropic. This phenomenon has been considered by Faro and Hill (Ref. 42). In tunnels of moderate size, the expansion may be considered isentropic and the charts of Ref. 8 for equilibrium flow with variable specific heat, are valid.

Heat-capacity lag is more likely to occur, however, in a recompression process from test section conditions, if stagnation temperature is approached. The case of most interest is the pitot tube. Using the data on relaxation time τ downstream of normal shocks obtained by Blackman (Ref. 43) in the Princeton shock tube, an estimate has been made of the relaxation distance $V\tau$ behind normal shocks for $6 < M < 10$ in wind tunnels heated so that the saturation line is reached in the test section. For a stagnation pressure of 100 atmospheres, the relaxation distance does not vary much with Mach number and is about 15 mm.

For pitot probes at hypersonic speed, the shock detachment distance is about 0.1 diameters so that for probes of the usual size (about 1 mm.) the relaxation distance is two orders of magnitude larger than the length of the compression region from upstream of the shock to the mouth of the probe. The compression through the shock wave itself is known to correspond to a value of $\gamma = 1.4$ under these conditions (see for instance Ref. 44). For small pitot probes, the subsonic compression may also be considered instantaneous relative to the relaxation time. Consequently the compression for free-stream static to pitot pressure is given by Rayleigh's pitot-tube formula with $\gamma = 1.4$.

If the calibration method is based on stilling section stagnation pressure (upstream of the nozzle) and pitot pressure, the error incurred by using tables for $\gamma = 1.4$ = constant depends on the rate of expansion through the nozzle. If equilibrium flow in the nozzle can be assumed, the static pressure in the test section can be obtained by calculations such as those of Ref. 8 for variable γ. If the compression to pitot pressure is assumed to take place with $\gamma = 1.4$, the ratio p_i/p_0 is easily obtained and can be expressed as a multiple of the ratio corresponding to $\gamma = 1.4$ in the expansion as well as re-compression.

The asymptotic value (in the sense of the preceding subsection) of this multiple is shown for low pressure flows in Fig. IV-16 as a function of T_0, together with the Mach numbers M_A at which the asymptotic value is first reached.

(4) Some Numerical Results for Real Dry Air

Some feel for the practical consequences of the fact that air is not a perfect gas may be obtained by considering a few numerical examples. It has been shown that the behavior of air departs most markedly from that of a perfect gas at either high pressures or high temperatures.

Three isentropic expansions have accordingly been calculated, each with a pressure ratio of 400 to 1, as follows:

4 atm. to 0.01 atm. with $T_0 \cong 334°K$

40 atm. to 0.1 atm. with $T_0 \cong 447°K$

40 atm. to 0.1 atm. with $T_0 \cong 1111°K$.

The first expansion is representative of a supersonic wind tunnel where neither high pressures nor high temperatures are involved. Negligible departures from perfect-gas behavior are to be expected and, in fact, it turns out that the difference in the Mach numbers calculated from real air properties and from $\gamma = 1.4$ tables is below the 0.1 percent inaccuracy level set up as a standard in this report.

Tables IV, V, and VI give the results of real air and perfect gas computations. For the calculations based on $\gamma = 1.4$ = constant, the real value of the stagnation sound speed has been used and V and a have been calculated from the tabulated ratios V/a_0 and a/a_0; the dynamic pressure has been calculated from the ratio q/p_0 (which is equivalent to setting $q = 0.7p^0M^2$). This procedure has been followed in all three cases considered.

The second expansion is representative of an unheated (except by the compressors) high pressure supersonic wind tunnel. Blowdown tunnels of this kind represent the most economical way of testing at high Reynolds numbers. In this kind of expansion, the pressure effect on γ predominates and any allowance for the small decrease in γ (due to temperature effect) at the beginning of the expansion would lead to results even further from the truth than those based on $\gamma = 1.4$. Results analogous to those of Table IV are given in Table V. Considerably larger errors could arise with lower values of T_0 and higher values of p_0 (limited perhaps to lower Mach numbers by the onset of air condensation).

The third expansion is representative of a heated hypersonic wind tunnel being operated at the low end of its Mach number range. The caloric imperfections would be expected to dominate the picture here. Therefore, in addition to those for real air and for $\gamma = 1.4$, calculations have been made for a thermally perfect gas with γ a function of temperature but not of pressure. Such calculations have previously been outlined in this section. Results are given in Table VI.

(d) Measurement of Change of Stagnation Pressure Along a Supersonic Nozzle

The expansion of air from a low speed through a supersonic nozzle to the test section is assumed to be an isentropic process in a perfect gas. Water vapor condensation, weak shock waves in the flow, effects of viscosity and thermal conductivity have been introduced as reasons for possible failure of the assumption of an isentropic process; while other indications have been given of the conditions under which the perfect gas relations may not hold. An experimental confirmation has been reported in Ref. 18 of the theoretical prediction that these errors are all of small magnitude in a supersonic wind tunnel at normal supply temperature and pressure.

In this experiment, the Mach number measured locally in the test section of a Mach number 3.5 nozzle by the ratio of pitot pressure to pitot pressure behind an oblique shock (parameter P_{10} of Table II) was compared with a measurement based on the ratio of stagnation pressure upstream of the nozzle to pitot pressure in the test section (P_3). The dewpoint in these tests was about -46°C; there were no weak shock waves visible in the nozzle; the stagnation temperature was 43°C, and the stagnation pressure 2.5 atmospheres. Under these conditions errors due to viscosity and heat conduction, weak shock waves, water condensation, and imperfect gas effects should be negligible.

The ratio of stagnation pressure upstream of the nozzle to stagnation pressure in the test section was found to be .998 ± .003. Although this result is not surprising in view of the discussions, its value lies in its justification of the use of local pitot and upstream stagnation pressure (parameter P_3) as an accurate, and at the same time simple method of calibrating a supersonic wind tunnel at these operating conditions.

(e) Probe Errors

Inserting a probe into the flow will distort the field slightly and hence the Mach number will be altered and the measurement dependent on probe geometry. Besides the alteration in potential flow caused by insertion of a probe, its own boundary layer will displace the flow and produce viscous forces.

The probe reads its prescribed property only in regions of uniform flow. There must be no gradient of pressure or velocity in the vicinity of the probe which must, moreover, be aligned with respect to the velocity vector. Actually these conditions will not be satisfied exactly even in an empty tunnel, and where the flow field about a model is under investigation, they may be grossly violated.

Some estimates of each of these effects on the most important measuring methods will be given in this section.

(1) Boundary Layer Displacement Effects on the Measurement of Surface Pressures

Among the pressure measurements discussed in Section III are measurements of surface pressure on cones, wedges, and so-called "static-pressure" probes. Given the shape of such a probe and assuming potential flow, it is possible to relate the pressure at any point on the surface to the free stream static pressure and Mach number. In practice, however, the measured surface pressures will differ from those calculated by potential theory.

One of the causes of this difference is the displacement effect of the boundary layer. In other words, the experimental pressure distribution corresponds more nearly to that calculated about a body whose surface is displaced outwards everywhere by the boundary layer thickness, with a normal velocity through the new surface equal to the normal velocity at the edge of the boundary layer. For the purposes of this discussion, the difference between the pressures calculated with and without consideration of the boundary layer will be considered an error; an evaluation of its magnitude will be presented in this section.

Although there is a mutual interaction between an outer potential flow and a boundary layer, for most practical purposes, it is sufficient to calculate the boundary layer from the undisturbed potential flow. Instead of considering the edge of the boundary layer and the normal velocity there as the new boundary conditions for the potential flow, the conventional procedure is simply to modify the body by moving its boundary outwards a distance δ^* everywhere.

Here δ^* is the displacement thickness of the boundary layer, defined by

$$\delta^* = \int_0^\infty \left(1 - \frac{\rho u}{\rho_e u_e}\right) dy \tag{72}$$

in two-dimensional flow and

$$\int_{r_0}^{r_0+\delta^*} \frac{r}{r_0}\, dr = \int_{r_0}^{\infty} \left(1 - \frac{\rho u}{\rho_e u_e}\right) \frac{r}{r_0}\, dr \tag{73}$$

in axi-symmetric flow where the surface is approximately aligned with the free stream. The subscript e refers to the condition just outside of the boundary layer; while r is the radial distance from the center of the body of radius r_0. The justification for this procedure is given for subsonic flows by Preston in Ref. 45 and for supersonic flows by Young in Ref. 46.

The methods of calculating the change in the potential flow brought about by a small change in body shape are, of course, quite different in subsonic and supersonic flows. Only the latter will be considered here.

At moderate to high supersonic Mach numbers, the flow along the surface of a body of revolution is very nearly simple wave flow. The widespread use of shock-expansion theory for three-dimensional flows as discussed, for instance, by Eggers et al (Ref. 47) is grounded on this fact. At low supersonic Mach numbers, on the other hand, the rate of change of pressure with the slope of the meridian is much slower than in simple wave flow. The problem of finding $dp/d\theta$ in such flows may be formulated in terms of finding the ratio it bears to $dp/d\theta$ in simple wave flow at the same Mach number.

The crux of the problem is then to find a simple parameter of the flow to which this ratio is uniquely related. It is postulated here that this parameter is the local "two-dimensionality" of the flow in a certain sense. Consider a section of the flow field perpendicular to the axis of symmetry and at a distance x from the body vertex. The region in which the flow changes from free stream conditions to those at the body surface is bounded by the traces of the body and shock surfaces, the two circles shown in the sketch. At high Mach numbers the shock is close to the body, as in (a) of Fig. IV-17, and the body radius is nearly equal to the shock radius. In this sense the flow is "nearly two-dimensional." At low supersonic Mach numbers, the body radius is much as in (b) of Fig. IV-17, and the flow is far from two-dimensional.

It will now be assumed that the ratio of $dp/d\theta$ to its simple-wave value is a unique function of the ratio of the radius of the body to that of the shock circle. Further, since the configurations of interest are quite slender and the deviation from simple-wave flow becomes appreciable only at low supersonic Mach numbers, it will be assumed that the shock surface is not too far from the free stream Mach cone whose apex is at the nose of the body. In other words, it is postulated that, in general,

$$\frac{dp}{d\theta} = \left(\frac{dp}{d\theta}\right)_{\text{simple wave}} F\left(\frac{\sqrt{M_e^2-1}\, r_0}{x}\right). \tag{74}$$

This approximation is used mostly because of its simplicity; its validity has not really been checked but it is probably good enough for the present purpose. It will certainly fail downstream of the point of maximum thickness. Numerical values for $F[(\sqrt{M_e^2-1}\, r_0)/x]$ have been obtained from flight tests on parabolic bodies.

Now the displacement effect of the boundary layer is equivalent to turning the inviscid flow through an angle $d\delta^*/dx$ where x is the coordinate along the surface. The associated pressure change is therefore simply

$$\frac{\Delta p_s}{p_s} = \frac{1}{p}\frac{dp}{d\theta}\frac{d\delta^*}{dx}$$
$$= \frac{\gamma M_e^2}{\sqrt{M_e^2-1}} F\left(\frac{\sqrt{M_e^2-1}\, r_0}{x}\right)\frac{d\delta^*}{dx}. \tag{75}$$

The probe shapes of most interest are the cylinder (with conical or ogival nose) and the cone. If the boundary layer is laminar as it almost always will be, good approximations to $d\delta^*/dx$ for these shapes are

$$\frac{d\delta^*}{dx} = 0.86(1 + 0.277\,M_e^2)\sqrt{\frac{\nu_e}{u_e x}}$$

(cylinder or flat plate) (76)

and

$$\frac{d\delta^*}{dx} = 0.5(1 + 0.277\,M_e^2)\sqrt{\frac{\nu_e}{u_e x}}$$

(cone) (77)

when $\delta^* << r_o$.

These results must be modified when the boundary layer becomes an appreciable fraction of the body radius. Probstein and Elliot (Ref. 48) indicate that the value δ_1 of the definite integral on the right hand side of Eq. (73) is only slightly affected by the transverse curvature of the boundary layer. In other words, Eq. (76) and (77) are valid even for relatively thick boundary layers if $(d\delta_1/dx)$ is substituted on the left hand sides for $(d\delta^*/dx)$.

The true displacement effect is given in terms of δ_1 by

$$\int_{r_o}^{r_o+\delta^*} \frac{r}{r_o}\,dr = \delta_1$$

(78)

which implies

$$\frac{d\delta^*}{dx}\left(1 + \frac{\delta^*}{r_o}\right) = \frac{d\delta_1}{dx}$$

(79)

or

$$\frac{d\delta^*}{dx} = \frac{\dfrac{d\delta_1}{dx}}{\sqrt{1 + \dfrac{2\delta_1}{r_o}}}\,.$$

(80)

In other words, the transverse curvature effectively reduces the slope of the displacement surface of the boundary layer by the factor.

$$\frac{1}{\sqrt{1 + \dfrac{2\delta_1}{r_o}}}$$

where δ_1 is given by the "thin boundary layer" theory

$$\frac{\delta_1}{x} = 1.72(1 + 0.277\,M_e^2)\sqrt{\frac{\nu_e}{u_e x}}$$

(cylinder) (81)

$$\frac{\delta_1}{x} = (1 + 0.277\,M_e^2)\sqrt{\frac{\nu_e}{u_e x}}$$

(cone) (82)

The final results for the fractional error in static pressure may then be written (with $\gamma = 1.4$)

$$\frac{\Delta p^o}{p^o} = \frac{\dfrac{1.2\,M_e^2}{\sqrt{M_e^2-1}}(1 + 0.277\,M_e^2)\sqrt{\dfrac{\nu_e}{u_e x}}}{\sqrt{1 + 3.4(1 + 0.277\,M_e^2)\dfrac{x}{r_o}\sqrt{\dfrac{\nu_e}{u_e x}}}} \times F\left(\frac{\sqrt{M_e^2-1}\;r_o}{x}\right)$$

(cylinder) (83)

$$\frac{\Delta p_c}{p_c} = \frac{0.7 M_e^2(1+0.277 M_e^2)\sqrt{\frac{\nu_e}{u_e x}}}{\sqrt{M_e^2-1}\sqrt{1+2(1+0.277 M_e^2)\frac{x}{r_0}\sqrt{\frac{\nu_e}{u_e x}}}} \times F\left(\frac{\sqrt{M_e^2-1}\, r_0}{x}\right). \quad \text{(cone)} \qquad (84)$$

As a check of this theory, consider the experimental results on cone probes reported by Talbot in Ref. 49. For a 5-degree cone at M = 3.70 a comparison of theoretical and experimental results is shown in Fig. IV-18. The data were taken in a low density wind tunnel, and even at the highest Reynolds number, the boundary layer at the orifice location was quite thick, with $\delta_1/r_0 \sim .5$. The value of F in this case is essentially unity, and the theory is pure simple wave flow.

Extrapolating to the initial slope, the theoretical and experimental results are

$$\frac{\Delta p_c}{p_c} = -\frac{13}{\sqrt{Re_x}} \quad \text{(theory)} \qquad (85)$$

$$\frac{\Delta p_c}{p_c} = \frac{14}{\sqrt{Re_x}} \quad \text{(experiment)} \qquad (86)$$

The validity of the method for order of magnitude estimates of errors in the measurement of cone or static pressure is thus established.

In Fig. IV-19 a chart is presented which allows a rapid estimate of the error likely to be incurred in using probes of typical dimensions in supersonic wind tunnels. Also shown is an indirect experimental check, based on some measurements made at the University of Michigan and reported by Murphy (Ref. 50). Static and pitot pressure were measured in the test section of a supersonic wind tunnel while stagnation pressure was measured in the stilling section. From these pressures, the three possible ratios were computed and from each of these a Mach number was deduced using the appropriate formula of Section II.

Three different Mach numbers were obtained. There are three possible explanations for this result:

(1) Static pressure was measured incorrectly.

(2) Pitot pressure was measured incorrectly.

(3) There was a stagnation pressure loss in the expansion through the nozzle.

All of these possibilities are discussed in the referenced report. The available evidence indicates that the second and, for low dewpoints, third explanations can account only for negligible Mach number errors. The error in static pressure reading required to reconcile the three Mach numbers is shown for three nozzles in Fig. IV-19. These points have been obtained from Murphy's results by converting his apparent stagnation pressure loss to an apparent static pressure rise. Corrections have been applied for the small effects of water vapor condensation (D.P. < -32°C) and for the pressure field of the conical nose of the probe, to which the curve shown for $\ell/d = 12$ is applicable.

(2) Effects of Viscosity on Measurement of Pitot Pressure

At small Reynolds numbers, the decelerating flow immediately upstream of the mouth of a pitot tube is acted on by viscous forces which are not negligible in comparison with the inertia forces. Consequently the measured pressure may differ from the true stagnation pressure. Several investigations of this problem have been published, both experimental and theoretical; the most recent one of which is by Sherman (Ref. 51) who presents subsonic and supersonic results as well as comparisons with representative theories.

The theoretical results are generally of the form

$$C_\mu = \frac{p - p_{correct}}{\frac{1}{2}\rho V^2} = \frac{k}{Re} \tag{87}$$

where k is a constant. In other words

$$C_\mu Re = k \ . \tag{88}$$

Whereas Sherman's results at subsonic speed yield a constant value of $C_\mu Re$ for a fixed probe shape, the supersonic results for some probe shapes do not. The results which do not follow the theoretical trend are now believed to be erroneous. The assumption that all probe shapes should read the same pressure at very large Reynolds numbers is not believed to be justified when the diameter of the orifice becomes an appreciable fraction of the overall diameter of the probe.

The invariance of pitot-pressure reading with respect to bore size is discussed in the following subsection. It has been verified for square-nosed tubes for bore sizes only up to 2/3 of the outside diameter. There are reasons for expecting that it will not hold as the condition of zero wall thickness is approached. Both Sherman and Graves and Quiel (Ref. 52) have tested probes with very thin walls at supersonic speeds. Both sets of data show initially decreasing pitot pressures as the Reynolds number is reduced. These results are believed to be peculiar to large bore tubes. It is recommended that small bore ($\leq 1/3$ O.D.) probes be used, to which the following estimate of the viscous error applies.

The most reliable estimates of the effects of viscosity on pitot pressure readings can probably be based, for a given probe shape, on the results obtained for that shape at subsonic speeds. To apply them at supersonic speeds, one simply assumes that

$$C_\mu Re = k$$

is independent of M if C_μ and Re are based on the flow downstream of a normal shock.

The pitot pressure error estimated in this way for straight cylindrical probes in a wind tunnel is shown for a typical probe size as a function of Mach number in Fig. IV-20.

(3) Effects of Orifice Size on the Reading of Pitot Tubes

Strictly speaking, to measure the true stagnation pressure in a flow, only a probe with an infinitesimal orifice at the forward stagnation point is suitable. Long experience at subsonic speeds has shown that the pressure measured with a straight pitot tube remains constant as the inside diameter is increased to as much as half the outside diameter.

Similar conclusions have been reached at supersonic speeds by Holder and North (Ref. 53) and by Hill (Ref. 18) who found that the measured pressure was constant (to ± 0.05 percent) for bore sizes up to 2/3 the outside diameter at M = 3.5. The tube size and test conditions were such that the estimated error due to viscous effects was of the order of 0.02 percent.

The tests just referred to were run with straight cylindrical tubes cut off square. It is believed that with round-nosed tubes, the effect of bore size would be much greater at supersonic speeds. If the Mach number distribution over a hemisphere (approximately invariant above M = 2.5) is assumed to exist on the probe, it is possible to estimate the dropoff in surface pressure at the rim of an orifice relative to the stagnation point. If the bore size is one fifth the outside diameter, for instance, the pressure at the rim is about 3 percent lower than the pressure at the center of the bore.

(4) Effects of the Nose and Supporting Strut Pressure Fields on Static Probe Measurements

A static pressure probe generally consists of a nose section followed by a cylindrical section which in turn is terminated at its downstream end by some sort of support. The pressure is measured at some orifices or a slot located on the cylindrical section When such a probe is placed in a uniform stream, the measured pressure will differ from the static pressure of the airstream even if the effects of viscosity can be reduced to zero.

This difference represents, of course, the perturbation of the flow by the nose section and (especially in subsonic flow) by the support. The pressure at the orifices only approaches the static pressure as the cylindrical portion is made very long and the sources of the flow perturbations are moved far away.

A quantitative discussion of these effects in subsonic flow is given, for instance, by Kettle (Ref. 54). The influence of the nose is to lower the measured pressure below static and that of the support is to raise it. In principle, it should be possible to design a probe such that the two effects balance each other and a true measurement would be obtained. The usefulness of such a design would be lost, however, if the nose and support effects varied with airspeed.

At subcritical speeds (flow subsonic everywhere) such variations occur primarily because of change in boundary layer characteristics with Reynolds number. At supercritical airspeed (local supersonic regions in the flow) the nose effect varies rapidly with Mach number and the support effect is drastically modified.

To minimize the effects on the probe boundary layer of changes in Reynolds number and stream turbulence, Kettle suggests designing a nose with a low suction peak. It is impossible to avoid completely the region of adverse pressure gradient, in which the boundary layer stability is low, but the magnitude of the gradient can be held low by careful design.

At high subsonic speeds, as the Mach number increases above the lower critical value, the static pressure reading generally begins to increase above the true value. At this point the shock wave terminating the supersonic region of the flow is upstream of the orifices and the pressure rise across it affects the probe reading. The maximum value of this error is of the order of 5 percent for typical probes. It may occur either below or above the sonic speed.

At low supersonic speeds the support effects are very important. The detached bow wave associated with the flow about the support may be located ahead of the orifices on the probe, in which case they will read a pressure which again is too high. All the errors in the transonic range of airspeeds are troublesome because they cannot be estimated quantitatively. For reliable measurements of static pressure at transonic speeds a probe calibration is necessary.

At sufficiently high supersonic speeds, the support interference disappears at least for inviscid flows. Relatively simple theories are available for calculating the nose effect, which, as in incompressible flow, is such as to give a static pressure reading below the true value. Generally it has been considered (see, for instance Ref. 55) that the error is negligible if the orifices are at least 10 diameters downstream of the shoulder of the nose.

A more precise estimate of the error, and of its dependence on probe geometry and Mach number, may conveniently be obtained from slender-body theory. The pressure coefficient on the cylindrical portion of the probe is the so-called "interference pressure coefficient" of the forebody as discussed by Fraenkel (Ref. 56) and formulas for calculating it are given in his report.

For downstream ($\ell/D > 10$) the results may be expressed quite simply and turn out to be almost identical for conical and tangent-ogival noses. In terms of pressure coefficient the result is independent of M, so that the fractional error in static pressure increases like M^2 with increasing Mach number.

The result is, approximately

$$\frac{\Delta p}{p^0} = \frac{\gamma}{8}\left(\frac{MD}{\ell}\right)^2\left(1 - 0.7\,\frac{\ell_f}{\ell}\right) \tag{89}$$

for $\ell/D > 10$ where

D = the probe diameter

ℓ = the length of the cylindrical portion, up to the orifices

ℓ_f = the forebody length.

This equation has been plotted in Fig. IV-21 for $\ell_f = 5D$, together with indications of the accuracy required in p^0 to obtain M to 0.1 percent by the two common methods. It will be noticed that the 10 diameter criterion is inadequate above M = 1.5.

To return to the question of support interference in supersonic flow, obviously the pressure field of the support cannot propagate upstream against a supersonic flow. On the other hand it is well known that such an upstream propagation is possible in the boundary layer even when the main stream is supersonic. A general discussion of shock-wave boundary interaction is of course beyond the scope of this report. For the present purpose it is appropriate to restrict the problem to (1) boundary layers initially laminar, and (2) configurations similar to that of Fig. III-2 b with rather small (< 10 degrees) nose angles.

The two-dimensional analog to this configuration is a wedge located on a flat plate or a deflected control surface on a flat wing. A recent experimental study at the Naval Supersonic Laboratory of the two-dimensional case by Sweeney (Ref. 57) shows that (1) any surface deflection greater than about 2 degrees will cause a laminar boundary layer to separate, and (2) the upstream extent (from the corner) of the pressure disturbance is approximately equal to 550 θ where θ is the momentum thickness of the boundary layer just before the pressure begins to rise.

Within the accuracy of the experiment, the distance $550\,\theta$ was found to be independent of M, Re, and pressure rise over the range of these variables covered. The same order of upstream influence was found by Lee at the University of Toronto (Ref. 58) on an axi-symmetric configuration. Lee also found a dependence on pressure rise, but this was for nose angles greater than 10 degrees.

It will be assumed that, for the cases likely to arise in supersonic wind tunnel practice, the extent of upstream influence found by Sweeney is of the right order of magnitude. The influence of transverse curvature will be neglected and a factor of safety of 1.2 will be applied.

In terms of diameters, then, zero support interference will be obtained if the static probe diameter begins to increase at a distance downstream of the pressure orifices given by

$$\frac{\ell_s}{D} = \frac{450}{\sqrt{Re_D}} \sqrt{\frac{\ell}{D} + \frac{5}{3}}$$

for a typical configuration with a nose fineness ratio of 5.

The required probe length is shown for two typical probe sizes in Fig. IV-22 as a function of Mach number.

(5) The Yaw Sensitivity of Pitot Tubes

The yaw sensitivity of conventional pitot tubes has been the subject of a number of investigations in subsonic flow. Some results for probes with hemispherical heads and various ratios of bore to outside diameter are given by Pankhurst and Holder in Ref. 15, for instance. In supersonic flow, very few detailed results have been published. Largely devoted to unconventional designs, Refs. 59 and 60 by Gracey, et al, give a comparison of supersonic and subsonic results.

For low angles of yaw (< 15 degrees) the few comparisons available suggest that the Mach number dependence is eliminated if the results are given in the form of

$$\frac{\Delta p_i}{q} \text{ vs. } \alpha$$

for subsonic flow, and

$$\frac{\Delta p_i}{q'} \text{ vs. } \alpha$$

for supersonic flow, where

$$q' = p_i(\text{pitot}) - p^\circ \text{ (static in free stream)}.$$

As $M \rightarrow \infty$, $q' \rightarrow p_i$ and, according to this hypothesis, the $\Delta p_i/p_i$ curve for hypersonic flow should be identical with the $\Delta p_i/q$ curve for incompressible flow. For hemispherical heads, the Mach number distribution in hypersonic flow has been given (theoretically and experimentally) in Ref. 61. For a pitot tube with a very small bore size, the effect of yaw would be represented by this pressure distribution.

It turns out that this hypersonic result, in terms of $\Delta p_i/p_i$, does indeed check closely the incompressible result in terms of $\Delta p_i/q$ given by Pankhurst and Holder. The method of extrapolating subsonic results to supersonic speeds discussed above is thus good enough for order of magnitude estimates.

Now the effect of yaw on pitot tube readings depends strongly on the nose shape and on the ratio of the ratio of bore to outside diameter. As this ratio increases, the yaw sensitivity decreases. From the experimental data available an estimate of the yaw effects has been made for square-ended cylindrical tubes with relatively small (~ 1/3 O.D.) bore sizes. This estimate is presented in Fig. IV-23 together with the experimental result for a hemispherical head with a very small bore size in hypersonic flow ($M > 2.5$). Approximate criteria for supersonic flow are: (1) for < 1 percent error, yaw < 10 degrees; (2) for < 0.1 percent error, yaw < 3 degrees.

(6) The Yaw Sensitivity of Cones and Static Pressure Probes

In subsonic flows at least, it is well known that static pressure probes are much more sensitive to yaw than pitot tubes. When an accurate value of the static pressure is desired, the importance of a good alignment of the probe with the flow is well appreciated. The exact variation of static pressure with yaw angle varies from probe to probe, but qualitatively the effect of yaw is always to lower the measured pressure when averaged around the circumference.

To align the probe with the stream and to get a true reading, it is only necessary to adjust its orientation until the maximum reading is found. Both qualitatively and quantitatively the effects at supersonic speed are similar to those at low speeds.

According to linearized theory for all speeds, the average pressure coefficient around a body of revolution at any axial station is

$$c_p = -\alpha^2 . \tag{90}$$

The fractional error in surface pressure is then

$$\frac{\Delta p_s}{p_s} = -\frac{q}{p_s}\alpha^2 \tag{91}$$

where p_s is the surface pressure. On the right hand side of this equation for making order of magnitude estimates, p_s may be replaced by the stream static pressure both for static pressure probes and for cones in supersonic flow.

Several experimental investigations have confirmed that Eq. (91) correctly represents the order of magnitude of the yaw effect on cones and static probes, at least up to $\alpha = 15$. The results quoted by Goldstein (Ref. 62) for the NPL standard tube are in agreement with the theory. So are the results for a 7.5 degree cone at $M = 1.60$ given by Cooper and Webster (Ref. 17) and those for a number of static probe designs at the same Mach number given by Holder, North, and Chinneck (Ref. 55).

The variation of the error in static pressure or cone pressure with yaw angle is shown (approximately) in Fig. IV-24 for various Mach numbers.

If the plane of misalignment of the probe to the stream can be predicted it is possible to locate the orifices of a static probe so that the effect of yaw is minimized. Linear theory predicts zero c_p due to yaw of locations ± 30 degrees from the stagnation points. One would expect experimental results to follow this prediction more closely on the windward side than on the lee side.

In Ref. 63, Walter and Redman report the results of some development tests on static probes designed to be insensitive to yaw in one plane. As expected, these probes work better for positive angles than negative angles of yaw. Favorable orifice locations were found to be $\theta = \pm 33$ degrees from the windward stagnation point for moderate Mach numbers up to $M = 2.5$ and $\theta = \pm 52$ degrees for higher Mach numbers. The yaw angle ranges for errors < 2% of static pressure were found to be -8 degrees < α < 16 degrees at $M = 1.5$ ($\theta = \pm 33$ degrees) and -4 degrees < α < 11 degrees at $M = 2.9$ ($\theta = \pm 52$ degrees).

(7) Effects of Velocity Gradients on Probe Measurements

Mach number measurements in boundary layers and wakes are typical examples of the use of pitot tubes in flows with large velocity gradients. A well-known source of error in such measurement in low-speed flows is the displacement in the plane of the gradient of the apparent location of a pitot tube. In other words the pitot tube measures the total pressure not on a streamline, aligned with its axis, but on one displaced towards the region of higher velocities.

The standard quantitative result for this problem is that of Young and Mass (Ref. 64) who found that for conventional square-tipped cylinders the displacement was of the order of 0.2 times the tube O.D., more or less independent of the magnitude of the gradient. Their investigation was carried out in the wake of an airfoil in essentially incompressible flow. A similar investigation in supersonic flow has been reported by Johanneson and Mair (Ref. 65).

Davies has studied a similar effect in supersonic laminar boundary layers (Ref. 66) at M = 2.5. He found a displacement which varied across the boundary layer and was of the same order as that observed by Young and Maas, but of the opposite sign. According to Monaghan (Ref. 67) this result is neither confirmed nor denied by other investigations of probe errors in supersonic boundary layers.

Another kind of test in which gradient effects are important is in the calibration of a pitot static tube, for instance for flight application. Here an error arises if there are velocity gradients in the wind tunnel. The Mach number at the nose of the probe may be different from the Mach number at the static orifice locations. To get the uniform stream calibration of the static reading, the latter should be compared with the static pressure corresponding to the measured Mach number at the static orifice station rather than at the nose of the probe.

Similar difficulties occur when it is desired to obtain a precise cone calibration in a wind tunnel. A first order allowance for the effects of nonuniform flow may be made by using the empty tunnel Mach number at the orifice station as the reference Mach number.

(8) Effects of Stream Turbulence

The effects of stream turbulence on the readings of pitot static tubes have been analyzed for incompressible flows by Goldstein (Ref. 68). The effect of turbulence is to increase the pitot pressure reading. The amount of this increase is equal to the dynamic pressure multiplied by the square of the turbulence intensity $(V'/V)^2$

$$(p_i)_{\text{measured}} = p_i + \frac{1}{2}\rho (V')^2 \tag{92}$$

Under most circumstances this correction is negligible outside turbulent boundary layers and wakes. The difficulty in applying it is obvious, since the turbulence level is not known without a separate measurement. When both pitot tube and hot-wire measurement have been made in turbulent flow, the theoretical prediction of the pitot tube reading has been confirmed.

No specific theoretical or experimental information is available on the performance of pitot tubes in turbulent supersonic flows. Almost certainly the reading will be too high, as in subsonic flow, but the magnitude of the effect may be quite different. Ribner (Ref. 69) has presented a theory for the interaction of turbulence with a normal shock; it is valid only when the eddy size is small compared with the frontal area of the shock.

If the assumption is made that the order of magnitude predicted for the downstream turbulence is correct even for the shock size associated with a pitot tube, then the effect of the shock is to increase the turbulence level by the speed ratio across the shock. For moderate Mach numbers this speed ratio is of the order of the upstream Mach number. Because the downstream dynamic pressure is a small fraction of the total pressure, the effect is still small.

Approximately, the fractional error in pitot pressure would be

$$\frac{\Delta p_i}{p_i} = \frac{1}{2} M \left(\frac{V'}{V}\right)^2 \tag{93}$$

for moderate M < 6.

The effect of turbulence on the reading of a static probe was also investigated by Goldstein (Ref. 68). The transverse components of fluctuating velocity give rise to an "impact" pressure on the sides of the tube and on the static orifices.

Goldstein's equation is

$$p^{\circ}\,\text{measured} = p^{\circ} + k_s \rho (v'^2 + w'^2) \tag{94}$$

where k_s is a numerical factor depending on the arrangement of the pressure orifices and the kind of turbulence (degree of anisotropy).

Fage (Ref. 70), from experiments in pipe and channel flow, deduced that the constant is about 1/4 for isotropic turbulence. The pressure rise is then one-third the dynamic pressure multiplied by the square of the turbulence intensity; it is negligible except possibly in turbulent boundary layers and wakes.

In supersonic flow the dynamic pressure may be an order of magnitude larger than the static pressure, and the fractional error in the latter quantity might become measurable, particularly where, as in wind tunnels, the lateral fluctuations are larger than the longitudinal.

(f) Influence of the Boundaries and Model on Mach Number in Subsonic Wind Tunnels

(1) Tunnel Speed

When actually testing a model in a wind tunnel (as distinct from calibration) the problem of Mach number determination comes up in one of two ways. Either one wants to test at a given Mach number and requires a procedure to set the tunnel accordingly or one is running the tunnel at some known pressure level and power setting and would like to compute the Mach number of the test.

In either case it is necessary to define the concept of tunnel Mach number. If the intake (or stilling section) conditions and the mass flow through the tunnel could be kept constant while the model was removed, the tunnel Mach number could be defined as the (mean) Mach number in the empty tunnel at the location previously occupied by the model. In the absence of measuring inaccuracies, this is the Mach number obtained during calibration for the same intake conditions and the same mass flow. The crux of the problem is then duplication, while running with a model, of the mass flows run during calibration.

One device which immediately fixes the mass flow for given intake conditions is a sonic throat. Choked flow either upstream or downstream of the test section ensures that the mass flow is fixed by the intake conditions with or without the model. The sonic throat does even more than this, of course. In a supersonic tunnel, the entire Mach number distribution is fixed downstream of the throat. In a transonic tunnel, with the throat downstream of the test section, the mean Mach number at any station is fixed by the cross-sectional area. The only way in which the intake conditions can affect these Mach numbers in either case is through the effective change in tunnel geometry as the boundary layer thickness changes, or, when the throat is downstream, through the changes in effective throat area caused by the passage of the model wake.

The minor boundary layer effects in supersonic tunnels can be taken care of by calibrating over the operating range of stagnation pressure and temperature, or as a function of Reynolds number/cm in the test section. The wake effect in the subsonic tunnel cannot be taken care of as easily and reliable values of tunnel Mach number probably cannot be obtained by relying on a downstream choke. Such a choke will always be useful as a flow stabilizing device but the Mach number should be obtained by the procedure applicable to unchoked tunnels.

Common practice in low-speed wind tunnels is to determine the speed from simultaneous measurements of total head in the intake and static pressure on the wall of the test section, well upstream of the model location. In compressible flow this method is still applicable, for the ratio of these two pressures is a direct function of the mean Mach number at the measuring station. This in turn is related to the mean Mach number at the model station by the ratio of the cross-sectional areas.

Calibration conditions in the empty tunnel can therefore be duplicated by setting the same values of total head and wall static pressure at the so-called "tunnel speed hole." The ratio of these two pressures determines the empty tunnel Mach number uniquely except for the changes in boundary-layer thickness with Reynolds number, which can be accounted for by calibration as stated above.

In the intake or stilling section, where the total head is to be measured, the velocity is usually sufficiently low so that static pressure is a good approximation to stagnation pressure. The error here is less than 0.1 percent if the cross-sectional area is more than 16 times the area for sonic flow.

The "tunnel speed hole" must be located sufficiently far upstream of the model station so that the pressure there is not influenced by the model. In a closed tunnel, it is fortunate that the constriction effect of the walls partly cancels the upstream propagation of the pressure disturbances caused by the model (see Thom, Ref. 71). Both his calculations and some unpublished work at MIT indicate that about 1.5 tunnel heights or diameters ahead of the model station will be sufficient in the cases most likely to be encountered.

While the flow perturbation at the "tunnel speed hole" due to the model can in this way be made negligible, that at the model due to its support system generally cannot. In most high-speed tests the models are held from the rear by a sting which in turn is supported by some kind of strut. The flow perturbations associated with this kind of a support system will extend upstream into the region occupied by the model.

Reasonably accurate settings of tunnel speed can only be made if the calibration is done with the support system in the tunnel. The so-called empty tunnel in the preceding discussion should therefore be empty only in the sense that the model is absent. This is important not only for tunnel speed setting but also for applying blockage corrections on the basis of wall pressure measurements, as discussed later.

(2) General Consideration of Wall Interference

Even when the tunnel speed is set correctly, there is no assurance that the flow about the model is similar to that in flight at the same speed. A solid tunnel wall will, in fact, restrict the expansion of the streamlines about the model while the equilibrium conditions at an open jet boundary will require them to expand further than in free flight. Strictly speaking, the flow pattern in the wind tunnel is not duplicated in flight at any speed. If the model is small compared with the tunnel dimensions, however, the flow in the tunnel does very nearly correspond to flight at some speed. Intuitively it seems that this flight speed will be higher than the tunnel speed in a closed wind tunnel and lower in an open tunnel.

This reasoning is confirmed by mathematical calculations of the influence of the airstream boundaries. Such calculations are practical only for flows governed by linear equations, so that super position of solutions is possible. If the velocity potential of the free airflow about the model is ϕ_0, it is necessary to find the interference potential ϕ_1 such that the sum $\phi_0 + \phi_1$ satisfies the conditions on the airstream boundaries. Insofar as the effect of the walls can be represented by a simple change in speed, this latter is given by $\partial \phi_1 / \partial x$ at the centroid of the model, where x is the coordinate along the tunnel axis. The velocity along the wall is of course $\partial (\phi_0 + \phi_1)/\partial x$.

For convenience in the calculation of ϕ_0 the model is usually represented by a system of sources and sinks or, if it is very small compared with the size of the test section, by an equivalent doublet. The fact that the wake of the model is confined in an airstream of finite size also alters the effective speed of the test and, following a suggestion by Prandtl, the wake flow is replaced by a source flow for calculation purposes. The representation of lifting models requires, in addition, a system of vortex lines. While the interference potential associated with lift affects the flow angle at the model, it does not influence the speed and will therefore not be considered here.

Some of the interference potentials imply the existence of not only an interference velocity at the model, but also of a spurious velocity gradient. The latter plays no part in the correction of the test speed but must be taken into account in order to correct the drag and pitching moment.

Calculations of wind tunnel interference are generally performed for incompressible flow and extended to high subsonic flow by the Prandtl-Glauert-Göthert rule (Ref. 72). They are obtained in the first place in the form of velocity perturbations $\Delta V/V$, from which the corrections to Mach number and dynamic pressure follow

$$\frac{\Delta M}{M} = \left(1 + \frac{\gamma - 1}{2} M^2\right) \frac{\Delta V}{V} \tag{95}$$

$$\frac{\Delta q}{q} = \left(2 - M^2\right) \frac{\Delta V}{V} \tag{96}$$

where the reference quantities are the uncorrected values.

In the rest of this section the available methods for obtaining $\Delta V/V$ in closed wind tunnels will be discussed briefly.

(3) Theoretical Estimates of Solid Blockage

The speed correction corresponding to the flow about the model in the absence of any wake is called the solid blockage. If its magnitude is referred to the volume of the model, the influence of the wing and body profile shapes is very small, at least for the thin sections used in high-speed flight.

The formulas are generally given in the form

$$\left(\frac{\Delta V}{V}\right)_B = \frac{1}{(1-M^2)^{3/2}} \frac{(Vol)_B}{A^{3/2}} \lambda_B \tau_B \tag{97}$$

for bodies and

$$\left(\frac{\Delta V}{V}\right)_W = \frac{1}{(1-M^2)^{3/2}} \frac{(Vol)_W}{A^{3/2}} \lambda_W \tau_W \tag{98}$$

for wings, where Vol is the model volume and A is the test section area.

The factors λ_B and λ_W depend only on model shape for slender bodies

$$\lambda_B \cong 0.90 \tag{99}$$

and for thin wings

$$\lambda_W \cong 0.95\,. \tag{100}$$

The factor τ_B depends only on the shape of the tunnel cross-section; τ_W depends, in addition, on the ratio of wing span to tunnel width and on the reduced sweep angle

$$\Lambda_0 = \tan^{-1}\left(\frac{\tan \Lambda}{\sqrt{1-M^2}}\right) \tag{101}$$

where Λ is the midchord sweep angle. For wings of very small span, $\tau_W = \tau_B$. Values of τ_B and of τ_W for straight untapered wings are given by Herriot (Ref. 73) for a circular tunnel and a number of rectangular shapes.

The effect of sweep, which is to reduce the interference velocity, is given by Hensel (Ref. 74) for a 1 x $\sqrt{2}$ rectangular tunnel. In general, the values of τ are of the order of unity. Evans (Ref. 75) has developed an approximate representation for tapered wings of arbitrary sweep.

The experimental results available suggest that the corrected Mach number should be used in the compressibility term, $(1 - M^2)^{3/2}$.

(4) Theoretical Estimates of Wake Blockage

In a closed wind tunnel the equation of continuity implies that the reduced stream density ρV in the wake, relative to the undisturbed stream, must be accompanied by an increase in stream density in the main flow. The speed of the airstream must increase as it flows past the model. For one thing, this increase imposes a pressure gradient on the model whose effect must be removed from the drag measurements. For another, it requires a correction to the test speed which will now be considered and which is called wake blockage.

The basis of all calculations of wake blockage is the representation of the wake flow by a source flow, as suggested by Prandtl (see Ref. 76). The strength of the source is made proportional to the dissipative drag (i.e. excluding induced drag) of the model. In high-speed flow the required source strength is also a function of Mach number.

While slightly different Mach number effects are obtained by various authors, an adequate representation of all their results may be expressed as

$$Q = \frac{D}{V}\left[1 + (\gamma - 1) M^2\right] \tag{102}$$

where Q is the mass flow of the source, and D is the drag force (excluding induced drag).

The location of the source is generally taken to be at the centroid of the model volume. At great distances this representation of the flow field is adequate; in the vicinity of the model it has been shown that additional sources and sinks are needed to represent the initial portion of the wake. Their inclusion in the theoretical calculations would be very difficult; it is worth noting that the "velocity ratio" method of applying blockage corrections (discussed below) takes them into account approximately.

Given the simple source representation of the wake, the blockage can be calculated by the superposition of velocity potentials as already outlined. It can also be obtained directly from mass flow considerations.

The velocity perturbations obtained for a single source confined in a long duct of area A are:

a. Zero interference at the model

b. $$\frac{\Delta V}{V} = \pm \frac{1}{2}\left(\frac{1}{1 - M^2}\right)\left(\frac{Q}{\rho V A}\right) \tag{103}$$

for downstream (+) and upstream (-).

That a correction must be applied even though the interference velocity at the model is zero is at first sight surprising. Actually, the basis of the correction is that the tunnel speed is measured essentially "far upstream" where the interference velocity is not zero.

The reading is too low by just the amount given in Eq. (103), so that a positive correction is required amounting to

$$\left(\frac{\Delta V}{V}\right)_{\text{Wake}} = \left(\frac{1 + (\gamma - 1)M^2}{2(1 - M^2)}\right)\frac{D}{\rho V^2 A} \tag{104}$$

where again it should be noted that only the dissipative drag is associated with the formation of a wake, so that the value used for D must exclude induced and tunnel buoyancy drags.

Again it seems that the corrected Mach number is the best value to use in the compressibility terms.

(5) "Velocity-Ratio" Method for Solid and Wake Blockage

From the free-air and interference potentials it is just as easy to calculate the velocity perturbations at the wall as at the model. The perturbations at the wall can be deduced from measurements of wall pressures, with and without the model. To obtain only the effect of the model it is of course necessary to measure the reference pressures with the model support system installed. A comparison of such measurements with theory provides an indirect check of the blockage corrections, since they are obtained from the same solution for the velocity potential.

Among others Evans (Ref. 75) and Göthert (Ref. 77) have obtained good verification of the theory in this way. Göthert has suggested that the wall pressures be used to determine the blockage corrections empirically in routine tests. The wall perturbations depend of course on the same quantities as the blockage corrections.

Dividing one by the other most of these quantities are canceled and the result may be written

$$\left(\frac{\Delta V}{V}\right)_{B,\,model} = m_B \left(\frac{\Delta V}{V}\right)_{B,\,wall} \tag{105}$$

for bodies, and

$$\left(\frac{\Delta V}{V}\right)_{W,\,model} = m_W \left(\frac{\Delta V}{V}\right)_{W,\,wall} . \tag{106}$$

If the models are small enough (relative to the test section size) to be represented by equivalent doublets the "velocity ratios" m are rather like the factors τ introduced earlier in that m_B depends only on the shape of the tunnel cross section while m_W, in addition, depends on the wing-span to tunnel-width ratio and on the reduced sweep angle. Values of m_B and m_W are given for a circular tunnel by Göthert (Ref. 77) (straight wings only) and for a rectangular $1 \times \sqrt{2}$ tunnel by both Hensel (Ref. 74) and Evans (Ref. 75).

The doublet representation becomes inadequate at large values of the reduced chord/tunnel height ratio,

$$\frac{c}{\sqrt{1-M^2}\,H} \tag{107}$$

where c is the chord and H is the tunnel height (or diameter). Both Göthert and Evans have calculated the effect of increasing wing chord (or body length). They find that m increases as the ratio (107) increases, and roughly by as much as 30 percent when this ratio becomes unity.

The wake perturbation, being figured far upstream and downstream, is uniform across the tunnel, so that $m_{wake} = 1$. With swept wings this is not quite true because the sources, being distributed over a range of streamwise stations, do not give zero perturbation velocities at the model. For the small spans likely to be used in high-speed tests $m_{wake} = 1$ is very good approximation, however, at least for unstalled flows, for which the wake blockage is not too large a fraction of the whole.

The method of obtaining the total blockage from the measured wall perturbations may be illustrated by referring to the sketch of the variation of perturbation velocity along the test section wall (Fig. IV-25). For lifting models it is assumed that the pressures on the top and bottom walls have been averaged. Far downstream, the velocity perturbation reaches an asymptotic value B.

This is also the value on the centerline and, as shown in the section on wake blockage, represents twice the correction required

$$\left(\frac{\Delta V}{V}\right)_{Wake,\,model} = \frac{1}{2}\,B \, . \tag{108}$$

The solid blockage at the wall may then be obtained by subtracting B/2 from the total wall perturbation at the model station. For the test of a body alone or wing alone, the solid blockage at the model is then obtained directly from the appropriate velocity ratio

$$\left(\frac{\Delta V}{V}\right)_{B,\ model} = m_B C \tag{109}$$

or

$$\left(\frac{\Delta V}{V}\right)_{W,\ model} = m_W C \tag{110}$$

when $m_B \neq m_W$ unless the wing has a very small span.

For a wing-body combination with an appreciable span, a weighted mean value of m must be used. The weighting factors must be obtained from theoretical estimates of the relative contributions of the wing and body to the solid blockage, by the methods already given.

The velocity-ratio method of applying blockage corrections is considered more accurate than a purely theoretical estimate. It is generally assumed that the ratio of the perturbation at the wall and model is predicted more accurately than the absolute value of either. Furthermore, the velocity ratios are less than unity, so that the measured perturbations are larger than the blockage corrections.

Near sonic speed it is more desirable to correct down from a high observed Mach number than to correct upwards towards Mach 1 from the tunnel speed. Furthermore, as Göthert (Ref. 77) has pointed out, this method of correction is valid even when the flow over the model is supercritical and the Prandtl-Glauert-Göthert rule no longer holds there. At such speeds the rule may still be valid at the walls and the velocity-ratio method will then be correct.

Various investigators, for instance Maeder (Ref. 78), have obtained results which show (for instance by testing similar wings of three different sizes) that the blockage corrections are predicted correctly even when the region of supersonic flow about a model reaches halfway out to the tunnel walls. Under such conditions the purely theoretical methods will certainly fail.

(g) Some Aspects of Mach Number Measurements in "Ventilated" Transonic Wind Tunnels

In recent years transonic wind tunnels have been developed in many countries with slotted, porous, or perforated walls which, besides allowing tests to be run through sonic speed without choking the tunnel, may be designed to have zero blockage at subsonic speeds. In the United States the most common wall configurations are either perforated or have longitudinal slots.

For a given slot configuration or wall porosity, the solid and wake blockage corrections can be calculated by methods similar to those used for closed tunnels. The boundary conditions at the walls, which the sum of the free air and interference potentials must satisfy, are really inhomogeneous (particularly for slots) but for some applications, such as those considered by Baldwin, et al, (Ref. 79) and by Maeder (Ref. 80), may be replaced by equivalent homogeneous conditions.

The solid blockage is given by formulas similar to (97) and (98) with the factors τ_B and τ_W depending, in addition, on the fractional open area of the walls. For any wing-span to tunnel-width ratio and wing sweep, there are wall configurations which make $\tau_W = 0$. However, a wall designed to have zero blockage for bodies and small span wings will require a blockage correction if large span wings are tested and vice versa.

? This [illegible] the analysis based on [illegible]

In the case of walls with longitudinal slots, as long as there is any open area at all, the wake blockage is zero as for an open jet. With perforated walls the wake blockage cannot be eliminated.

In principle, the speed setting with a transonic throat could be accomplished in the same way as for a closed tunnel, with a "tunnel speed hole" at the upstream end of the test section. In the absence of wall interference, however, the upstream influence of the model in subsonic flow extends much further than the 1.5 tunnel diameters found for closed tunnels.

At low supersonic Mach numbers the upstream limit of model influence on the flow is of course the bow shock. In practice, the static pressure in the plenum chamber surrounding the ventilated test section is usually used to set tunnel speed. This pressure is close to free stream static in the test section; the Mach number computed on the basis of an isentropic expansion from stilling section to plenum pressure is very nearly the test section Mach number. More accurate results may be obtained by calibration; as in closed tunnels this should preferably be done with the model support system installed.

In a tunnel designed for zero blockage, the interference velocity at the model is theoretically zero at least up to the critical Mach number of the model. Comparisons with tests in flight or in very large wind tunnels indicate that the interference at the model is very low throughout the transonic speed range (except for the perturbations associated with shocks reflected from the walls).

It may be assumed that the interference velocities are low throughout the test section. This means that the flow velocity at any point on the tunnel walls is essentially the sum of the tunnel speed and the perturbation velocity in free flight at the same location relative to the model. At points where the streamline curvature in the unbounded flow is concave towards the model, and this condition extends all the way out along an equipotential line to the region of essentially unperturbed flow, the pressure is lower than free stream static and the velocity higher than that of the main stream.

Over most of the streamwise extent of a typical transonic test section, with a small-span model installed, these conditions are satisfied at points in the flow corresponding to the wall locations. With a model in the tunnel the plenum pressure will be in rough equilibrium, not with free stream static pressure, but with a pressure which is on the average somewhat lower.

In other words there is a model influence on the measurement of tunnel speed when it is measured by the plenum pressure just as there is when it is measured by an upstream wall orifice. The two effects are, however, in opposite directions; whereas the presence of a model tends to make the pressure at the "tunnel speed hole" read too high, it tends to make the plenum pressure read too low.

The magnitude of the model influence on plenum pressure would be very difficult to calculate in transonic flow. At speeds low enough for the Prandtl-Glauert-Göthert rule to be valid, one might expect a relation of the form obtained from conventional wall-interference theory,

$$\frac{\Delta M}{M} = \frac{1+\frac{\gamma-1}{2}M^2}{(1-M^2)^{3/2}} \; \frac{(\mathrm{Vol})}{A^{3/2}} \; K_T \, . \tag{111}$$

Covert (Ref. 81) has investigated this effect to some extent in the transonic test section at the MIT Naval Supersonic Laboratory. He measured wall pressures from which the true test section Mach numbers could be obtained far upstream. The difference between the empty tunnel calibration and that obtained with a 5 cm sphere in a 45 cm x 45 cm tunnel (solid side walls, longitudinal slots top and bottom) was found to decrease with increasing Mach number from $\Delta M \sim .015$ around $M = 0.7$ to $\Delta M \sim .005$ at $M = 1.1$ and above.

V. RECOMMENDED PROCEDURE FOR MEASURING MACH NUMBER

Specific techniques will be suggested here for Mach number calibration of an empty wind tunnel within the various speed ranges and for measurements of local Mach number in the nonuniform flow field about a wind tunnel model. Except at very low speeds or at hypersonic velocities where such precise knowledge of the Mach number is not required, efforts should be directed toward tunnel calibration measurement accurate to within 0.1 percent in Mach number. Due to the presence of flow nonuniformities, a local measurement of Mach number in a strongly varying flow field about a model must generally be made with lesser accuracy.

Computation of Mach number from pressure measurements is the generally recommended procedure since pressure measuring devices are easy to build and to use, and since manometers with various fluids and gages of many types are available with which the pressure may be measured to the desired accuracy in almost any range. In particular, at the present status of the art of measuring supersonic Mach number, the ratio of pitot pressure to stagnation pressure is most conveniently obtained.

Errors in the measurement of pitot pressure are generally much smaller and more easily corrected than is the boundary layer effect on static pressure measurement. The experiment cited in Section IV, moreover, indicates that stagnation pressure can be measured in the stilling section upstream of a supersonic nozzle since it does not change in the expansion through a reasonably shock-free nozzle to the test section.

Fig. V-1 shows the fractional error in measuring Mach number using three different pressure parameters. It is assumed that each parameter can be measured to an accuracy of 3 parts in 10,000, that the air is dry and that probes are properly aligned and constructed so that the only error is due to the boundary layer displacement effect on the static pressure measurement. It can be seen that the pitot-stagnation parameter P_3 is superior at supersonic speeds until the better sensitivity of the static pressure measurement overcomes the error due to boundary layer displacement effect at Mach numbers below about 1.4. It will be noted that there is a range of Mach numbers at which measurements of Mach number to 0.1 percent would require slightly greater precision in reading the pressure parameters than the 0.03 percent assumed here.

In subsonic flow, the ratio of pitot to stagnation pressure does not vary with Mach number and hence other techniques must be employed. The static pressure orifice then replaces the pitot tube. A further complication in subsonic calibration arises from the fact that inserting a model changes the Mach number everywhere from its empty tunnel calibration. The Mach number must then be adjusted either by applying a blocking correction (see Ref. 68) or by measuring the static pressure at the tunnel wall while the model is in the flow field.

The procedures recommended here are for tunnels working at approximately room temperature and atmospheric pressure at the stagnation condition. Hypersonic wind tunnels will be assumed heated sufficiently to avoid air condensation. In special installations using very high or very low pressures or operating at high stagnation temperatures, the recommendations may have to be revised in favor of the more complicated special techniques discussed in Section III.

(a) Empty Tunnel Calibration

(1) Subsonic Speeds, $M < 0.8$

The Mach number distribution in the test section can be determined from static and total pressure measurements using the subsonic pitot static probe described in Section III.

While the test region is calibrated in this manner, static pressure should be measured on the tunnel wall in the test section ahead of the model. The wall measurements are thus identified with the empty tunnel Mach number distribution in the test section, and when a model is in the stream, the wall static pressures will indicate approximately the free stream Mach number distribution. The wall static from taps placed around the test section at the station ahead of the model may be averaged by a so-called "piezometer ring" and this average used in place of the reading of one wall static pressure.

(2) Transonic Speeds, $0.8 \leqq M \leqq 1.4$

The ratio of pitot to stagnation pressure is still insensitive to Mach number in this range so that the calibration procedure requires static pressure measurements. As indicated in the part of Section IV devoted to nose and support effects on static pressure measurements, the transonic speed range is the most troublesome one for a static pressure probe. The recommended procedure then is to insert a long thin pipe in the test section of the tunnel extending forward through the contracting section of the nozzle. Static pressure is measured at various stations along the pipe, and Mach number deduced from the ratio of static to stagnation pressure.

In a tunnel with large contraction ratio such that the air upstream of the nozzle is essentially at stagnation condition, the stagnation pressure measured in the stilling section should be constant throughout the nozzle. Screens will help to remove any rotation or other variation in the stilling section. The entrance to the nozzle must also be smooth enough to avoid regions of flow separation. A survey of the stagnation pressure in the nozzle will indicate whether the entrance conditions have been properly designed.

The wall static pressure measurements recommended in the discussion of subsonic wind tunnel calibration should also be made in transonic tunnels to indicate test section Mach number when a model is in the flow.

At Mach numbers greater than one, the sensitivity formulas of Section III show that the Mach wave angle, visible in either schlieren or shadowgraph, is especially sensitive to Mach number. To use this parameter two families of Mach waves should be generated as illustrated in Fig. V-2. In this way the probes can be sufficiently far from the measuring point so that the nose shocks have degenerated into Mach waves; while the use of two probes cancels any effect of stream angularity.

As the Mach number approaches unity, the waves get fainter and finally become too obscure to identify. The procedure thus becomes useless around $M < 1.05$. This lower limit in Mach number depends upon the sensitivity of the optical system, the density of the flow, and the nature of the probe.

(3) Supersonic Speeds, $1.4 \leqq M \leqq 5$

In the usual range of supersonic testing, the pitot tube makes the best instrument when its reading is coupled with the stagnation pressure measured upstream of the nozzle. For reliable testing conditions, the tunnel air should be dry enough to avoid substantial errors due to water condensation and the supply air temperature should be sufficiently high to prevent air condensation at the higher Mach numbers. The stagnation pressure can generally be assumed constant through the nozzle and equal to the value measured upstream in the subsonic portion of the flow. The process is then isentropic. If shock waves exist in the nozzle flow, or imperfect gas or viscous effects are of a magnitude which might noticeably effect the stagnation pressure in the test section, then the method of measuring pitot pressure behind an oblique shock may be used to determine any loss in stagnation pressure.

The pitot probe will not be sensitive to small flow misalignments nor to viscous effects at normal tunnel densities. Other techniques (see Ref. 51) are employed when the density gets so low that viscous effects can no longer be ignored. To maintain an accuracy in Mach number computation to within 0.1 percent, careful measurement of pitot pressure is required and special manometer fluids or gages may be required when the pressure gets very low.

(4) Hypersonic Speeds, $M > 5$

The pitot probe is useful at hypersonic speeds too, although at high temperatures, corrections for imperfect gas effects may be required. Also viscosity and shock waves in the flow field are likely to invalidate the assumption of constant stagnation pressure through the nozzle. Fortunately, however, the quantities such as force coefficients usually measured in a wind tunnel are not very sensitive to small changes in Mach number in the hypersonic speed range.

(b) Local Measurements

(1) Subsonic Speeds, $M < 0.8$

The pitot-static probe can be used to make local Mach number measurements in a nonuniform flow field as about a model. The Mach number deduced from any measurement should be assigned to the point at which the static pressure is measured. In fact, in a good subsonic wind tunnel, the stagnation pressure is constant throughout the flow field; consequently besides this presumably known stagnation pressure, only local static pressures are needed to determine the Mach number distribution. The probe may be made small by eliminating the stagnation pressure orifice in the nose. In a nonuniform flow field, velocity gradients in several directions are likely to be present, hence for accurate Mach number determination, some effort should be made to align the probe with the stream direction.

(2) Transonic Speeds, $0.8 \leqq M \leqq 1.4$

In the subsonic range, the static probe may be used as described above except that a local pitot pressure measurement will be required too in any region downstream of shock waves. The Mach number is then determined from parameter P_2. Effects of probe nose and support pressure fields are best minimized by using a long slender support with the static pressure orifices far behind the nose, and as far as possible forward of a supporting holder.

At supersonic speeds above M = 1.05, two families of Mach waves may be generated as described for uniform transonic flow calibration, but they must be so placed and constructed that in the presence of flow irregularities, the waves will actually intersect at the point where the intersection appears in the optical system.

(3) Supersonic and Hypersonic, $1.4 < M$

A five-hole conical probe makes a suitable instrument for making local Mach number measurements in supersonic and hypersonic speeds. The ratio of cone surface pressure from the average of four holes around the cone to pitot pressure measured at the tip of the cone will give a measurement of Mach number. Errors due to flow angularity and boundary layer effects are indicated in Section IV. The cone surface pressure holes must be many tip diameters behind the pitot pressure tap, but by making the tip very small, the distance between pitot and cone surface pressure measurements may be kept down.

(c) Conclusions

Pressure measurements derive their usefulness, in part, from the long history of pressure-measuring instruments and techniques. Comparable advances in the development of the measurement of other properties may yet make the pitot tube obsolete. In particular, optical measuring devices have the desirable feature of being free from the probe errors discussed in Section IV.

At present the results are interpretable only in two-dimensional or axially-symmetric flow. Direct measurements of velocity and of the local velocity of sound are feasible at present but require much special equipment. The pressure measurement techniques are therefore attractive as long as the accuracy required remains within the capability of the method. Table VII lists the recommended measurement parameters.

REFERENCES

1. Morris, D. E., and Winter, K.G., "Requirements for Uniformity of Flow in Supersonic Wind Tunnels," Royal Aircraft Establishment, Technical Note Aero 2340, September 1954.

2. Liepmann, H. W., and Puckett, A. E., "Introduction to Aerodynamics of a Compressible Fluid," John Wiley and Sons, New York, 1947.

3. Tsien, H. S., "One Dimensional Flows of a Gas Characterized by Van der Waal's Equation of State," Journal of Math. and Phy., Vol. 25, No. 6, pp 301-324, 1947.

4. Tao, L. N., "Gas Dynamic Behavior of Real Gases," Journal of the Aeronautical Sciences Vol. 22, No. 11, pp 763-794, November 1955.

5. Hilsenrath, Joseph, et al, "Tables of Thermal Properties of Gases," National Bureau of Standards Circular 564, November 1955.

6. Hall, N. A., and Ibele, W. E., "Thermodynamic Properties of Air, Nitrogen, and Oxygen as Imperfect Gases," University of Minnesota, Engineering Experiment Station Technical Paper No. 85, December 1951.

7. "Handbook of Supersonic Aerodynamics," U. S. Navy Bureau of Ordnance, NAVORD Report 1488, Vol. 2, October 1950.

8. Ames Research Staff, "Equations, Tables, and Charts for Compressible Flow," National Advisory Committee for Aeronautics, Technical Report 1135, 1953.

9. Compressible Flow Tables Panel, "A Selection of Graphs for Use in Calculations of Compressible Air Flow," Clarendon Press, Oxford, 1954.

10. Keenan, J. H., and Kaye, J., "Gas Tables," John Wiley and Sons, Inc., New York, 1948.

11. Compressible Flow Tables Panel, "A Selection of Tables for Use in Calculations of Compressible Airflow," Clarendon Press, Oxford, 1952.

12. Tsien, H. S., "Superaerodynamics, Mechanics of Rarefied Gases," Journal of the Aeronautical Sciences, Vol. 13, No. 12, December 1946.

13. Tsien, H. S., "Wind-Tunnel Testing Problems in Superaerodynamics," Journal of the Aeronautical Sciences, Vol. 15, No. 10, October 1948.

14. "Handbook of Supersonic Aerodynamics," U. S. Navy Bureau of Ordnance, NAVORD Report 1488, Vol. 5, August 1953.

15. Pankhurst, R. C., and Holder, D. W., "Wind-Tunnel Techniques," Pitman, Ltd., 1952.

16. Kopal, Z., "Tables of Supersonic Flow Around Cones," Massachusetts Institute of Technology Technical Report 1, 1947.

17. Cooper, M., and Webster, R. A., "The Use of an Uncalibrated Cone for Determination of Flow Angles and Mach Numbers at Supersonic Speeds," National Advisory Committee for Aeronautics, Technical Note 2190, March 1951.

18. Hill, J. A. F. H., "On the Calibration of Supersonic Wind-Tunnels," Journal of the Aeronautical Sciences, Vol. 22, No. 6, pp 441-443, June 1955.

19. Baron, J. R., "Analytic Design of a Family of Supersonic Nozzles by the Friedrichs Method, Including Computation Tables and a Summary of Calibration Data," Wright Air Development Center Technical Report 54-279, June 1954.

20. Barry, F. W., "Determination of Mach Number from Pressure Measurements," A.S.M.E. Transactions, Paper 55-SA-28, 1955.

21. Ladenburg, R. W., "Physical Measurements in Gas Dynamics and Combustion," High Speed Aerodynamics and Jet Propulsion Series, Vol. 9, Part 1, Princeton University, 1954.

22. Ferri, A., "Elements of Aerodynamics of Supersonic Flows," MacMillan Company, New York, 1949.

23. Howarth, L., "Modern Developments in Fluid Dynamics, High Speed Flow," Vol. II, Clarendon Press, Oxford 1953.

24. Erdmann, S. F., "A New Simple Interferometer for Obtaining Quantitatively Evaluable Flow Patterns," National Advisory Committee for Aeronautics, Technical Memo. 1363, November 1953. Translation of "Ein Neues, Sehr Einfaches Interferometer zum Erhalt Quantitiv Auswertbarer Stromeingsbilder," Applied Sci. Res. Vol. B2.

25. Temple, E. B., "The Quantitative Measurement of Gas Density by Means of Schlieren Interference," Massachusetts Institute of Technology, Naval Supersonic Laboratory, Technical Report 132, November 1955.

26. Weltmann, R. N., Fairweather, S., and Papke, D., "Application of X-Ray Absorption to Measurement of Small Air Density Gradients," National Advisory Committee for Aeronautics, Technical Note 2406, July 1951.

27. Duneff, J., Hallett, R. K., and Hansen, C. F., "X-Ray Instrumentation for Density Measurements in a Supersonic Flow Field," National Advisory Committee for Aeronautics, Technical Note 2845, December 1952.

28. Kunkel, W. B., and Talbot, L., "Ion-Tracer Technique for Airspeed Measurement at Low Densities," National Advisory Committee for Aeronautics, Technical Note 3177, March 1954.

29. Boyd, B., Dorsch, R. G., and Brodie, G. H., "True Airspeed Measurement by Ionization-Tracer Technique," National Advisory Committee for Aeronautics, Research Memorandum E52C31, July 1952.

30. Lukasiewicz, J., and Rayle, J. K., "Effects of Air Humidity in Supersonic Wind Tunnels," Aeronautical Research Council, R and M 2563, 1953.

31. Hill, J. A. F., "Results of the Wind Tunnel Program on Water-Vapor Condensation Effects," Massachusetts Institute of Technology Naval Supersonic Laboratory Memorandum A and R 100-97, August 1952.

32. Baron, J. R., "Effect of Water Vapor Upon Impact Pressure Measurements in Supersonic Wind Tunnels," Massachusetts Institute of Technology Naval Supersonic Laboratory Memorandum A and R 126, March 1955.

33. Hansen, C. F., and Nothwang, G. J., "Condensation of Air in Supersonic Wind Tunnels and its Effects on Flow about Models," National Advisory Committee for Aeronautics Technical Note 2690, April 1952.

34. McLellan C. H., and Williams, T. W., "Liquefaction of Air in the Langley 11-Inch Hypersonic Tunnel," National Advisory Committee for Aeronautics Technical Note 3302, October 1954.

35. Grey, J., and Nagamatsu, H. T., "The Effects of Air Condensation on Properties of Flow and Their Measurement in a Hypersonic Wind Tunnel," Proceedings of the Third Midwestern Conference on Fluid Mechanics, University of Minnesota, 1953.

36. Wegener, P., et al., "NOL Hyperballistic Tunnel No. 4 Results I: Air Liquefaction," U. S. Naval Ordnance Laboratory NAVORD Report 1742, January 1951.

37. Buhler, R. D., "Recent Results on the Condensation Investigation," Hypersonic Wind Tunnel Memo. No. 1, Guggenheim Aeronautical Laboratory, California Institute of Technology, 9 July 1950.

38. Grey, J., "Effects of Air Condensation on Properties of Flow and Their Measurement in Hypersonic Wind Tunnels," Ph.D. Thesis, California Institute of Technology, 1952.

39. Howarth, L., "Modern Developments in Fluid Dynamics, High Speed Flow," Vol. I, Clarendon Press, Oxford, 1953.

40. Eggers, A. J., Jr., "One-Dimensional Flows of An Imperfect Diatomic Gas," National Advisory Committee for Aeronautics, Technical Report 959, 1950.

41. Kantrowitz, A., "Effects of Heat-Capacity Lag in Gas Dynamics," National Advisory Committee for Aeronautics Wartime Report L-457, January 1944.

42. Faro, I. D. V., and Hill, F K., "Experiments with Nitrogen in a Hypersonic Wind Tunnel," Paper Presented at U. S. Navy Symposium on Aeroballistics, Pasadena, California, May 1952.

43. Blackman, Vernon H., "Vibrational Relaxation in 0_2 and N_2" Princeton University Department of Physics Technical Report II-20, May 1955.

44. Glass, I. I., Martin, W., and Patterson, G. N., "A Theoretical and Experimental Study of the Shock Tube," University of Toronto, Institute of Aerophysics, Report No. 2, November 1953.

45. Preston, J. H., "The Calculation of Lift Taking Account of the Boundary Layer," Aeronautical Research Council, R and M 2725, November 1949.

46. Young, A. D., "The Calculation of the Profile Drag of Aerofoils and Bodies of Revolution at Supersonic Speeds," College of Aeronautics, Cranfield, Report No. 73, April 1953.

47. Eggers, A. J., Jr., Savin, R. C., and Syvertson, C. A., "The Generalized Shock-Expansion Method and Its Application to Bodies Traveling at High Supersonic Air Speeds," Journal of the Aeronautical Sciences, Vol. 22, No. 4, pp. 231-238, April 1955.

48. Probstein, R. F., and Elliott, D., "The Transverse Curvature Effect in Compressible Axially-Symmetric Laminar Boundary Layer Flow," Princeton University Department of Aeronautical Engineering Report 261, April 1954.

49. Talbot, L., "Viscosity Corrections to Cone Probes in Rarefied Supersonic Flow at a Nominal Mach Number of 4," National Advisory Committee for Aeronautics, Technical Note 3219, November 1954.

50. Murphy, J. S., "Evidences of an Inherent Error in Measurement of Total-Head Pressure at Supersonic Speeds," Aeronautical Engineering Review, Vol. 12, No. 11, November 1953.

51. Sherman, F. S., "New Experiments in Impact-Pressure Interpretation in Supersonic and Subsonic Rarefied Air Streams," National Advisory Committee for Aeronautics, Technical Note 2995, September 1953.

52. Graves, J. C., and Quiel, N. R., "Impact Pressure and Total Temperature Interpretation at Hypersonic Mach Number," Galcit Hypersonic Wind Tunnel Memo No. 20, 1954.

53. Holder, D. W., and North, R. J., "Experiments With Pitot Tubes in Supersonic Airstreams," Aeronautical Research Council Report No. 13,268, 1950.

54. Kettle, D. J., "Design and Calibration at Low Speeds of a Static Tube With Semi-Ellipsoidal Nose Shapes," Royal Aircraft Establishment, Technical Note Aero 2247, May 1953.

55. Holder, D. W., North, R. J., and Chinneck, A., "Experiments With Static Tubes in a Supersonic Airstream, Parts I and II," Aeronautical Research Council R and M 2782, 1953.

56. Fraenkel, L. E., "The Theoretical Wave Drag of Some Bodies of Revolution," Aeronautical Research Council, R and M 2842, May 1951.

57. Sweeney, M., Jr., "An Experimental Study of Supersonic Hinge Moment and Control Effectiveness," Thesis, Massachusetts Institute of Technology, 1956. Massachusetts Institute of Technology Supersonic Laboratory, WTR 109, January 1956.

58. Lee, J. D., "The Influence of High Adverse Pressure Gradients on Boundary Layers in Supersonic Flow," University of Toronto, Inst. of Aerophysics, Report No. 21, 1952.

59. Gracey, W., Coletti, D. E., and Russell, W. R., "Wind-Tunnel Investigation of a Number of Total-Pressure Tubes at High Angles of Attack, National Advisory Committee of Aeronautics, Technical Note 2261, January 1951.

60. Russell, W. R., Gracey, W., Letko, W. and Fournier, P. G., "Wind-Tunnel Investigation of Six Shielded Total-Pressure Tubes at High Angles of Attack," National Advisory Committee of Aeronautics, Technical Note 2530, November 1951.

61. Stine, H. A., and Wanlass, K., "Theoretical and Experimental Investigation of Aerodynamic-Heating and Isothermal Heat-Transfer Parameters on a Hemispherical Nose with Laminar Boundary Layer at Supersonic Mach Numbers," National Advisory Committee for Aeronautics, Technical Note 3344, December 1954.

62. Goldstein, S, "Modern Developments in Fluid Dynamics," Vol. I, Clarendon Press, Oxford, 1938, page 252.

63. Walter, L. W., and Redman, E. J., "Needle Static-Pressure Probes Insensitive to Flow Inclination in Supersonic Air Streams," U. S. Naval Ordnance Laboratory, NAVORD Report 3694, March 1954.

64. Young, A. D., and Maas, J. N., "The Behaviour of a Pitot Tube in a Transverse Total Pressure Gradient," Aeronautical Research Council, R and M 1770, 1937.

65. Johanneson, N. H., and Mair, W. A., "Experiments with Large Pitot Tubes in a Narrow Supersonic Wake," Aeronautical Research Council, Report No. 15,067.

66. Davies, F. V., "Some Effects of Pitot Size on the Measurement of Boundary Layers in Supersonic Flow," Royal Aircraft Establishment, Technical Note Aero 2179, August 1952.

67. Monaghan, R. J., "The Use of Pitot Tubes in the Measurement of Laminar Boundary Layers in Supersonic Flow," Royal Aircraft Establishment, Technical Note Aero 2369, May 1955.

68. Goldstein, S., "A Note on the Measurement of Total-Head and Static Pressure in a Turbulent Stream," Proc. Royal Soc. (A) Vol. 155, p 570, 1936.

69. Ribner, H. S., "Shock-Turbulence Interaction and the Generation of Noise," National Advisory Committee for Aeronautics, Technical Note 3255, July 1954.

70. Fage, A., "On the Static Pressure in Fully Developed Turbulent Flow," Proc. Roy. Soc. (A) Vol. 155, p 576, 1936.

71. Thom, A., "Blockage Corrections in a Closed High-Speed Tunnel," Aeronautical Research Council, R and M 2033, November 1943.

72. Göthert, B., "Ebene und Räumliche Strömung bei hohen Unterschallgeschwindigkeiten," Lilienthal Gesellschaft 127. Translated in "Plane and Three-Dimensional Flow at High Subsonic Speeds," National Advisory Committee for Aeronautics, Technical Memorandum No. 1105, 1946.

73. Herriot, J. G., "Blockage Corrections for Three-Dimensional-Flow Closed-Throat Wind Tunnels, with Consideration of the Effect of Compressibility," National Advisory Committee for Aeronautics, Report No. 995, 1950.

74. Hensel, R. W., "Rectangular-Wind-Tunnel Blocking Corrections Using the Velocity-Ratio Method," National Advisory Committee for Aeronautics, Technical Note 2372, June 1951.

75. Evans, J. Y. G., "Corrections to Velocity for Wall Constraint in Any 10 x 7 Rectangular Subsonic Wind Tunnel," Aeronautical Research Council, R and M 2662, April 1949.

76. Prandtl, L., and Tietjens, O. G., "Applied Hydro- and Aeromechanics," (Translation) McGraw Hill, New York, 1934.

77. Göthert, B., "Windkanal korrekturen bei hohen unterschallgeschwindigkeiten unter besonderer Berücksichtigung des geschlossenen Kreiskanals," Forschungsbericht Nr. 1216, Deutsche Versuchsanstalt für Luftfahrt, E. V., Institut für Aerodynamik, Berlin-Adlershof, May 1940. Translated in "Wind-Tunnel Corrections at High Subsonic Speeds Particularly For an Enclosed Circular Tunnel," National Advisory Committee for Aeronautics, TM 1300, 1952.

78. Maeder, P. F., "Investigation of Tunnel Boundary Interference On Two-Dimensional Airfoils Near the Speed of Sound," TR WT-6, Division of Engineering, Brown University, April 1951.

79. Baldwin, B. S., Jr., Turner, J. B., and Knechtel, E. D., "Wall Interference in Wind Tunnels With Slotted and Porous Boundaries at Subsonic Speeds," National Advisory Committee for Aeronautics, Technical Note 3176, May 1954.

80. Maeder, P. F., "Theoretical Investigation of Subsonic Wall Interference in Rectangular Slotted Test Sections," TR WT-11, Division of Engineering, Brown University, September 1953.

81. Covert, E. E., "On the Aerodynamic Field Around Bodies in the Naval Supersonic Laboratory Transonic Nozzle," Massachusetts Institute of Technology, Naval Supersonic Laboratory, A and R Memo 115, March 1955.

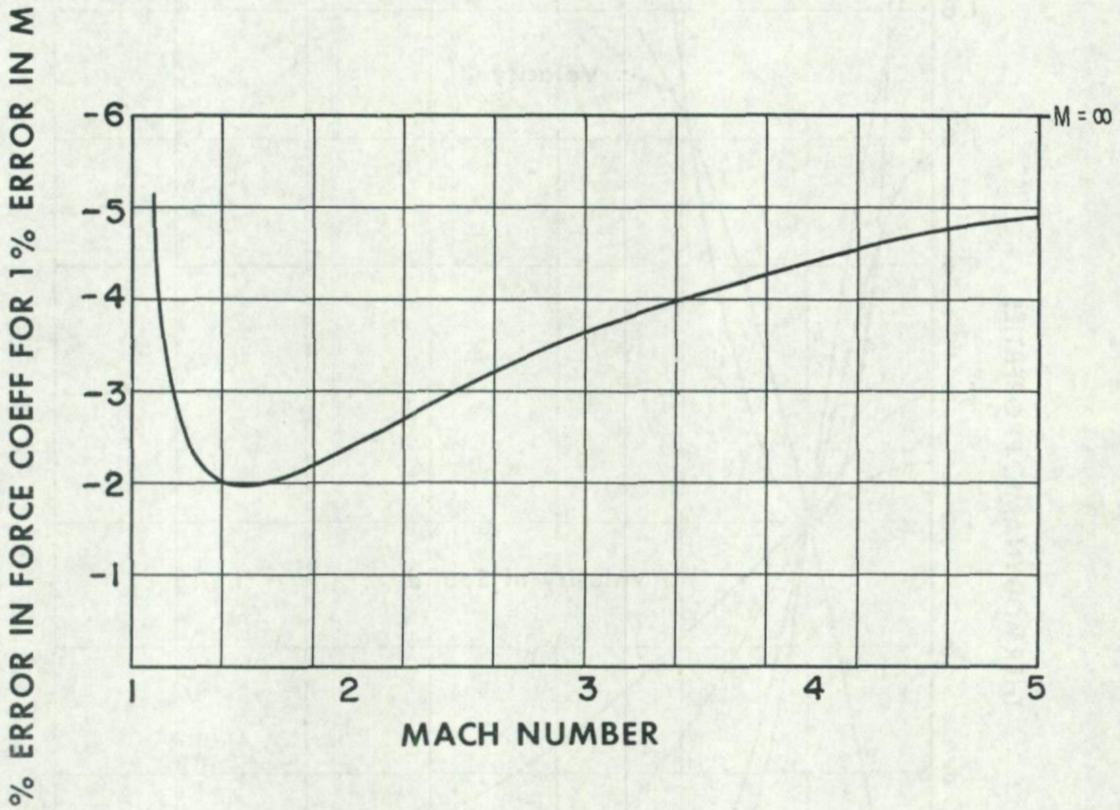

Fig. I-1. Percent error in force coefficient due to percent error in M.

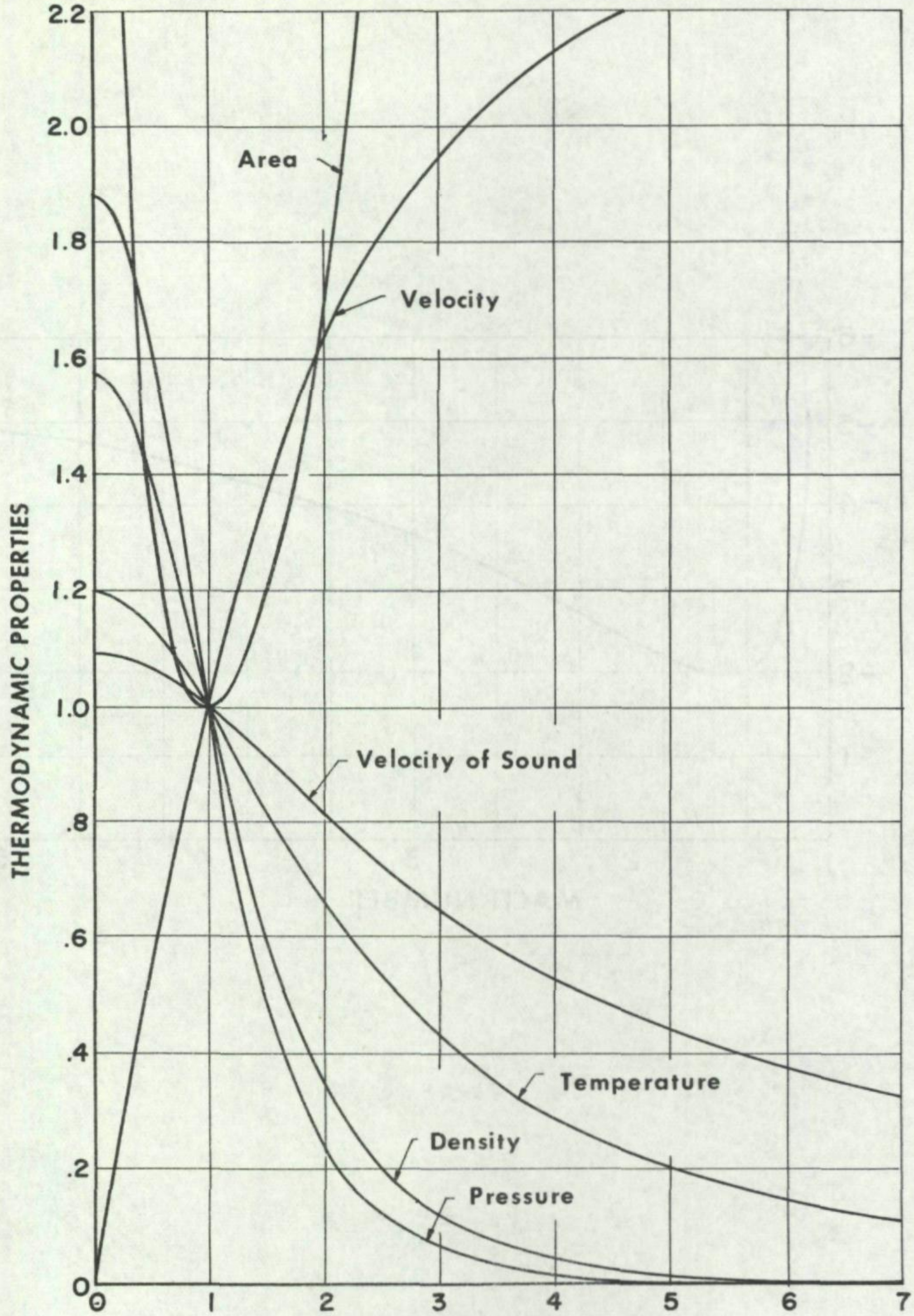

Fig. II-1. Thermodynamic properties in isentropic flow.

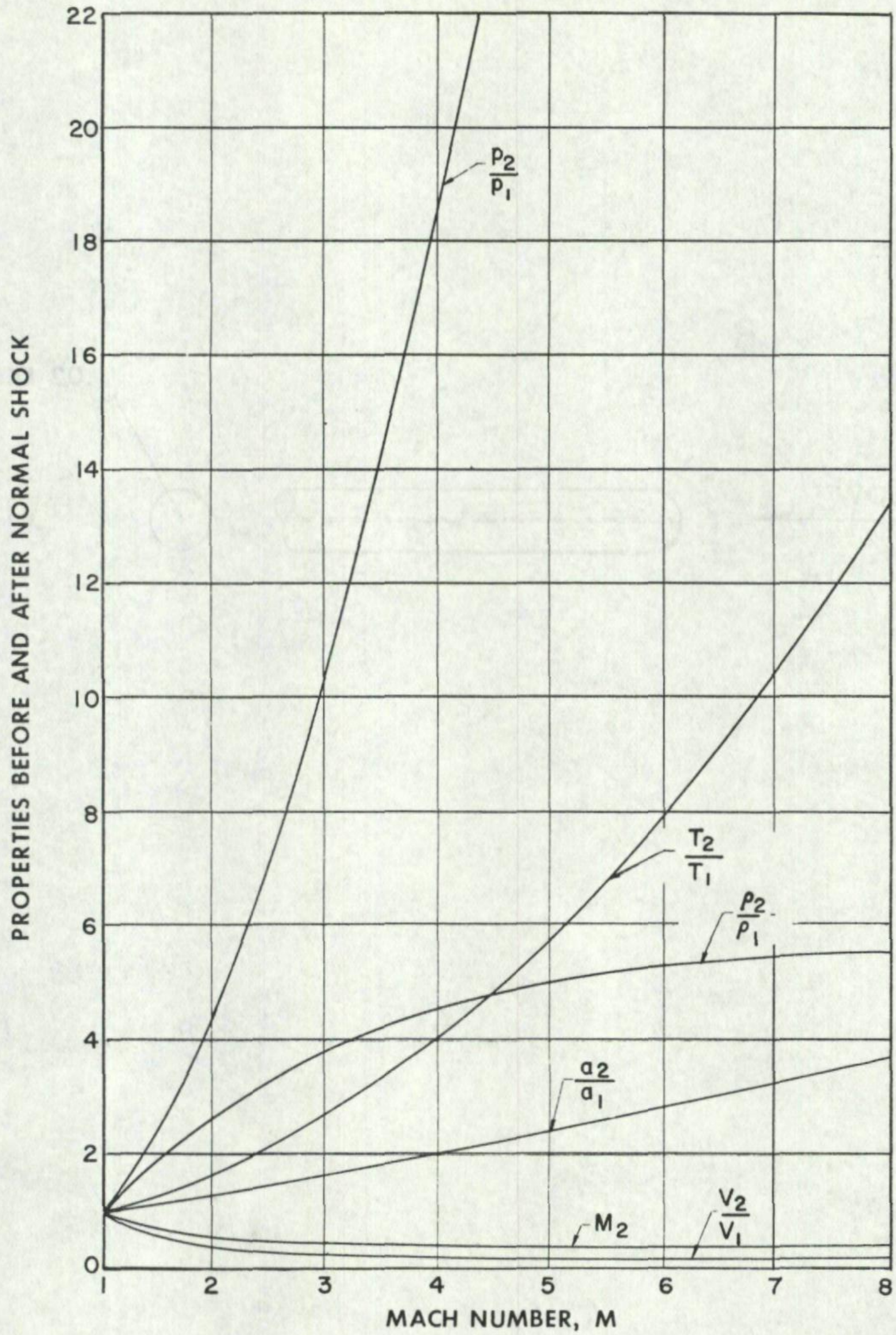

Fig. II-2. Normal shock functions.

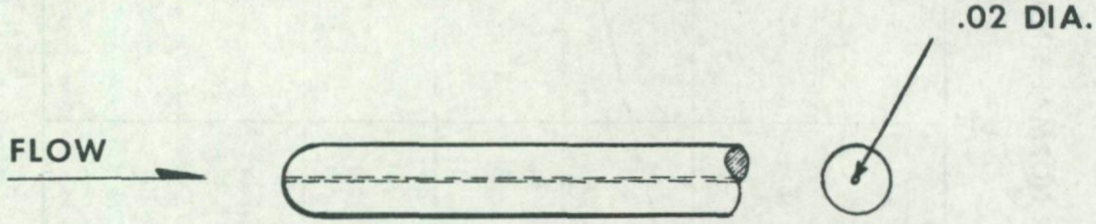

Fig. III-1. Stagnation pressure probes.

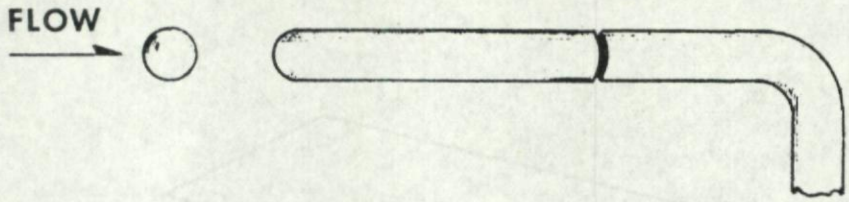

a) Subsonic Static Pressure Probe

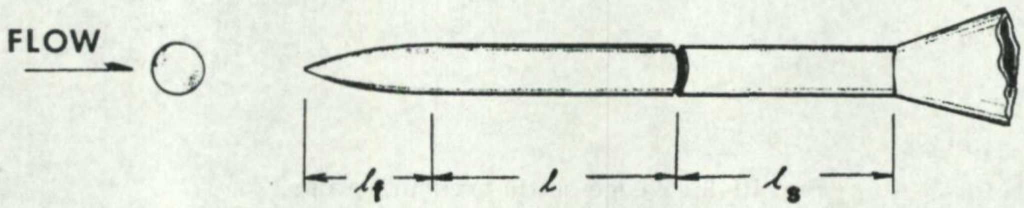

b) Supersonic Static Pressure Probe

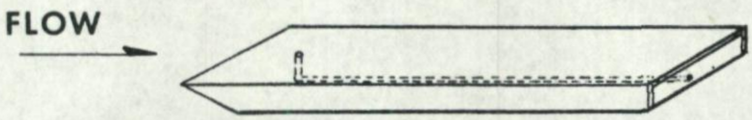

c) Flat Plate for Measuring Static Pressure in a Supersonic Stream

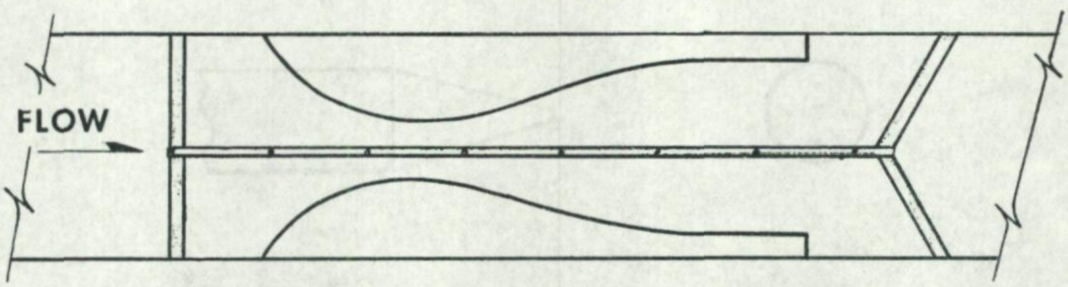

d) Static Pressure Tube in a Supersonic Nozzle

Fig. III-2. Static pressure probes.

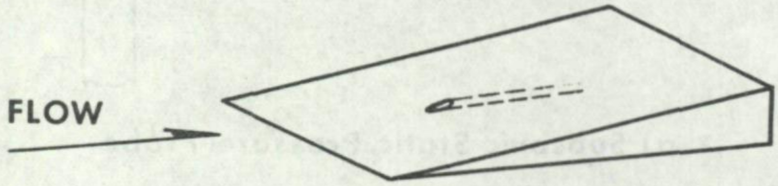

Fig. III-3. Wedge static pressure probe.

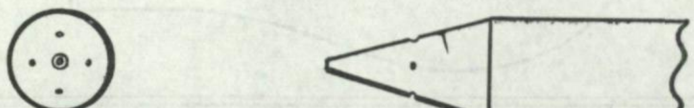

Fig. III-4. Five-hole conical probe.

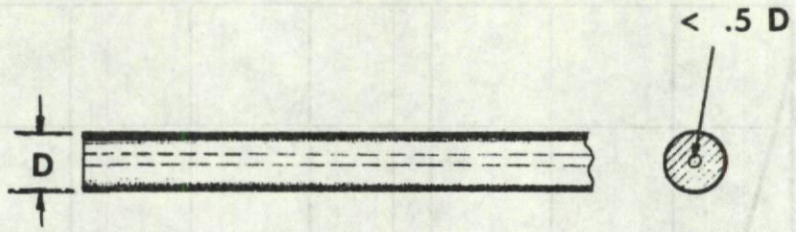

Fig. III-5. Pitot probe.

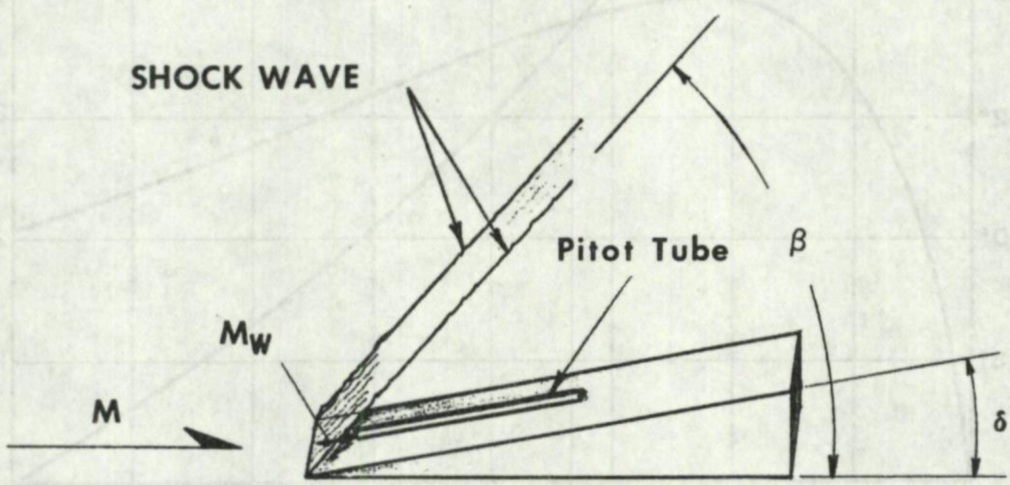

Fig. III-6. Arrangement for measuring pitot pressure behind an oblique shock.

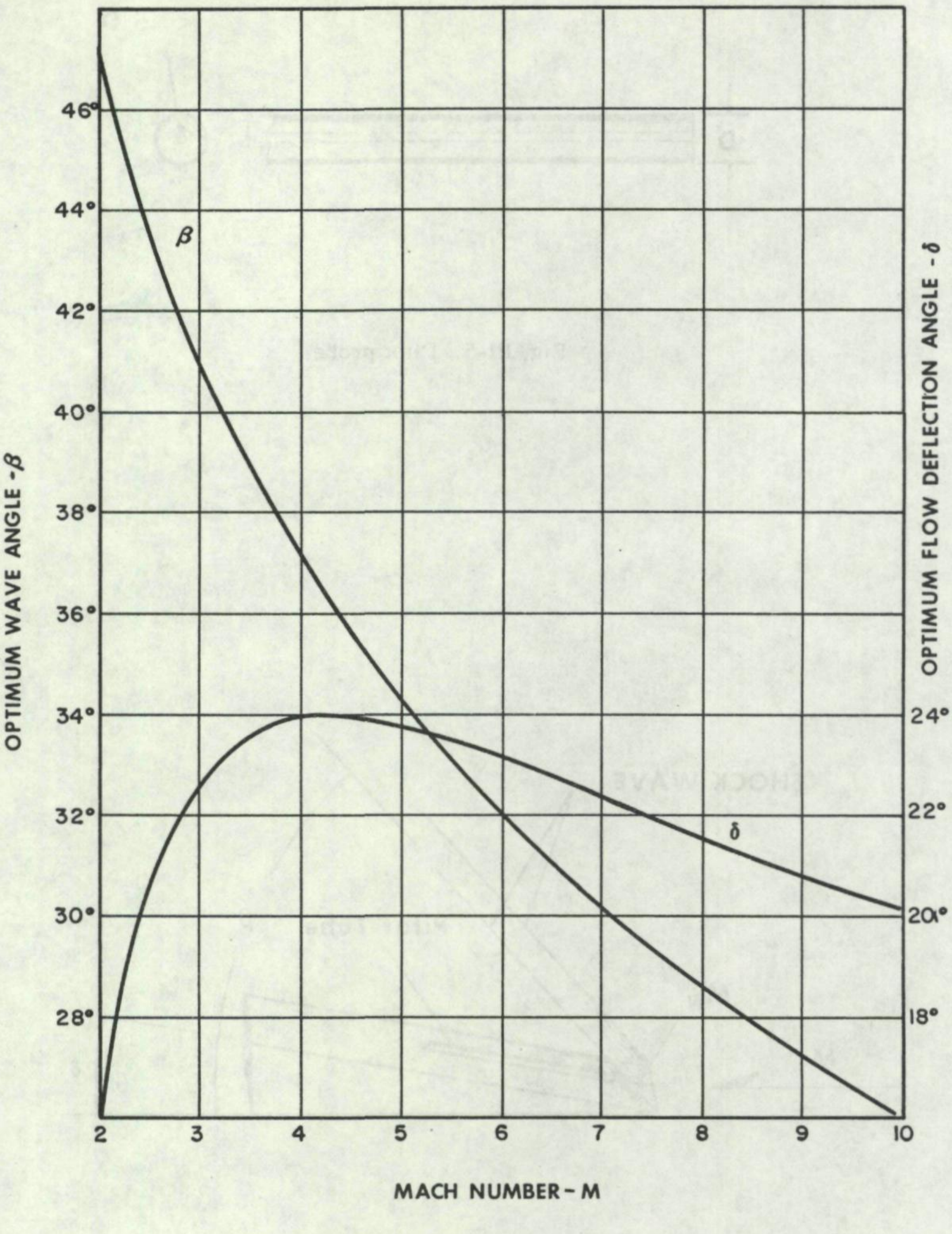

Fig. III-7. Optimum oblique shock wave angle and flow deflection angle for maximum downstream pitot.

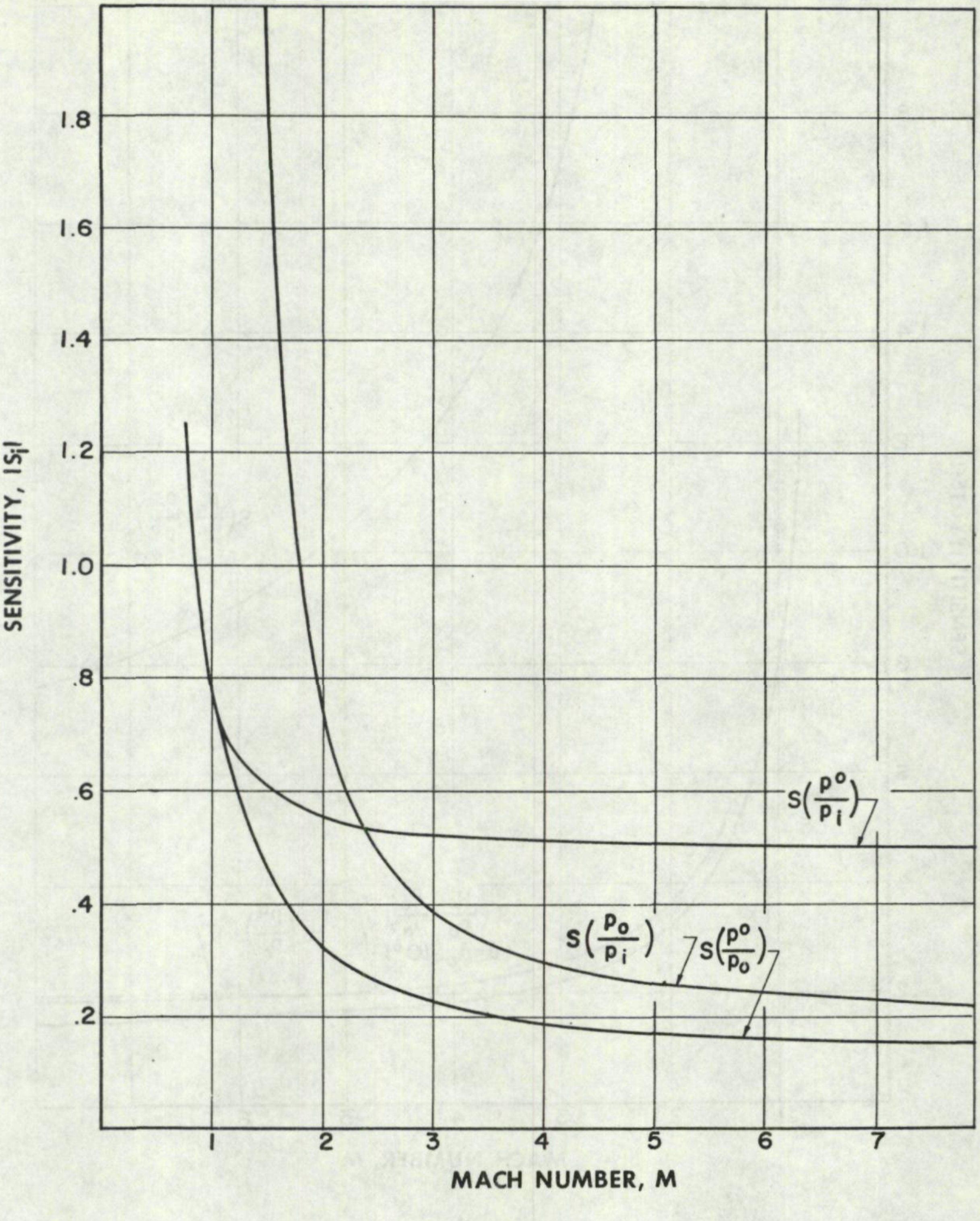

Fig. III-8. Sensitivities of pressure parameters.

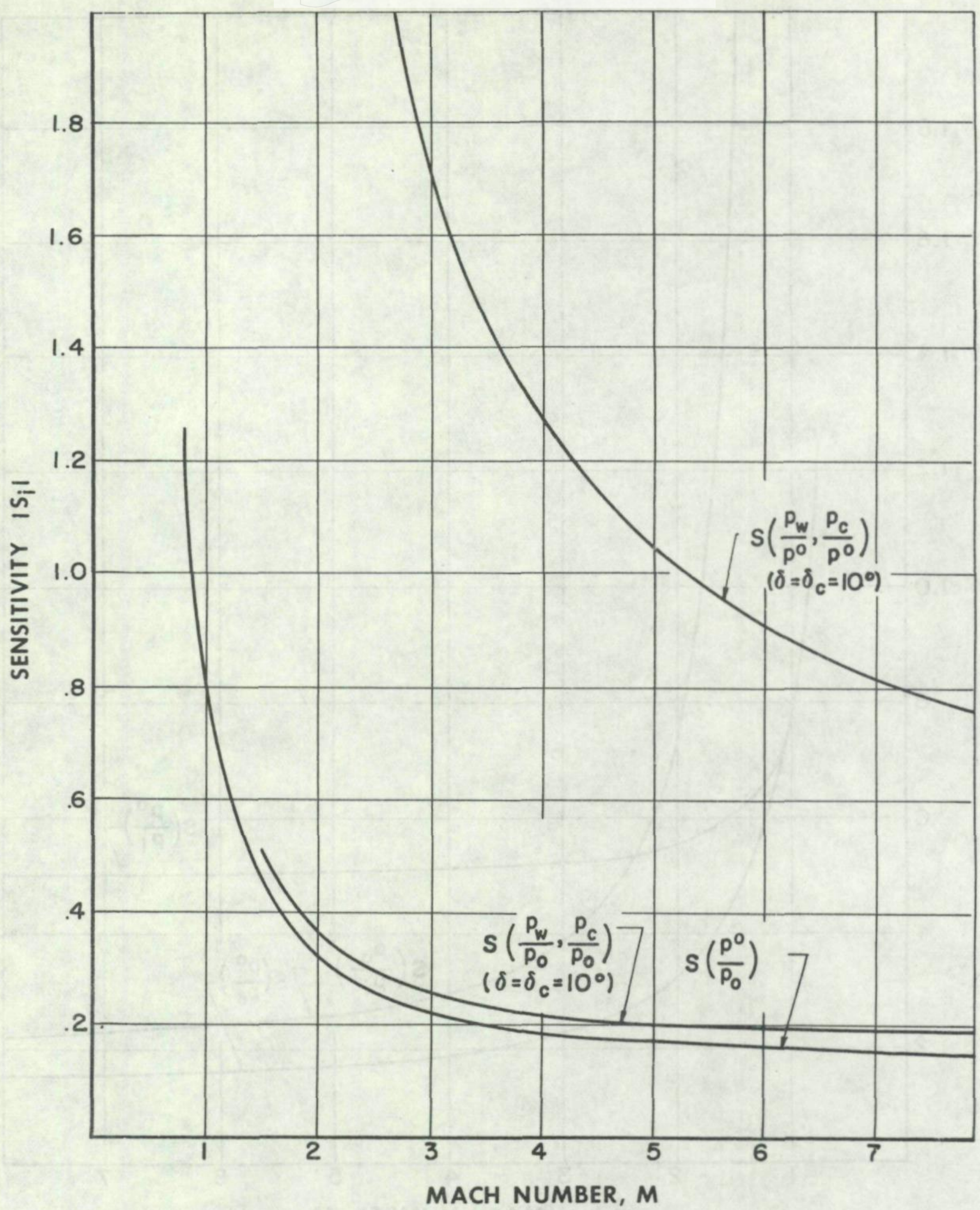

Fig. III-9. Sensitivities of parameters containing wedge or cone pressure and static or stagnation pressure.

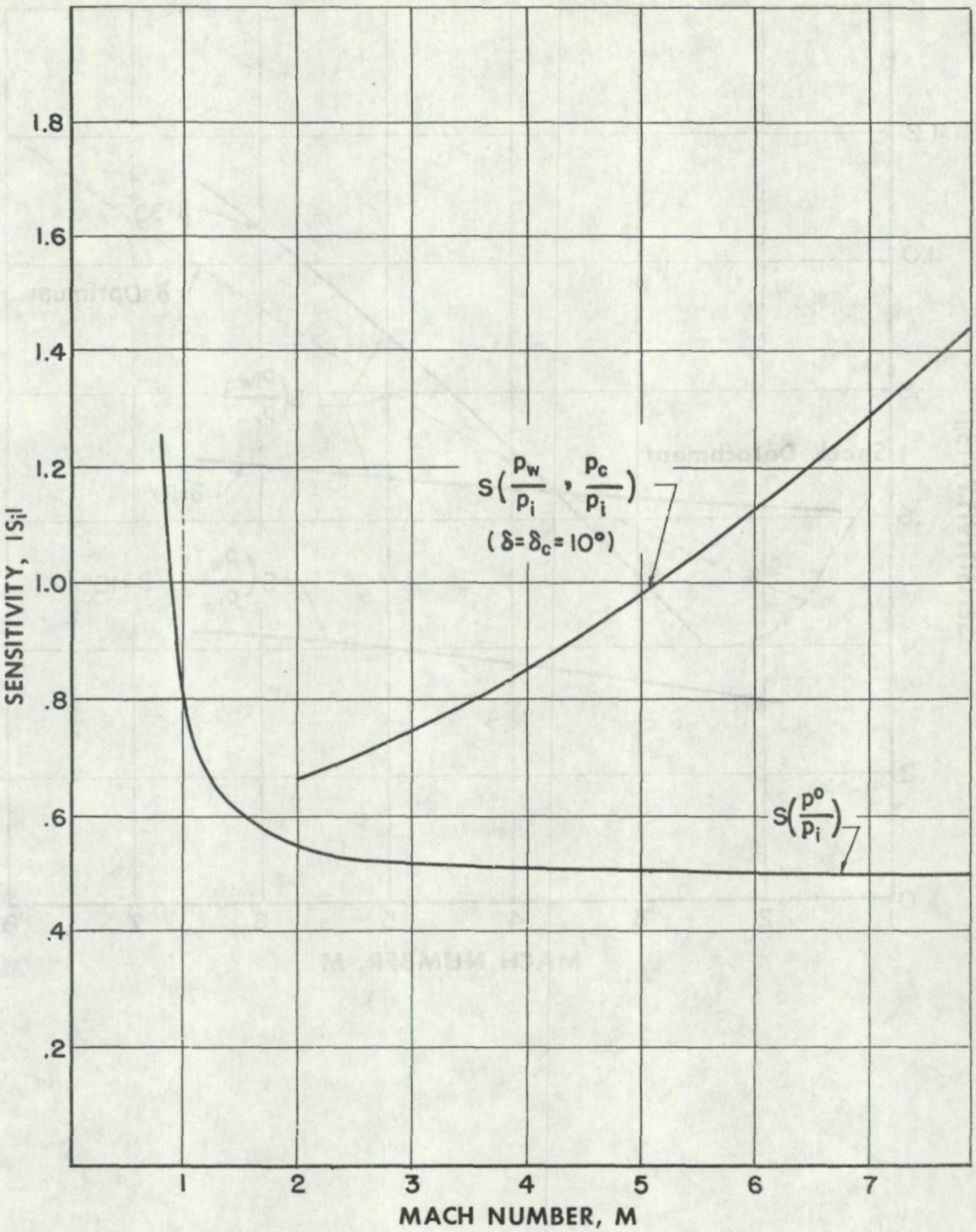

Fig. III-10. Sensitivities of parameters containing wedge or cone pressure and pitot pressure.

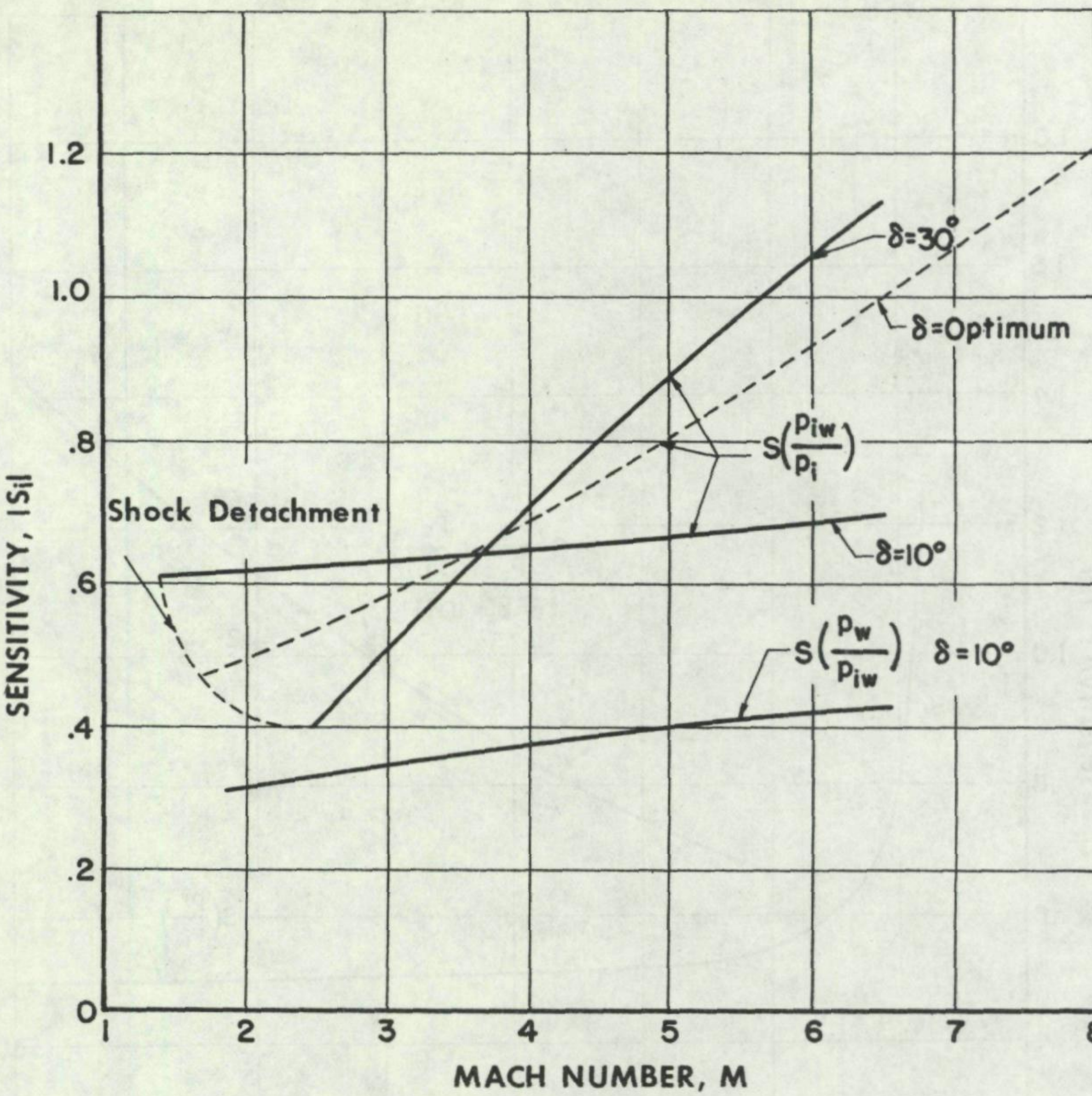

Fig. III-11. Sensitivities for impact pressure behind oblique shock.

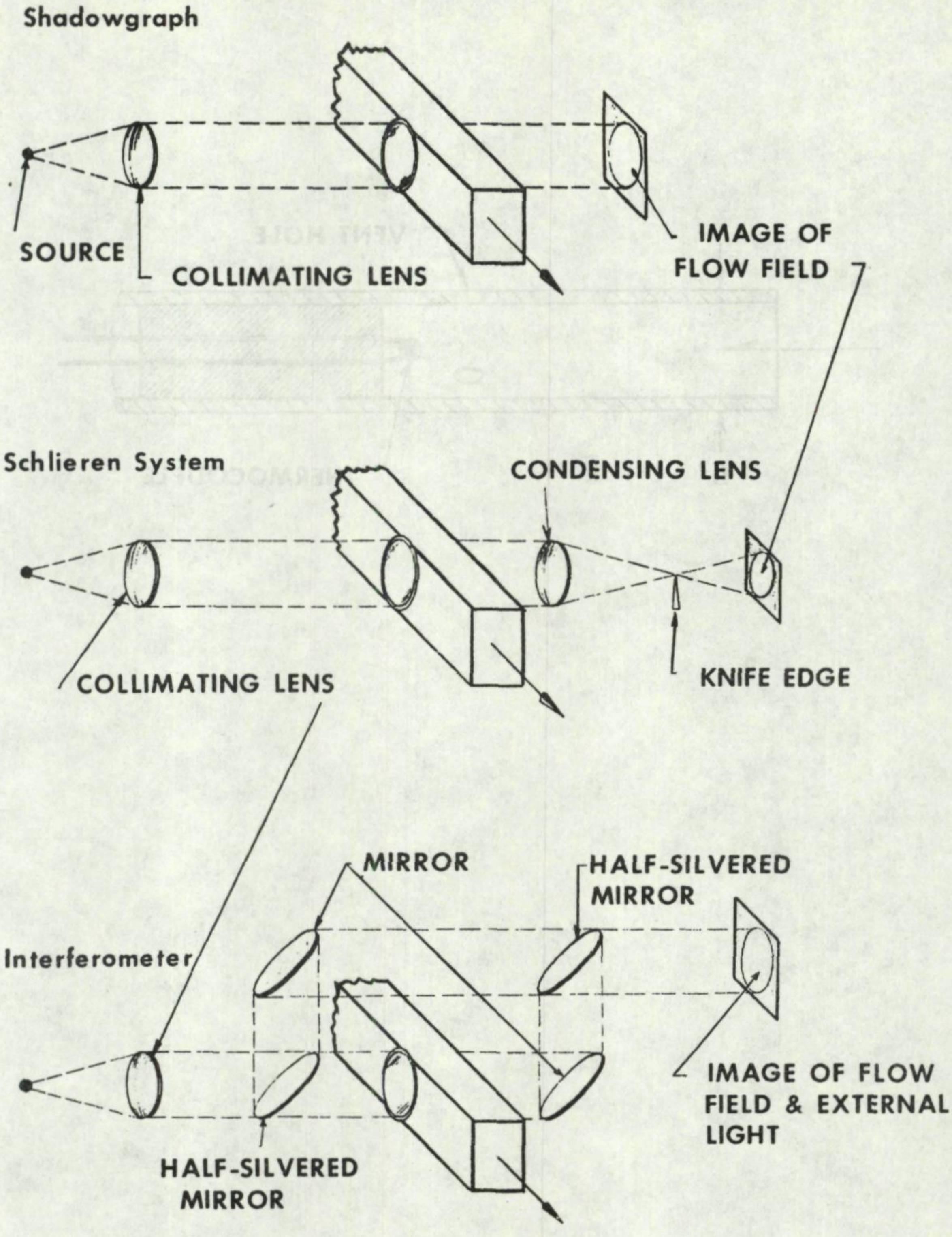

Fig. III-12. Optical systems for viewing compressible flow.

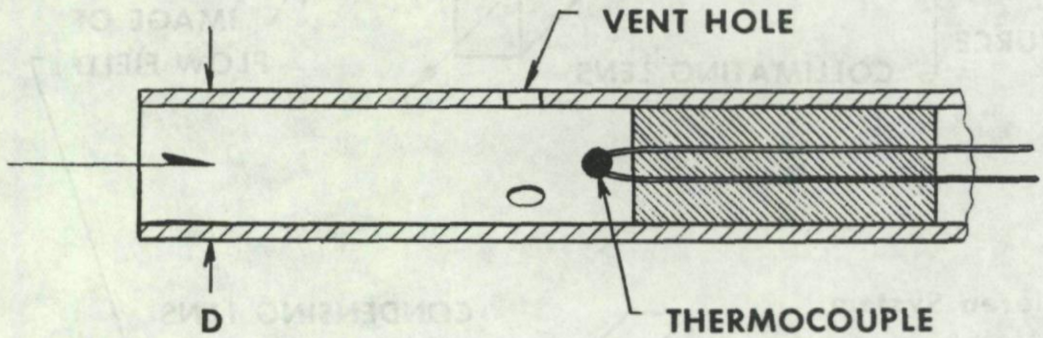

Fig. III-13. Total temperature probe.

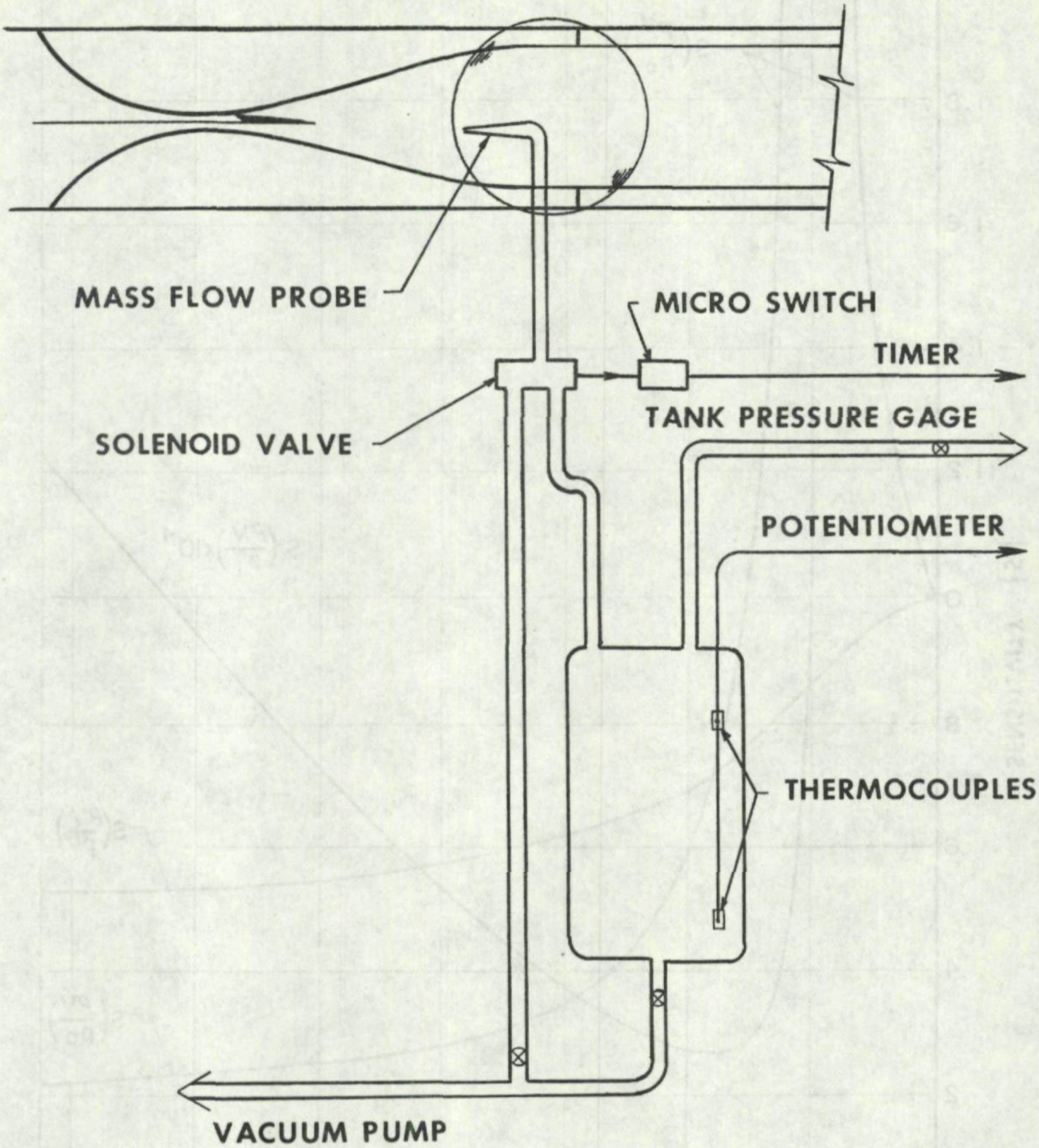

Fig. III-14. Mass flow probe system.

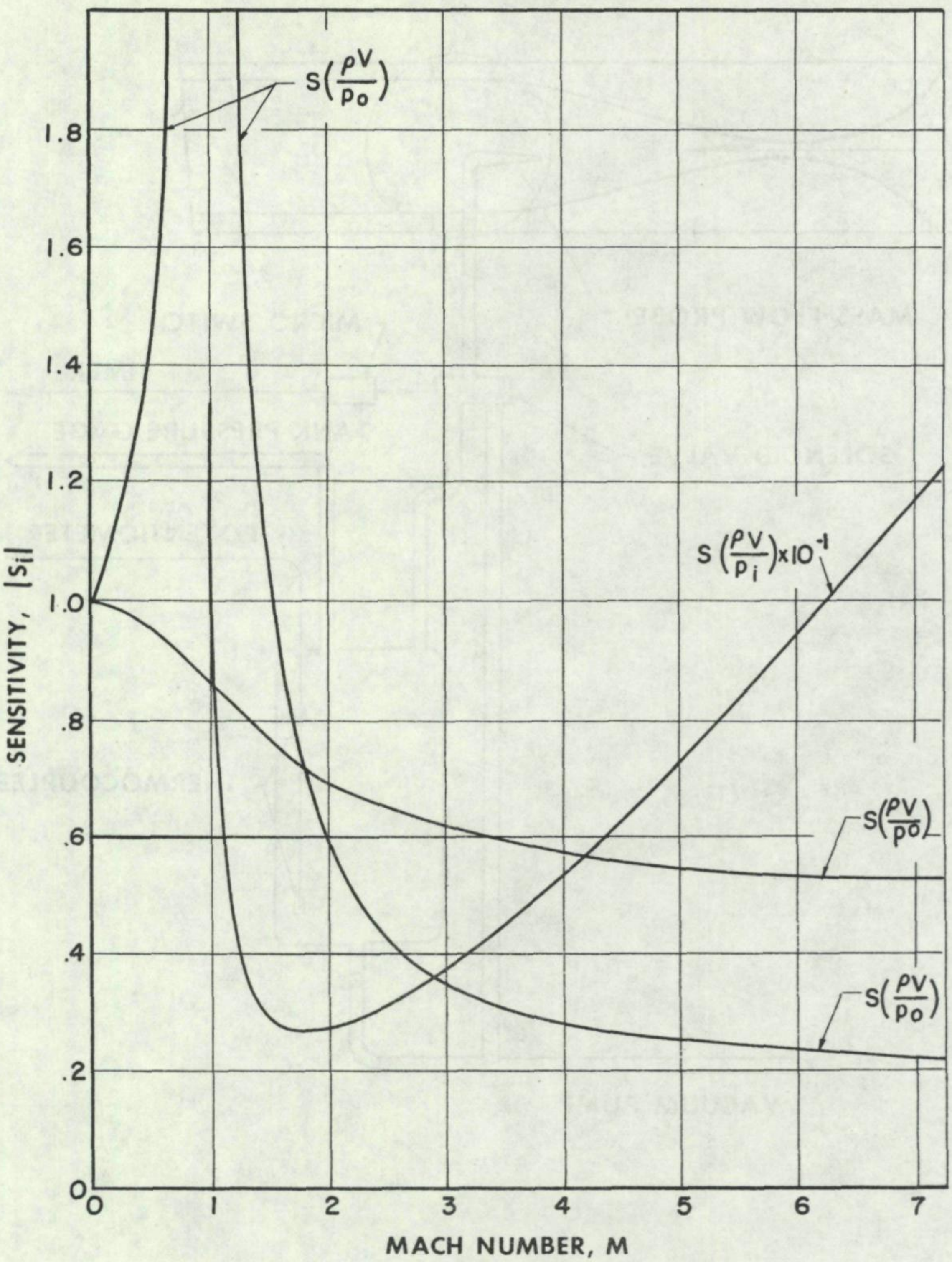

Fig. III-15. Sensitivities of mass flow parameters.

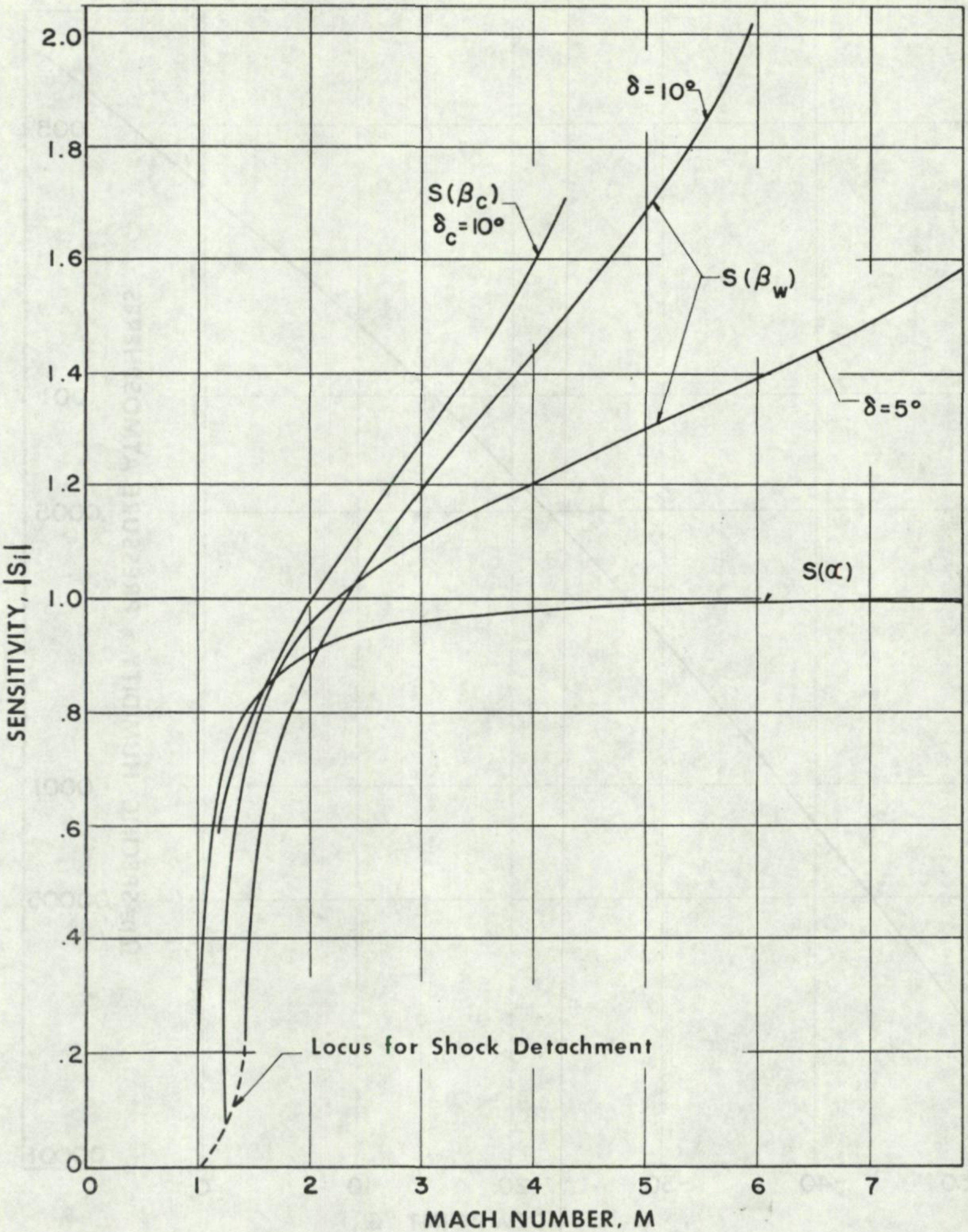

Fig. III-16. Wave geometry sensitivities.

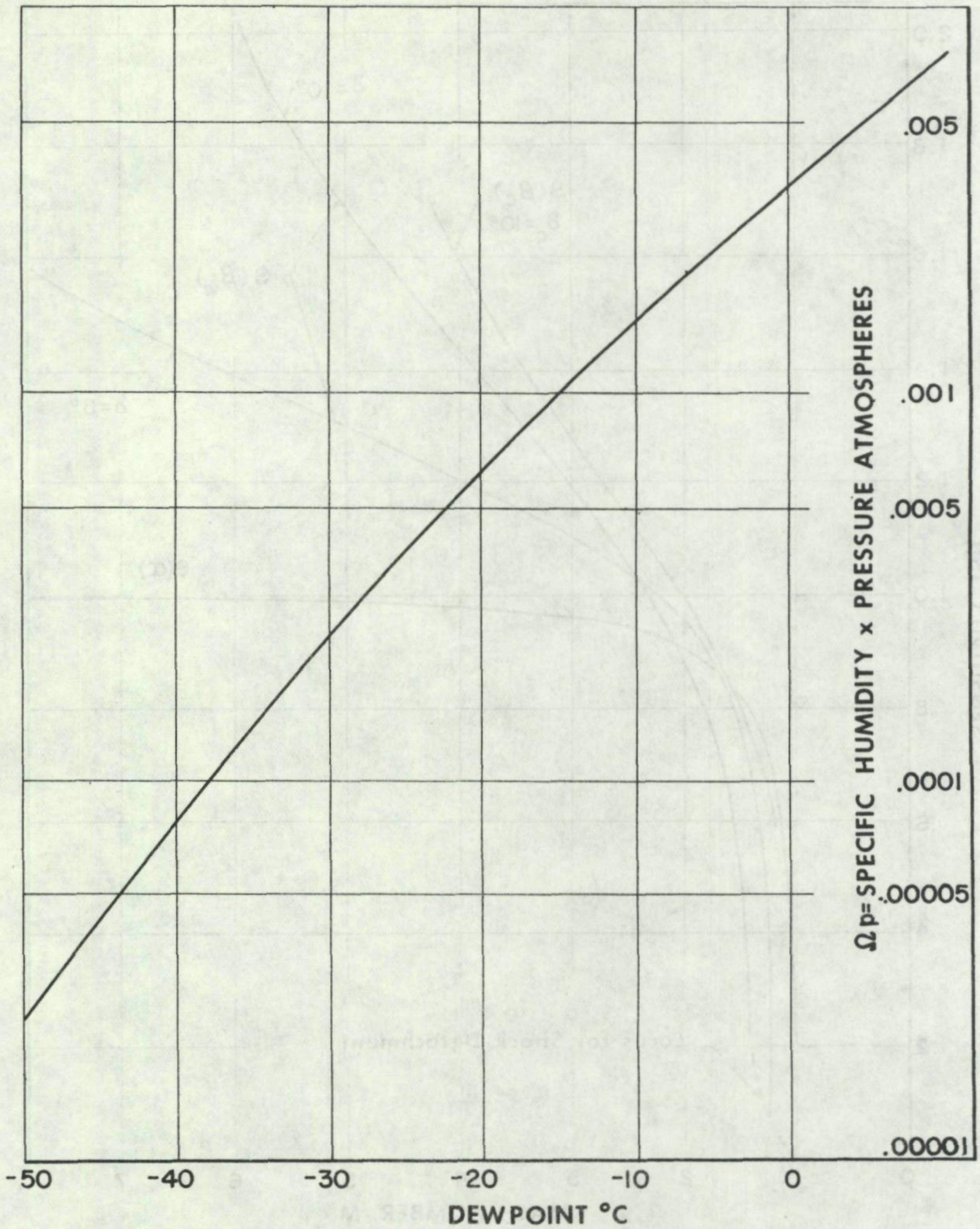

Fig. IV-1. Specific humidity, Ω , as a function of dewpoint.

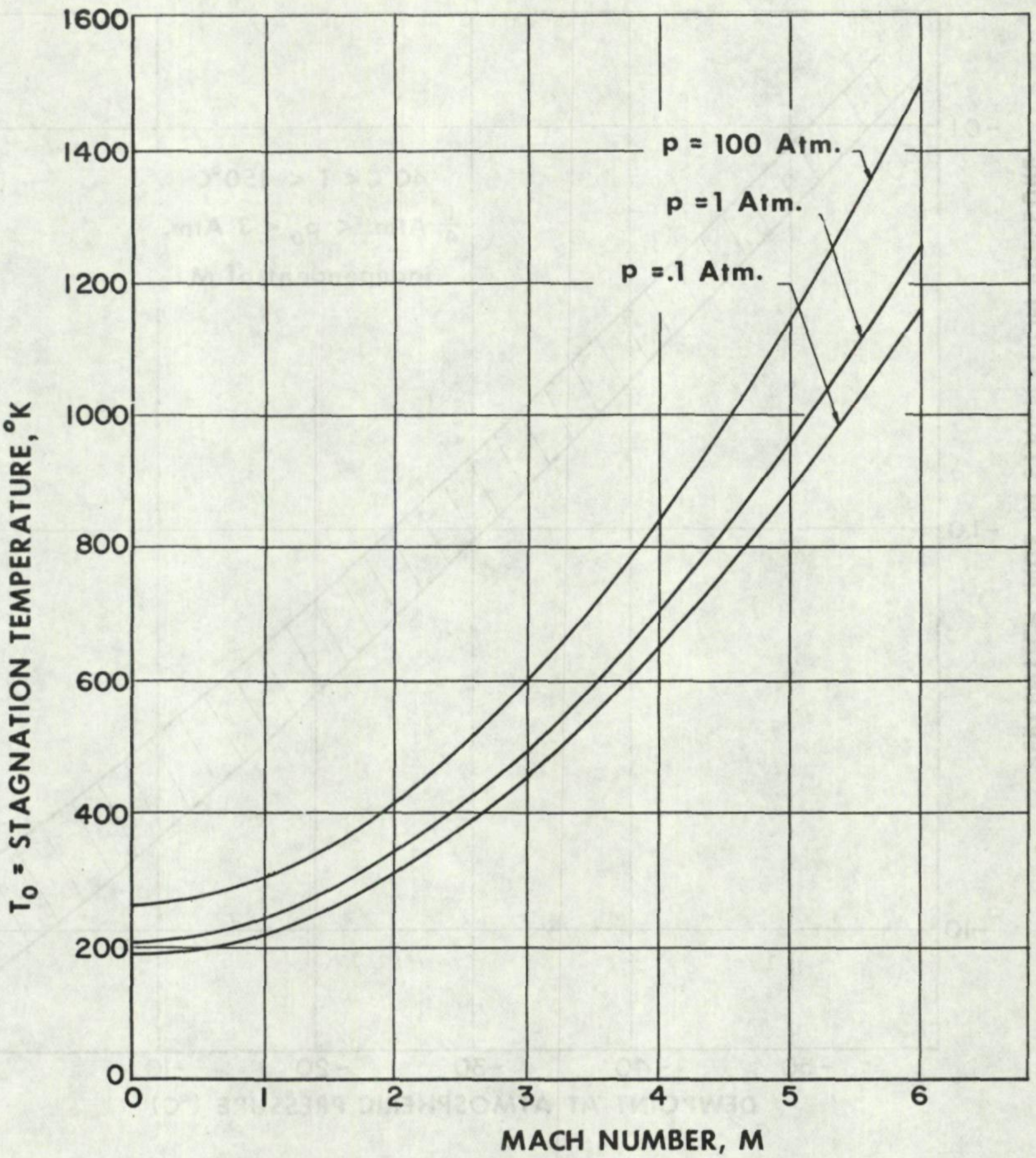

Fig. IV-2. Stagnation temperature for water condensation.
Free flow for specific humidity = .0001.

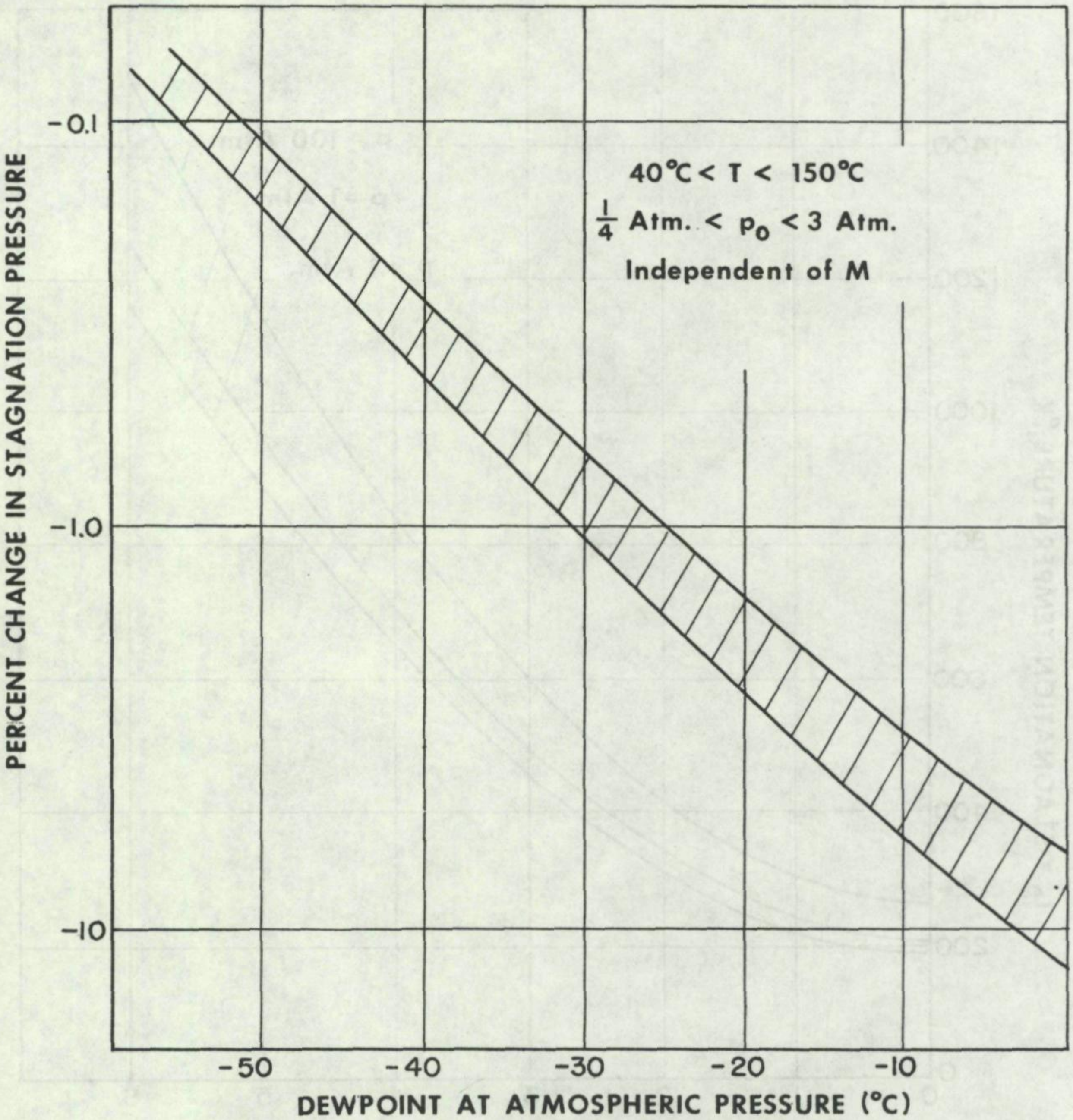

Fig. IV-3. Order of magnitude of the stagnation pressure loss accompanying water vapor condensation in supersonic wind tunnels.

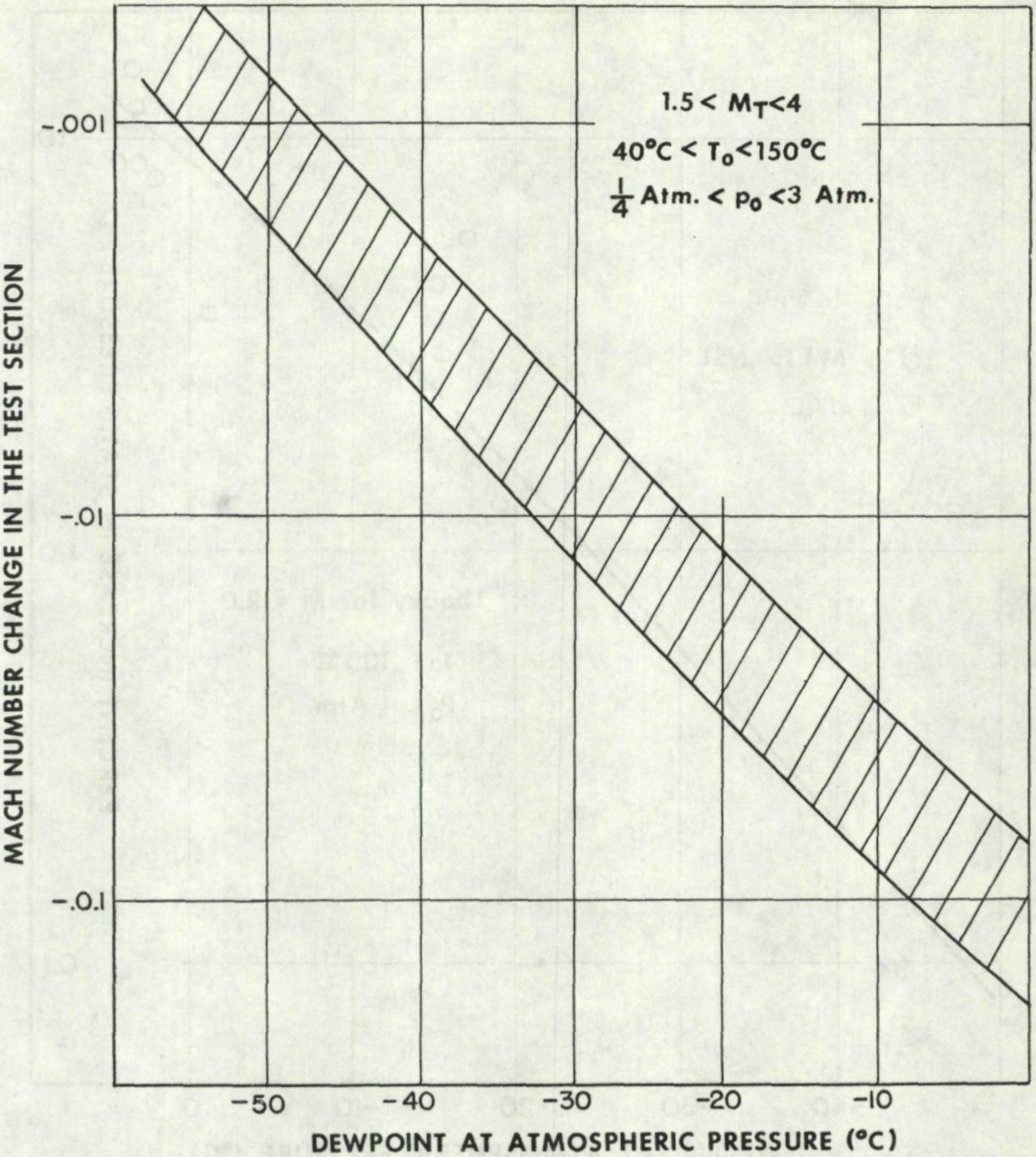

Fig. IV-4. Order of magnitude of the effects of water vapor condensation on test section Mach number in supersonic wind tunnels.

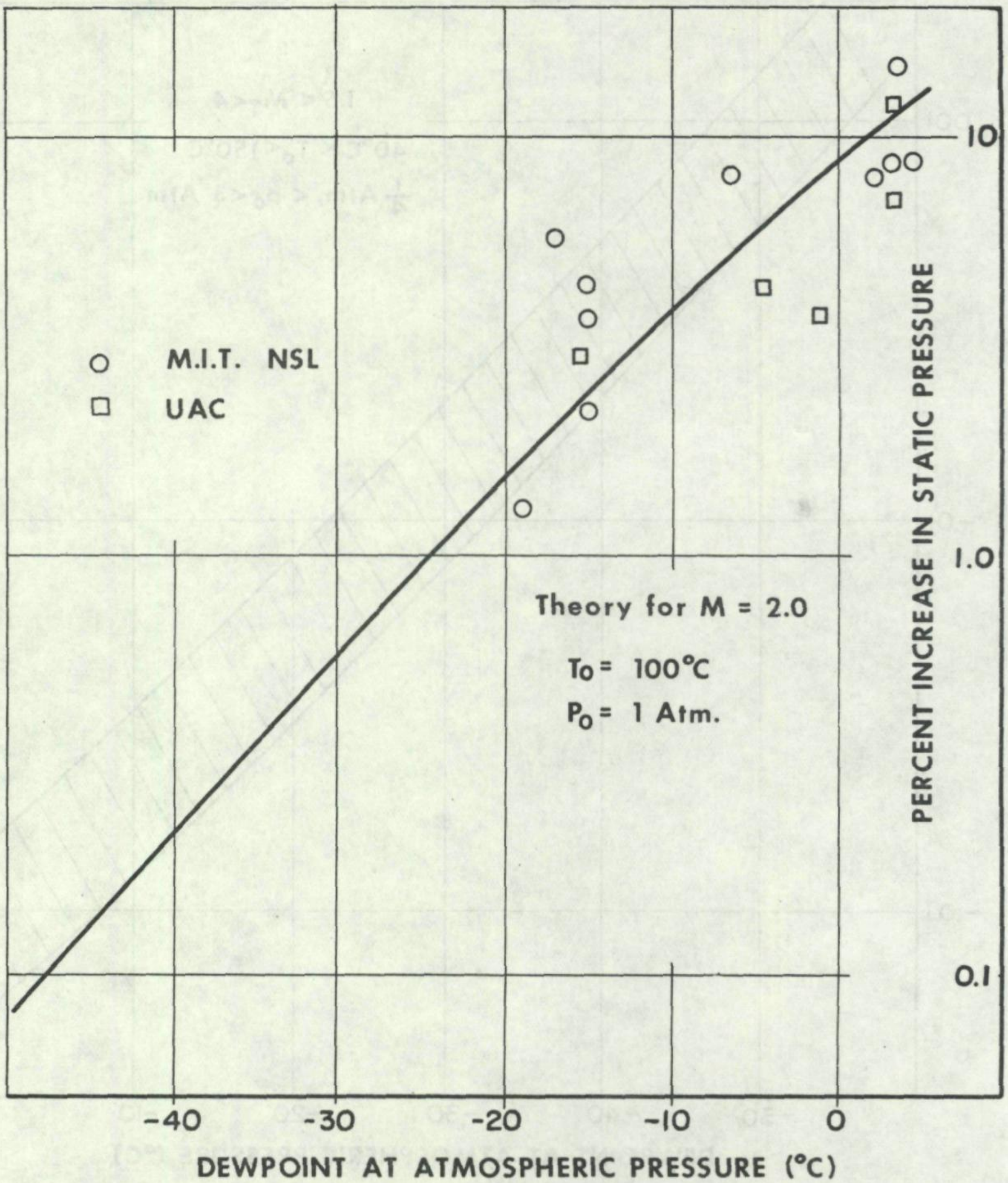

Fig. IV-5. Effects of water vapor condensation on test section static pressure (experimental).

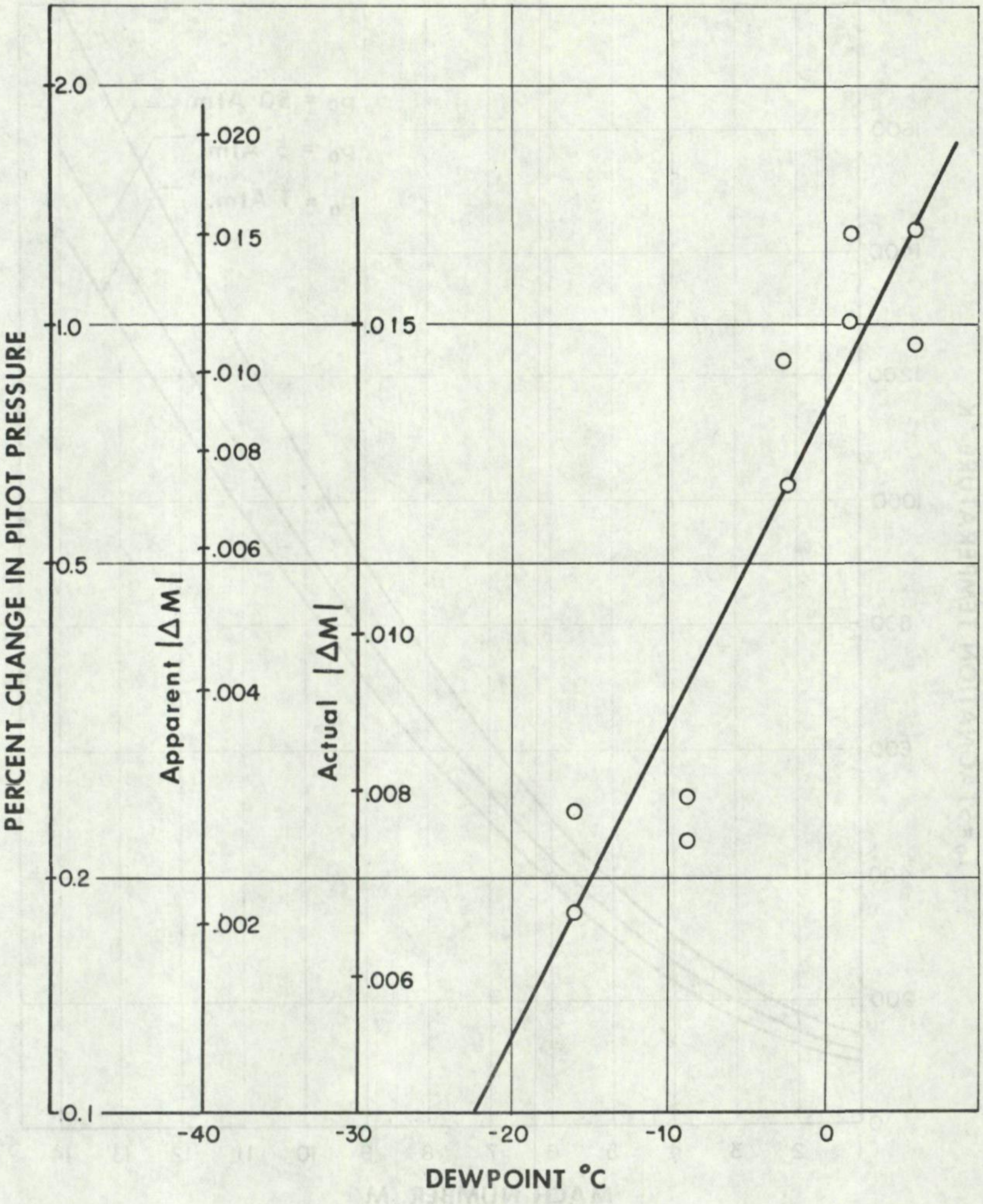

Fig. IV-6. Effect of water vapor condensation on pitot pressure in a M = 3.25 nozzle.

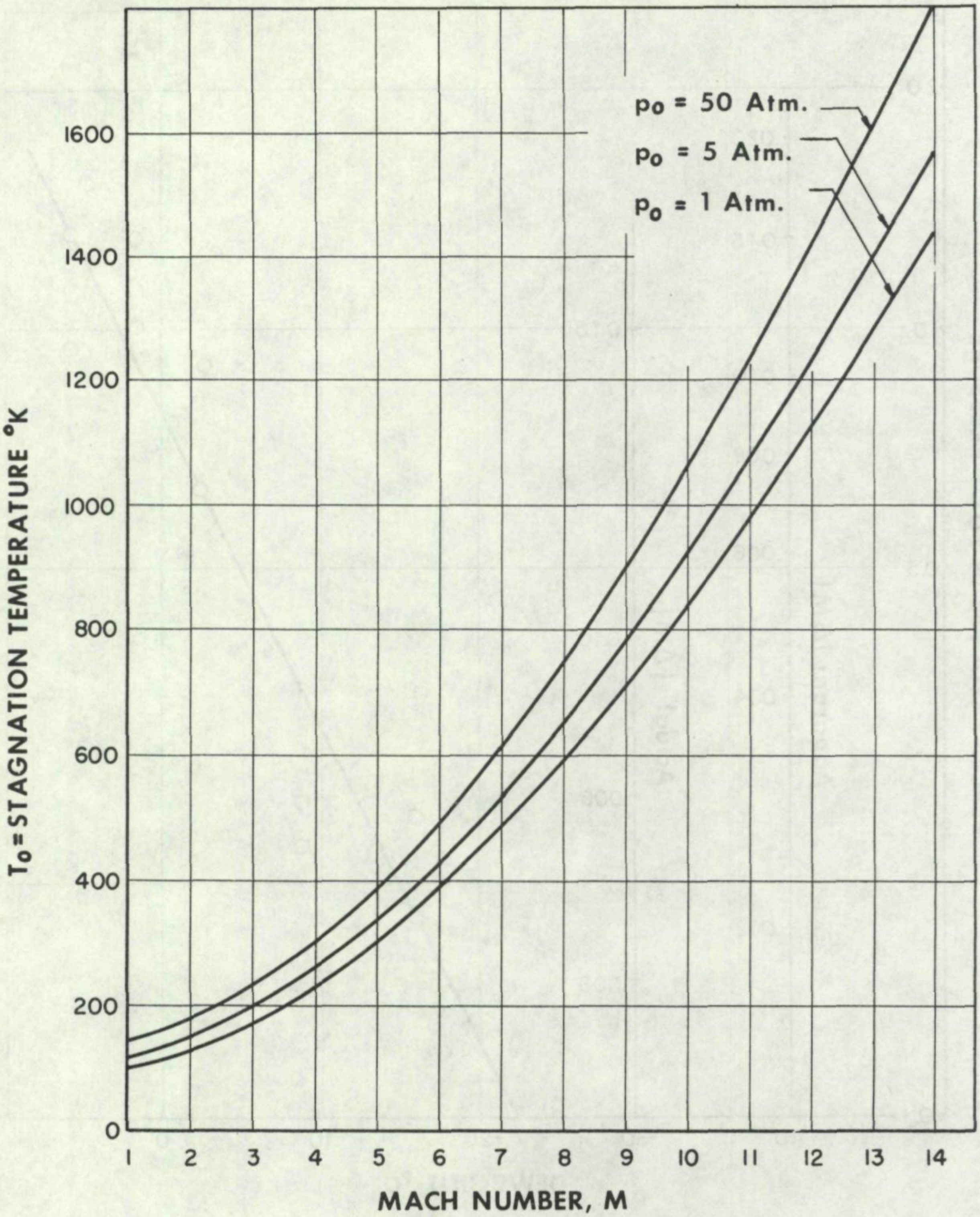

Fig. IV-7. Stagnation temperature for flow free of air condensation.

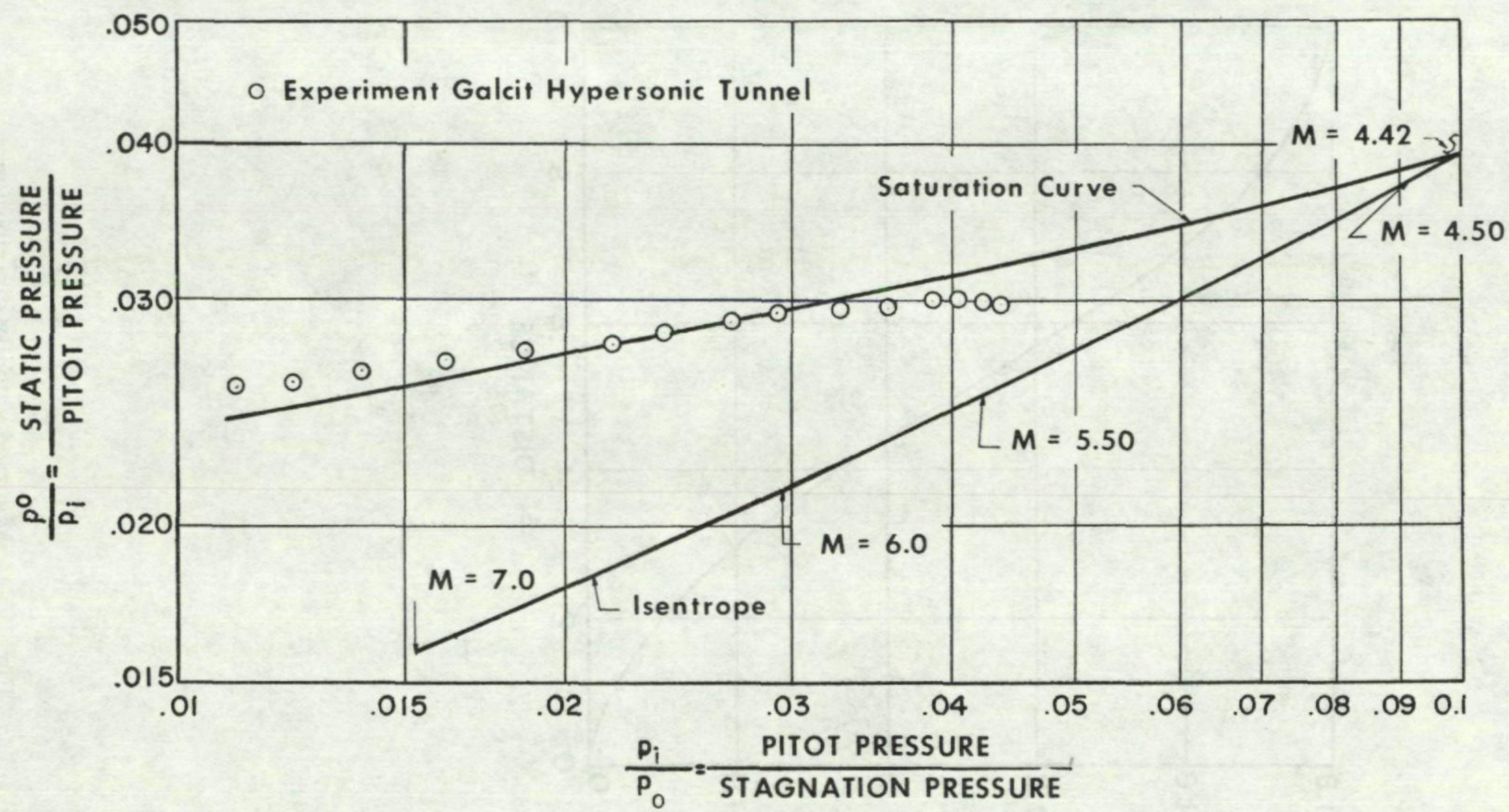

Fig. IV-8. Static-pitot pressure ratio versus pitot-stagnation pressure ratio, T_0 = 300° K, P_0 = 10.7 atm.

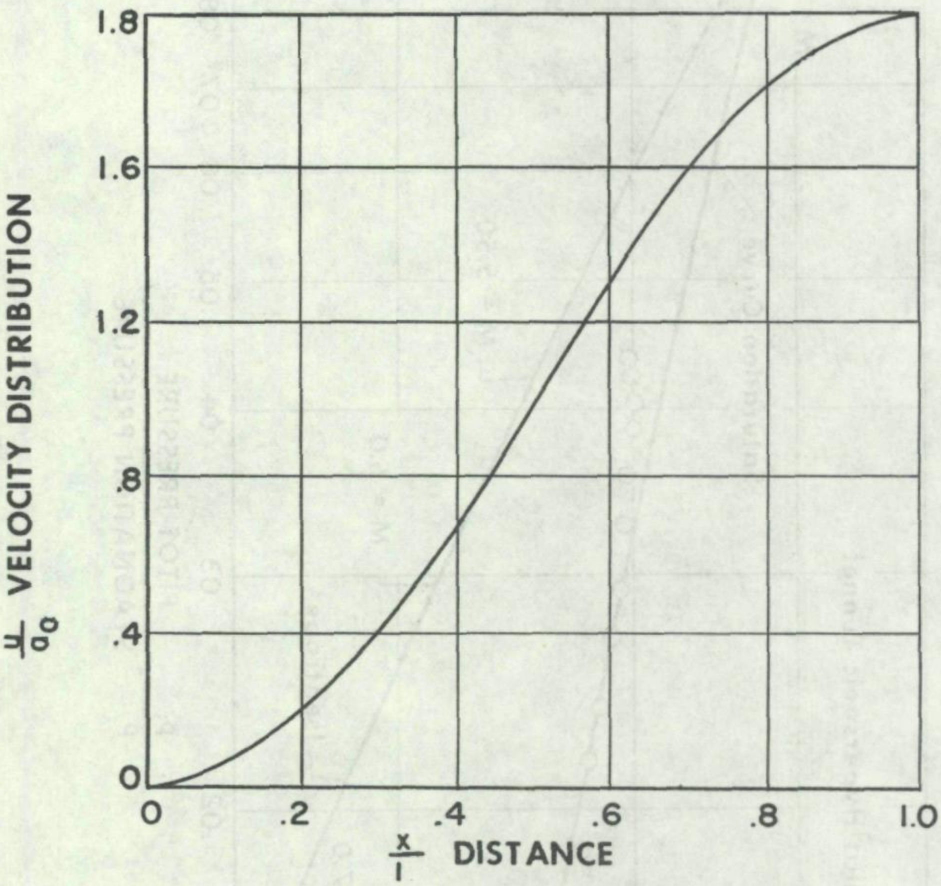

Fig. IV-9. Assumed velocity distribution.

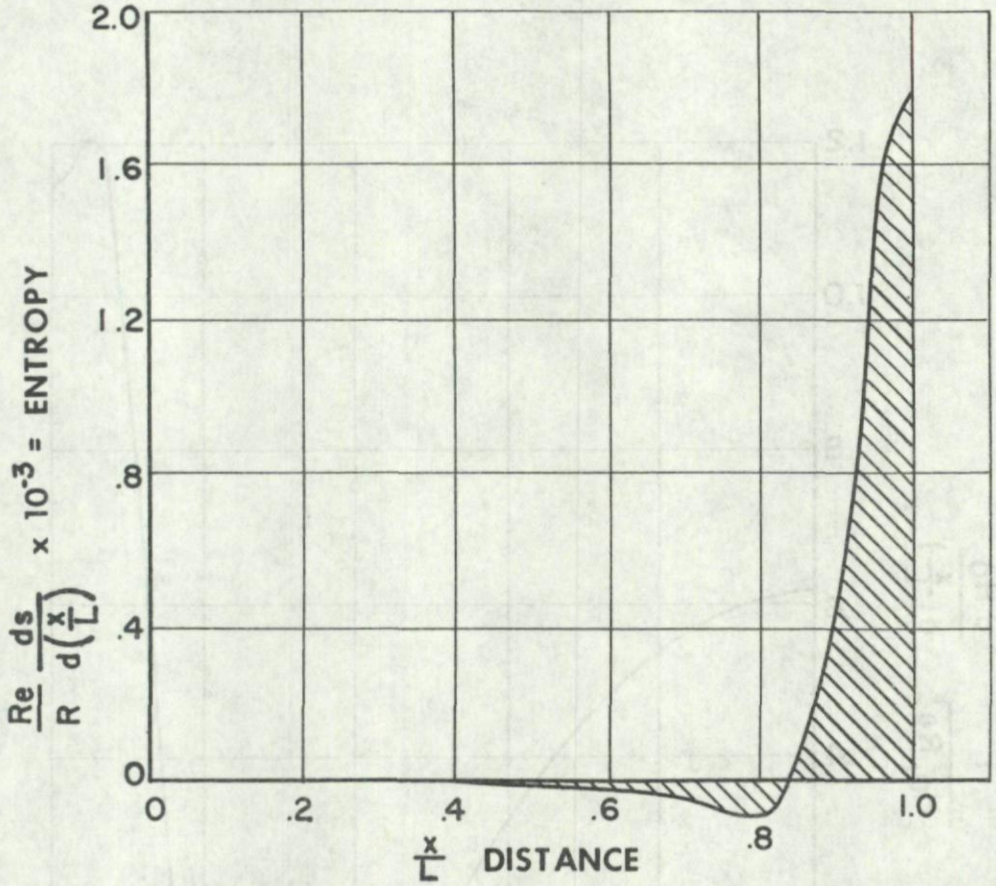

Fig. IV-10. Entropy change along the nozzle.

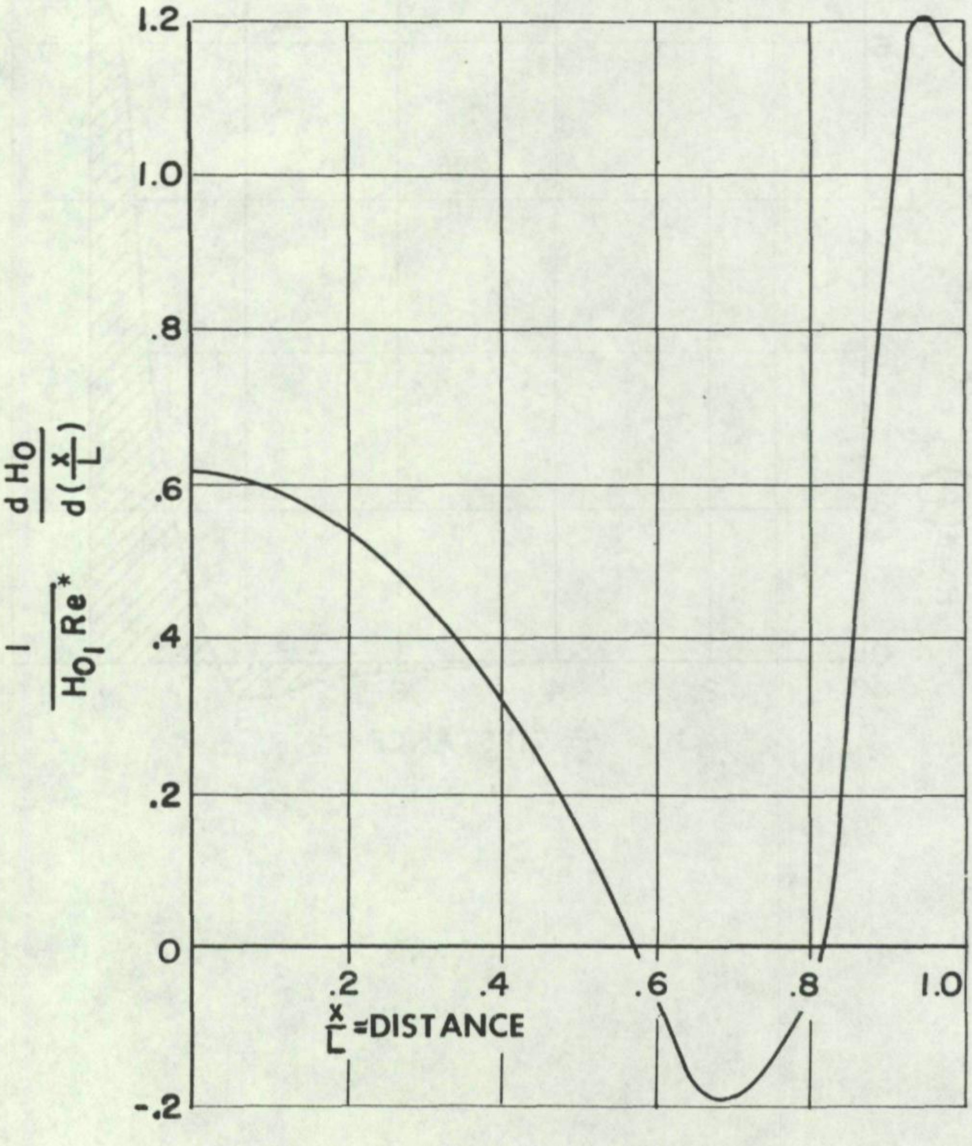

Fig. IV-11. Change in total enthalpy along the nozzle.

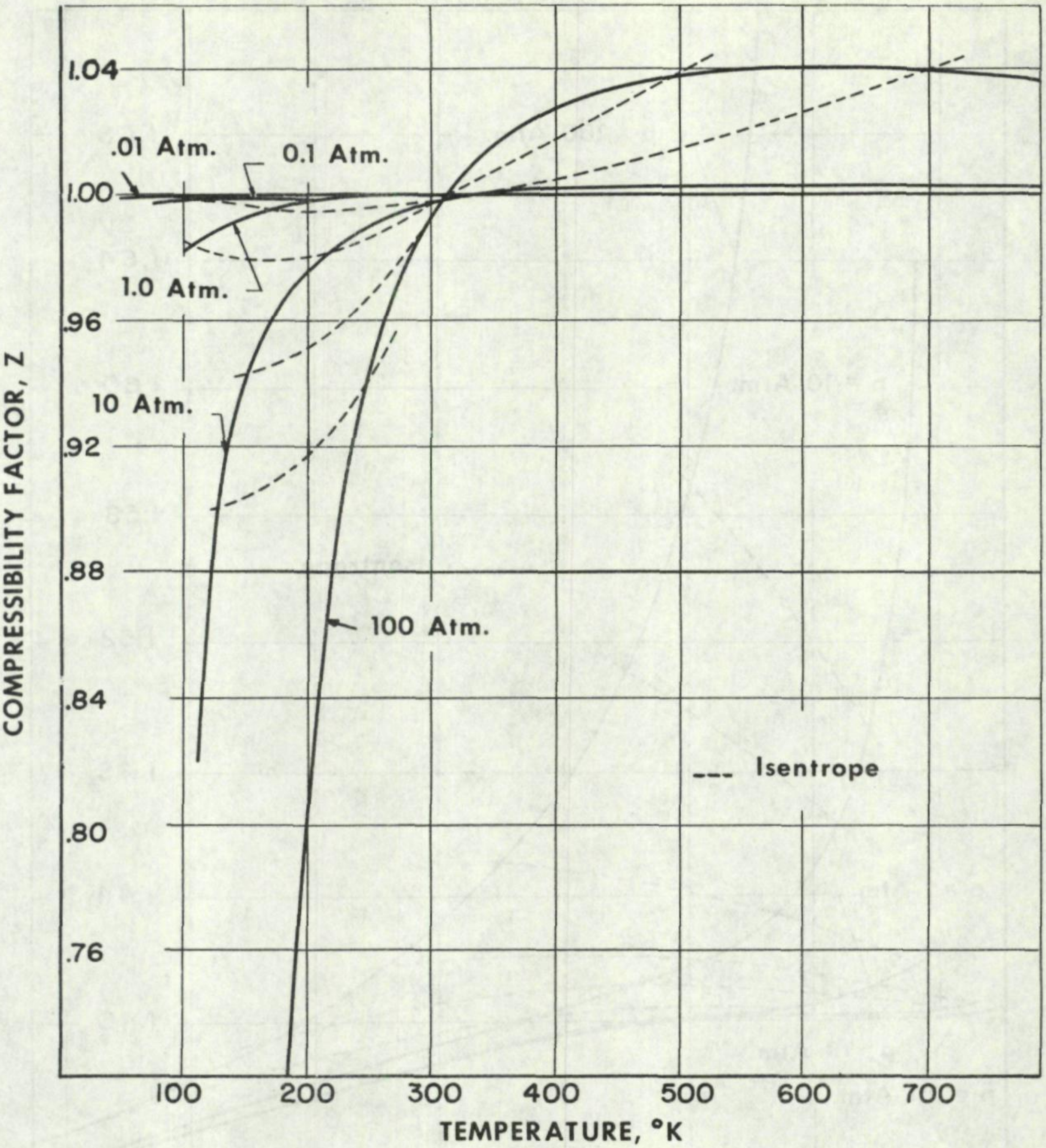

Fig. IV-12. Compressibility factor for air.

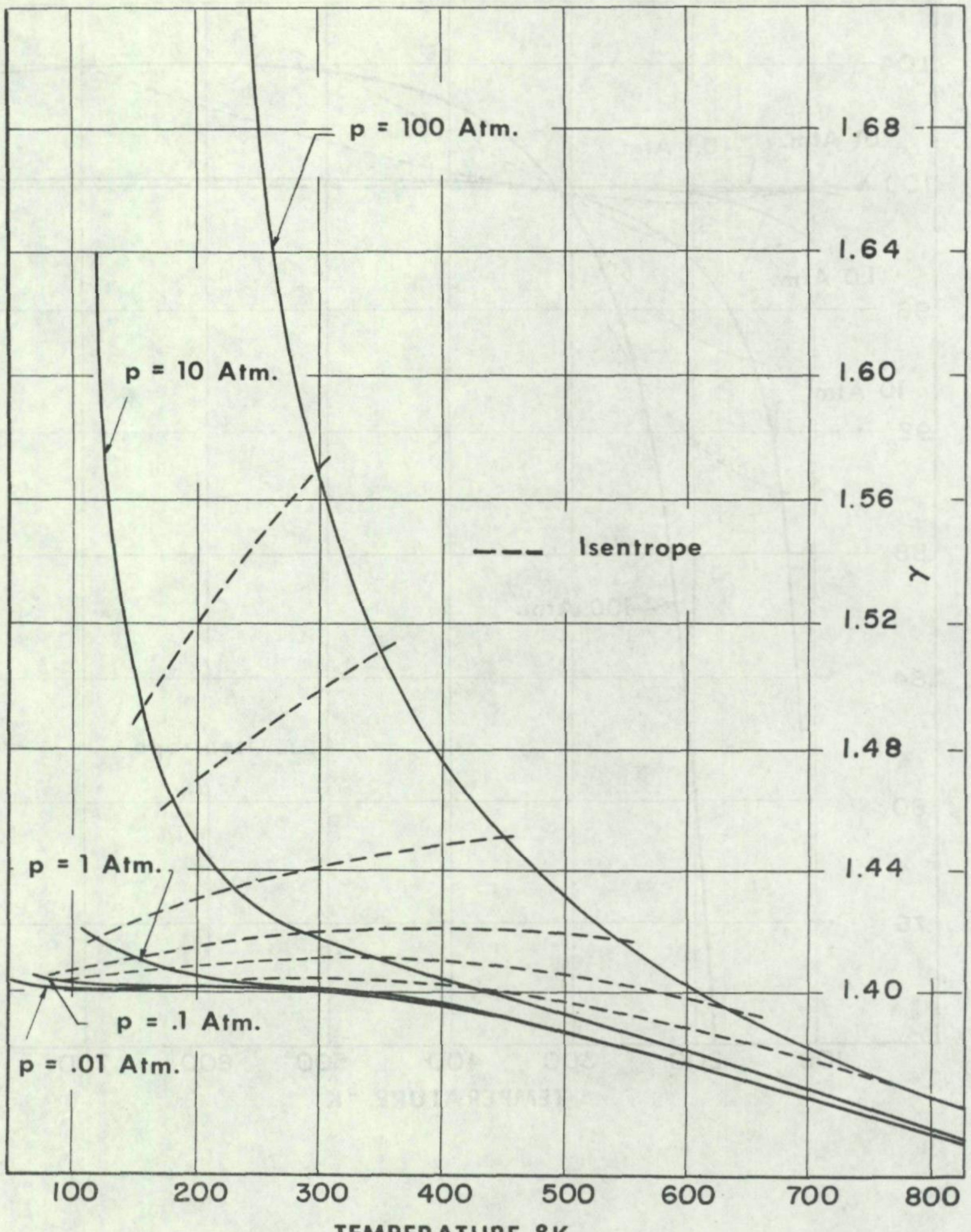

Fig. IV-13. Ratio of specific heats for air.

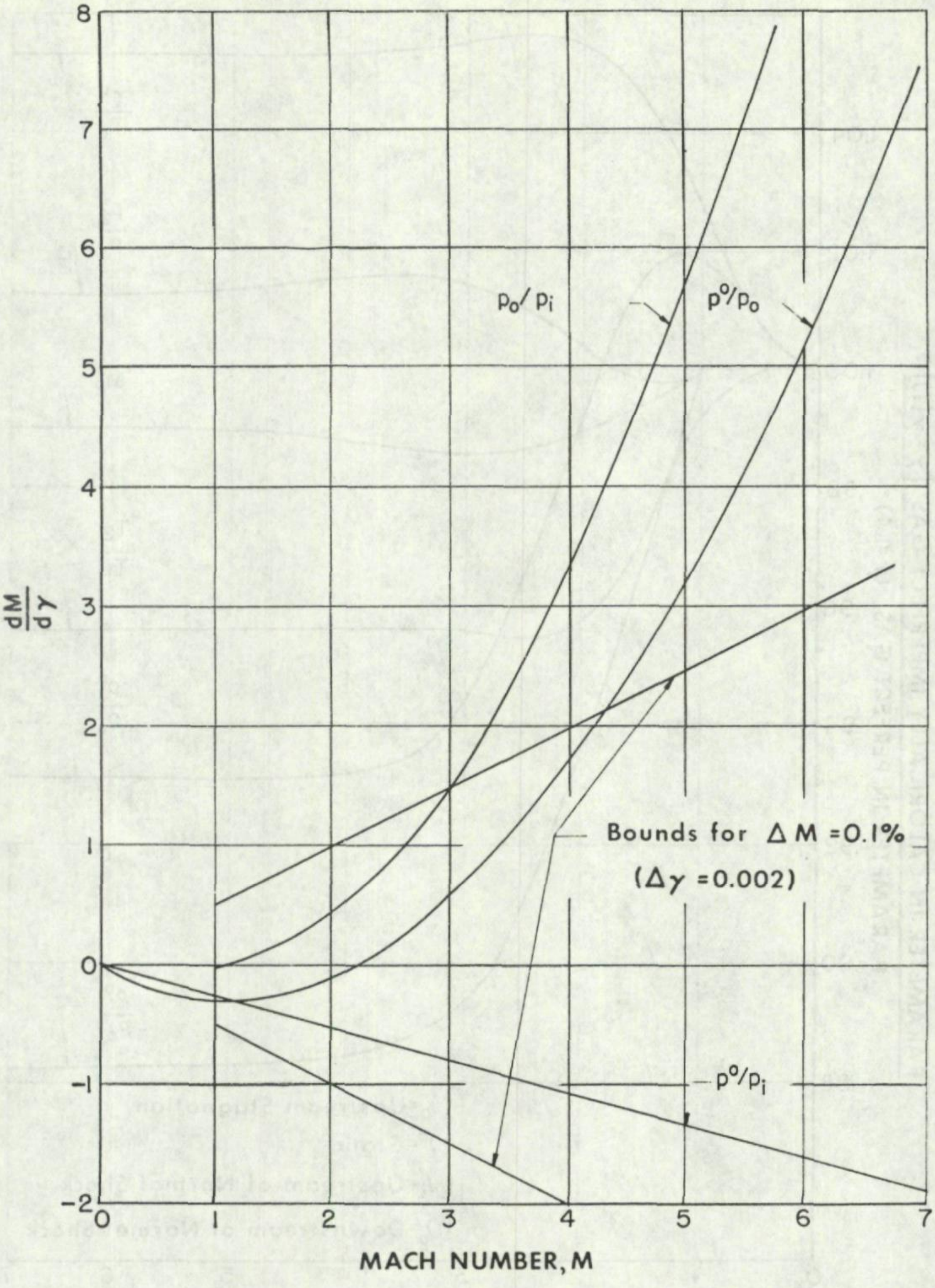

Fig. IV-14. Effect of γ uncertainty upon Mach number, assuming a constant γ process.

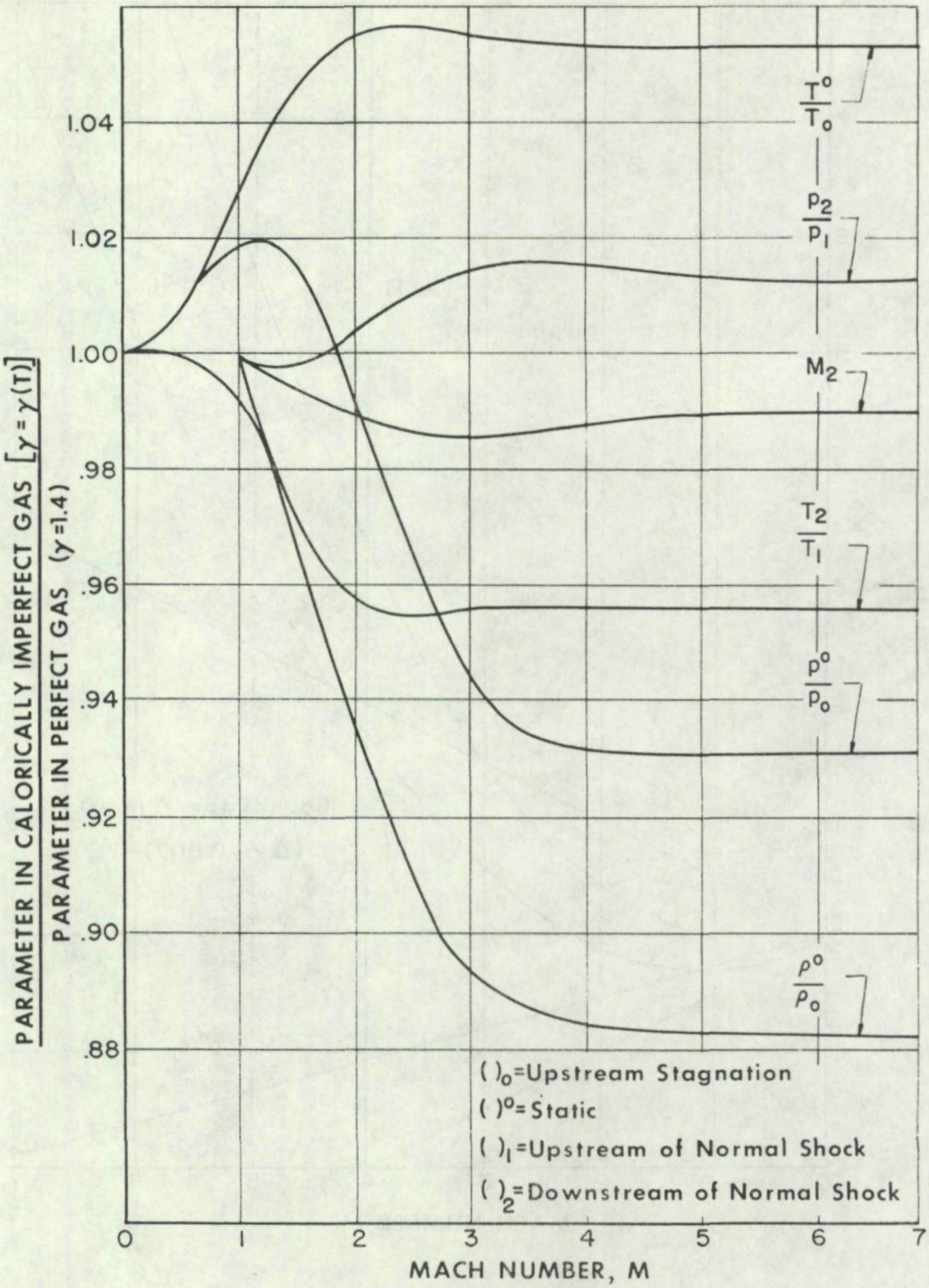

Fig. IV-15. Effects of caloric imperfections at T_0 = 1111° K.

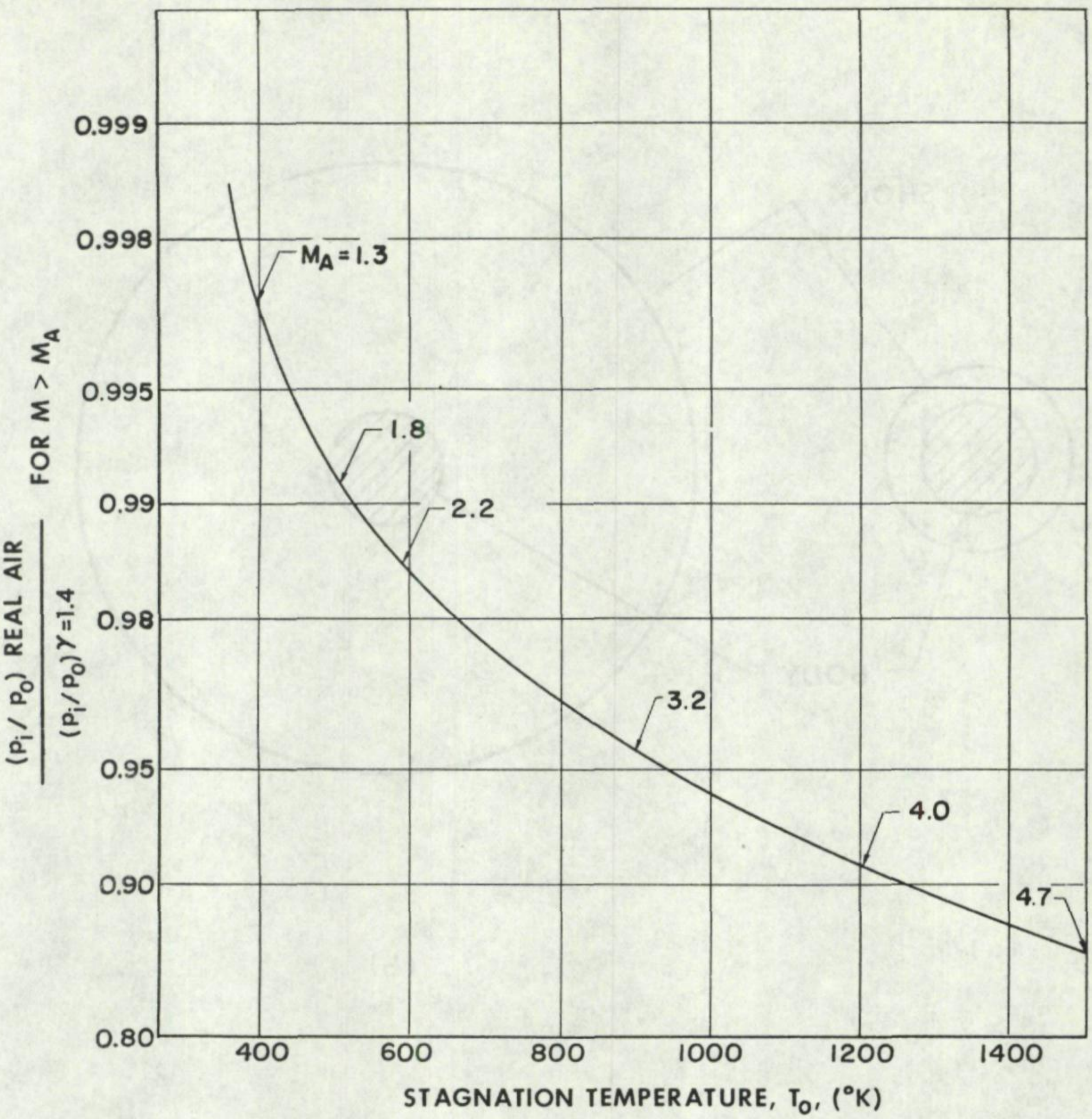

(Based on a real air isentrope passing through the state T = 300° K, p = .076 atmosphere and on the assumption that the recompression is very rapid compared with the relaxation time.)

Fig. IV-16. Asymptotic effect of high stagnation temperatures on the ratio of pitot pressure to stagnation pressure, p_i/p_o.

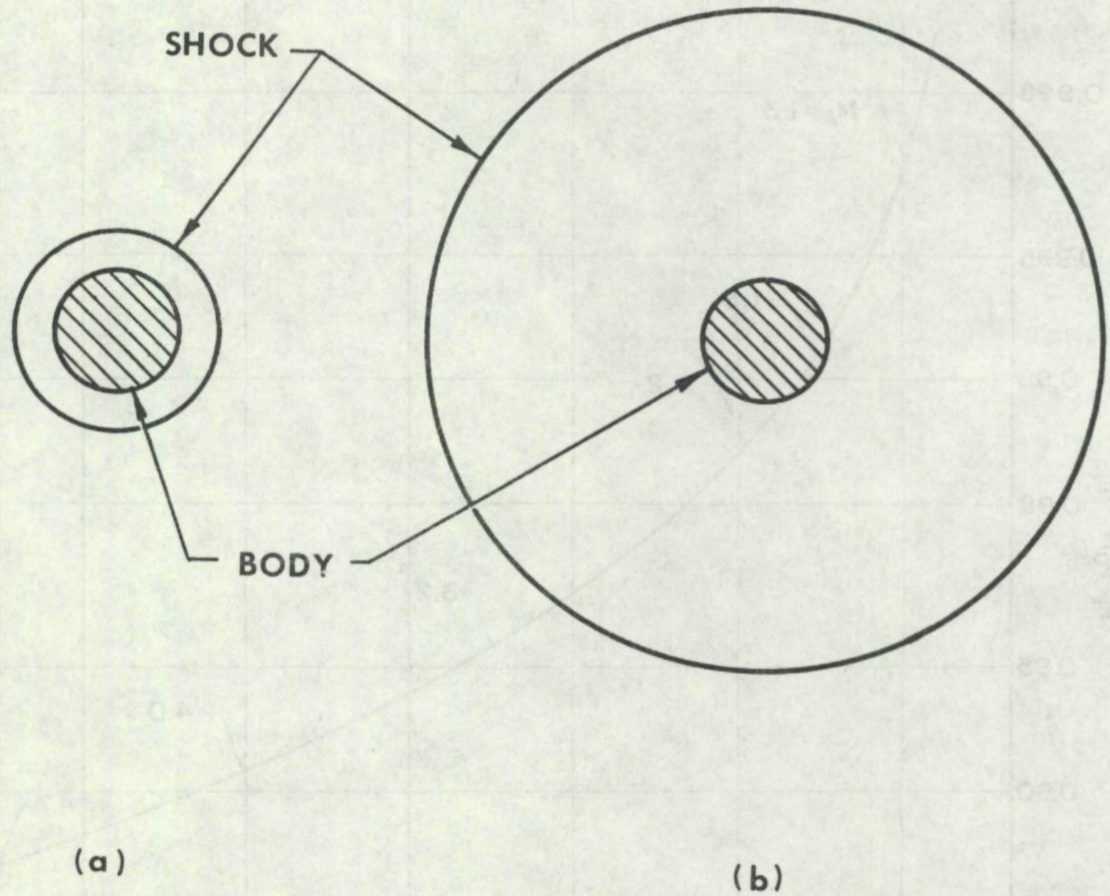

Fig. IV-17. Body and shock surface relations.

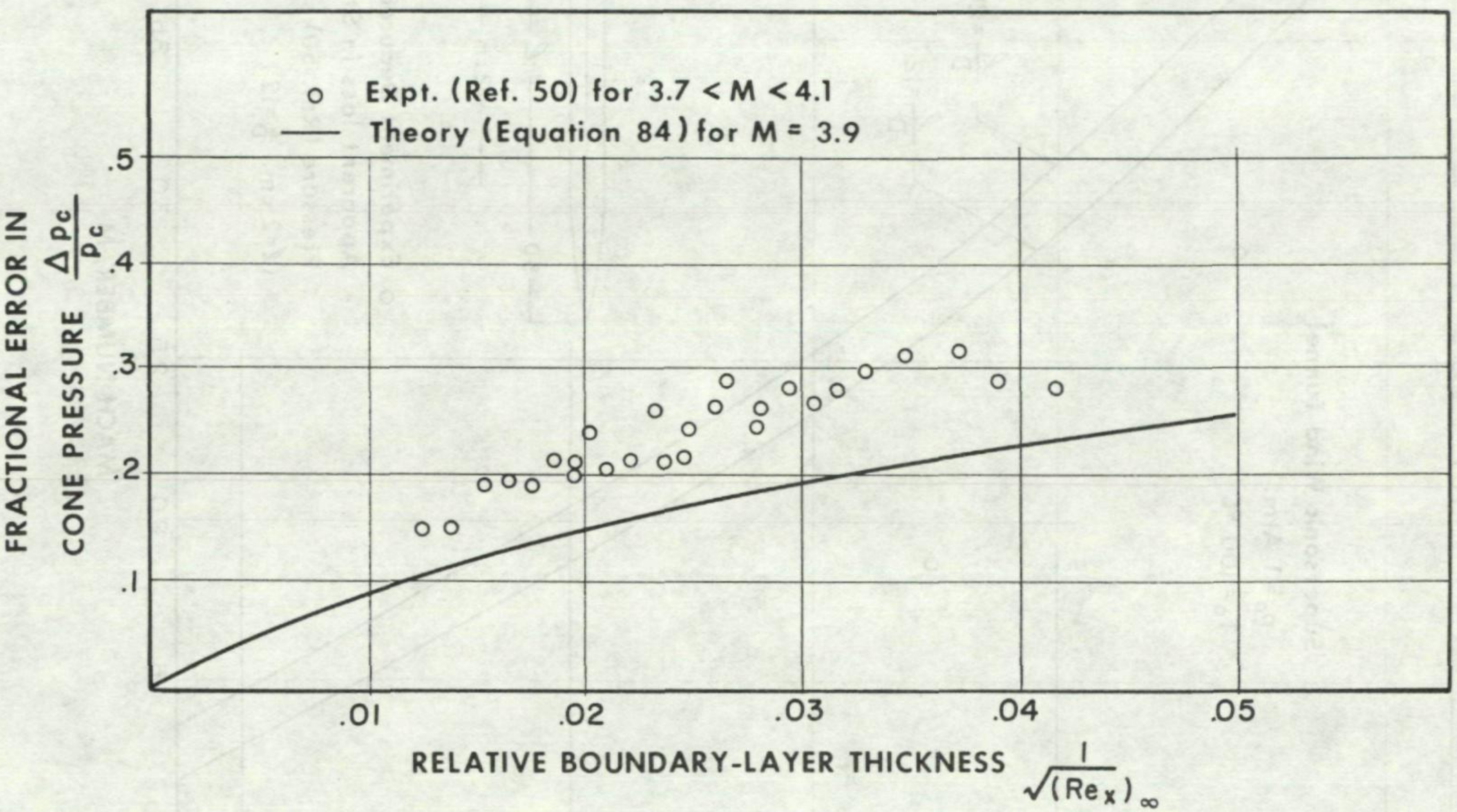

Fig. IV-18. Boundary layer displacement effect on surface pressures. Comparison of theory and experiment for 5° cone at $3.7 < M < 4.1$.

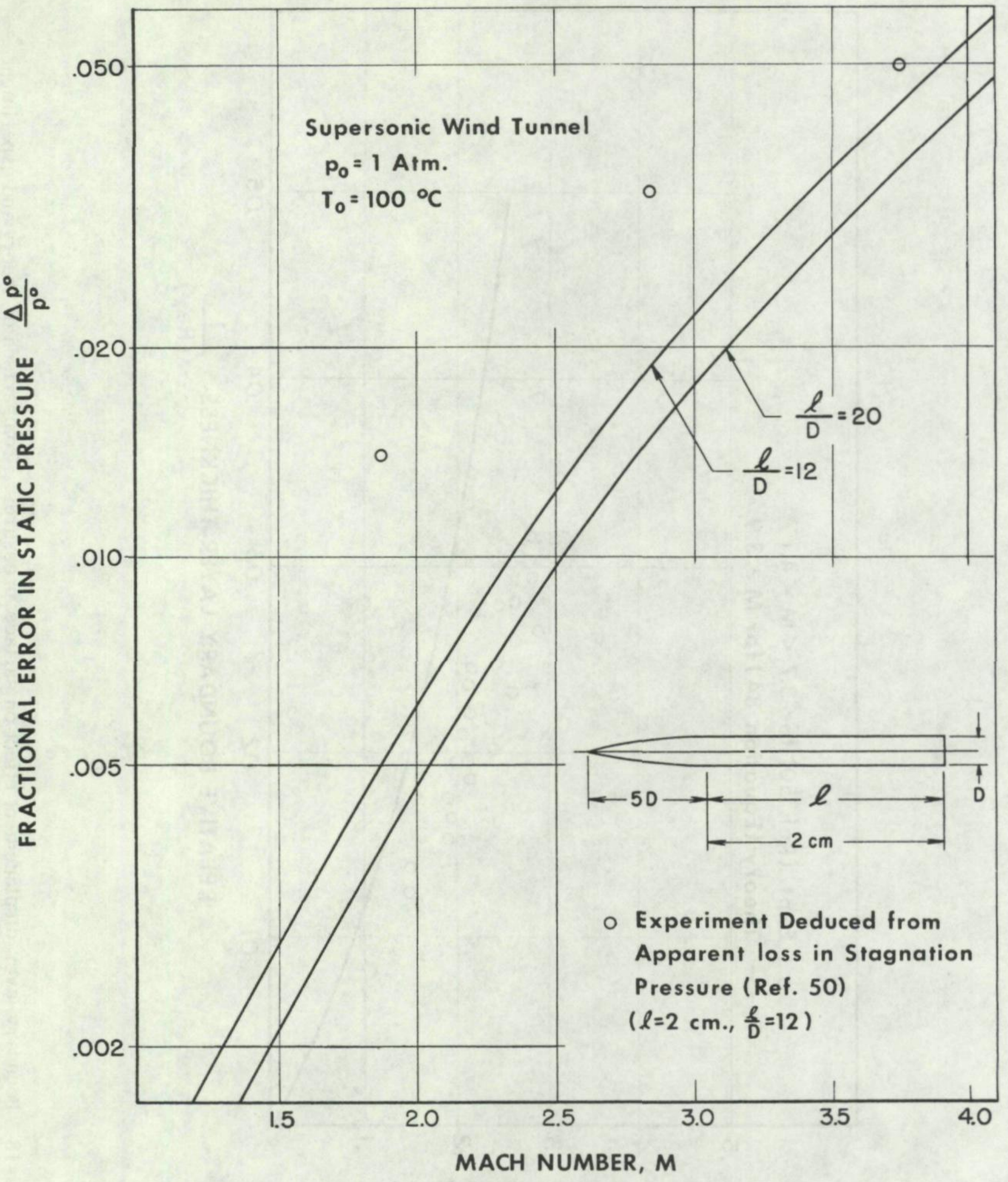

Fig. IV-19. Error in static pressure measurement due to boundary layer displacement effect.

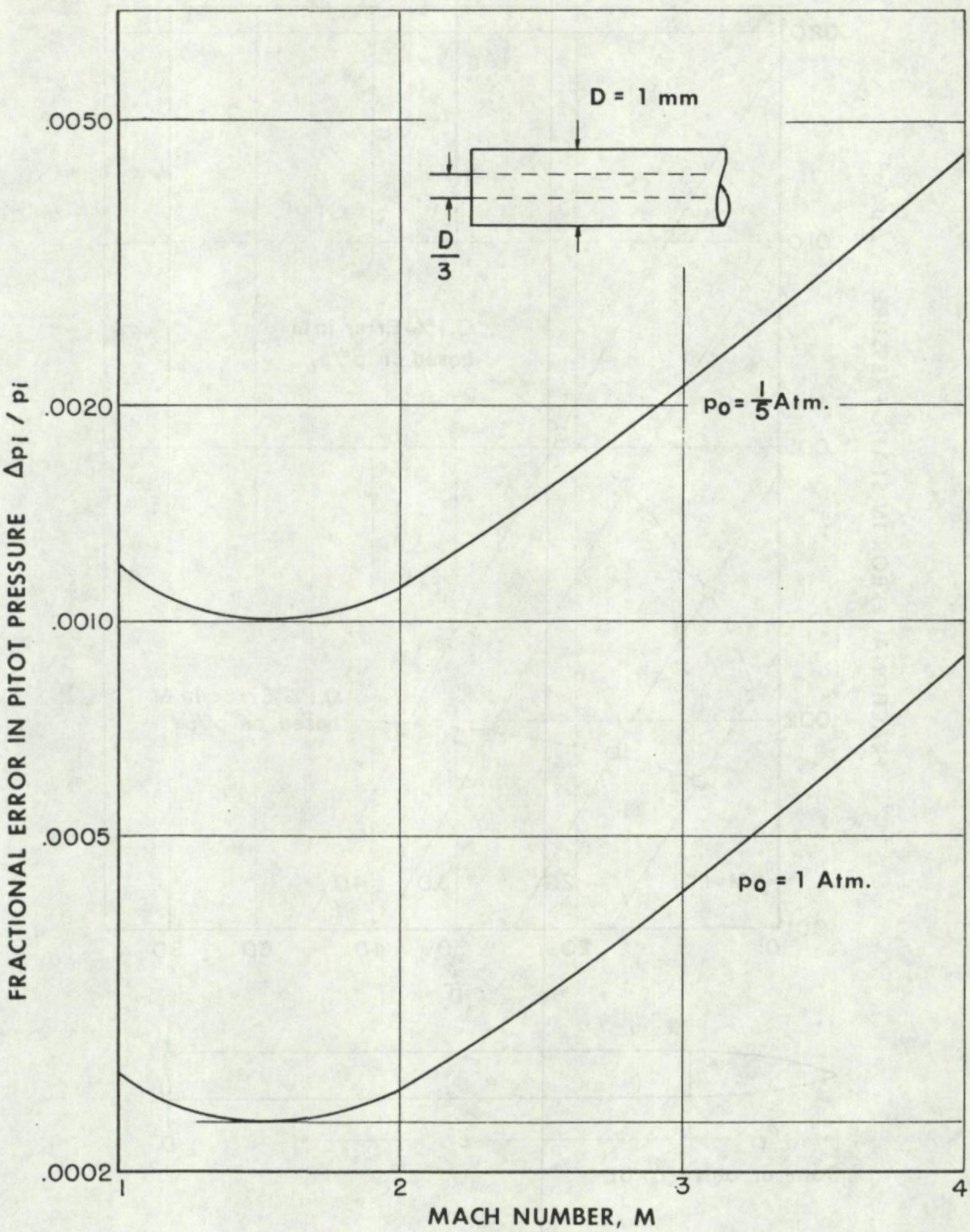

Fig. IV-20. Error in pitot pressure due to viscous effects at the probe.

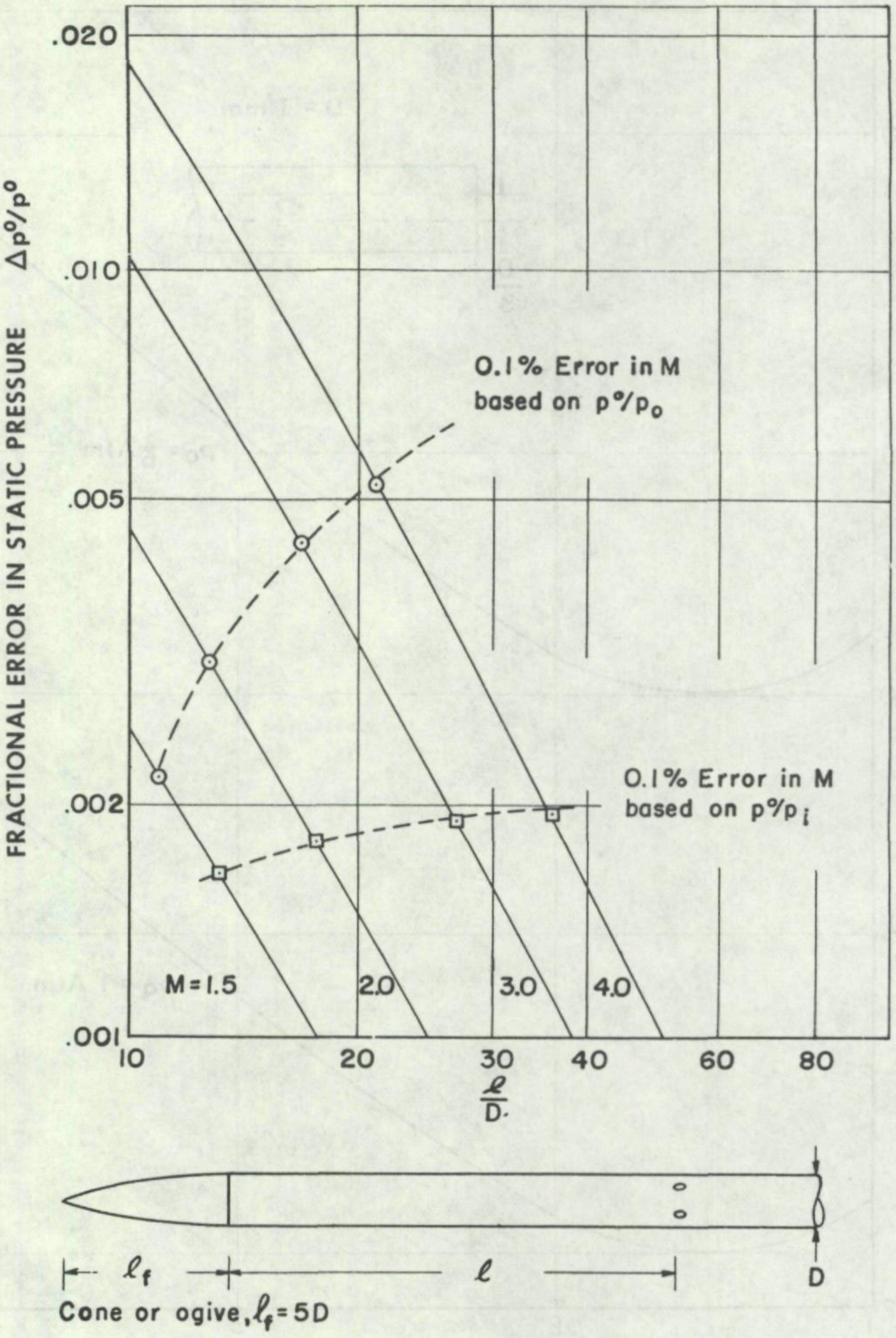

Fig. IV-21. Nose effect on static pressure probes in supersonic flow (based on slender-body theory).

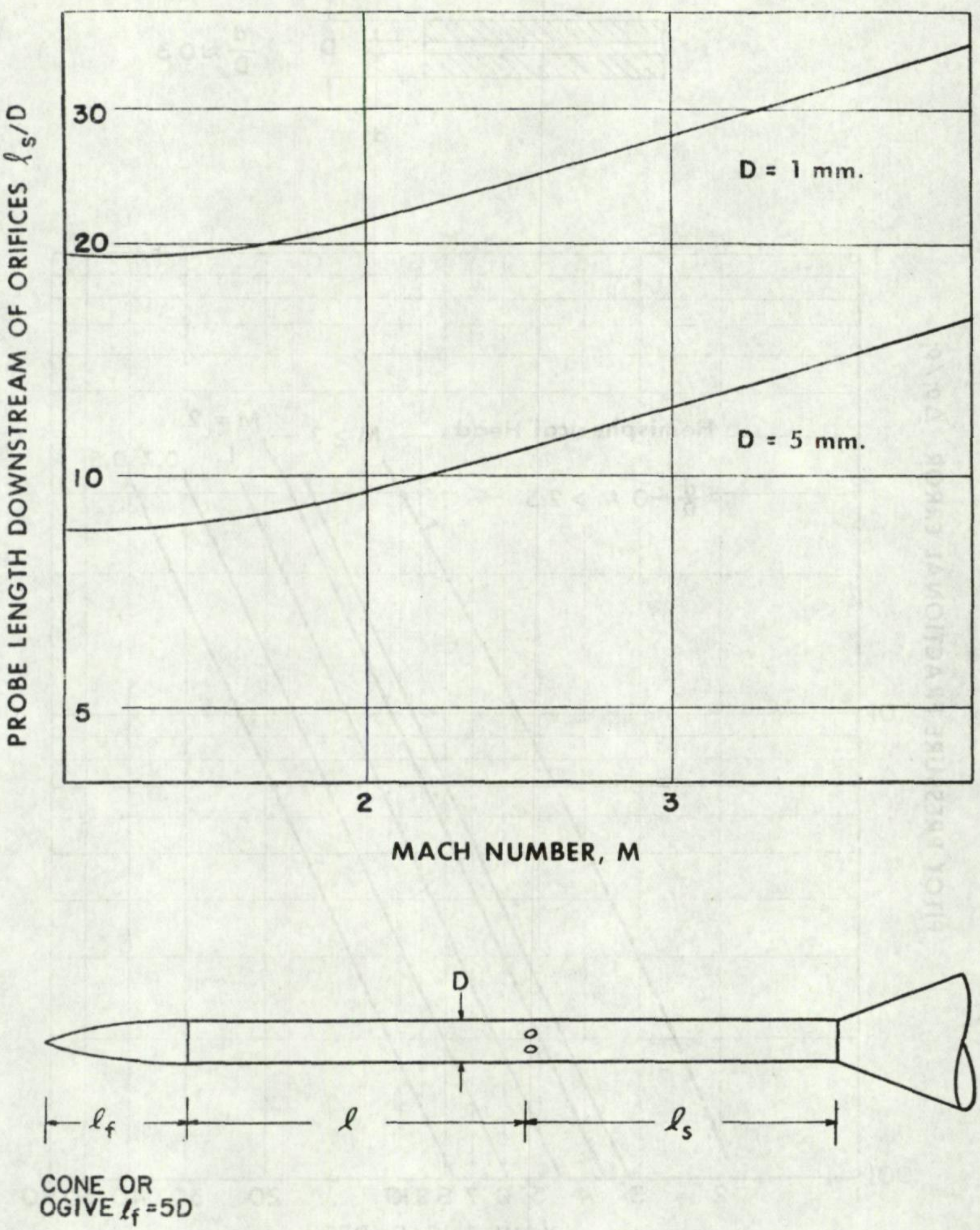

Fig. IV-22. Required length of static probe to avoid support interference through the boundary layer.

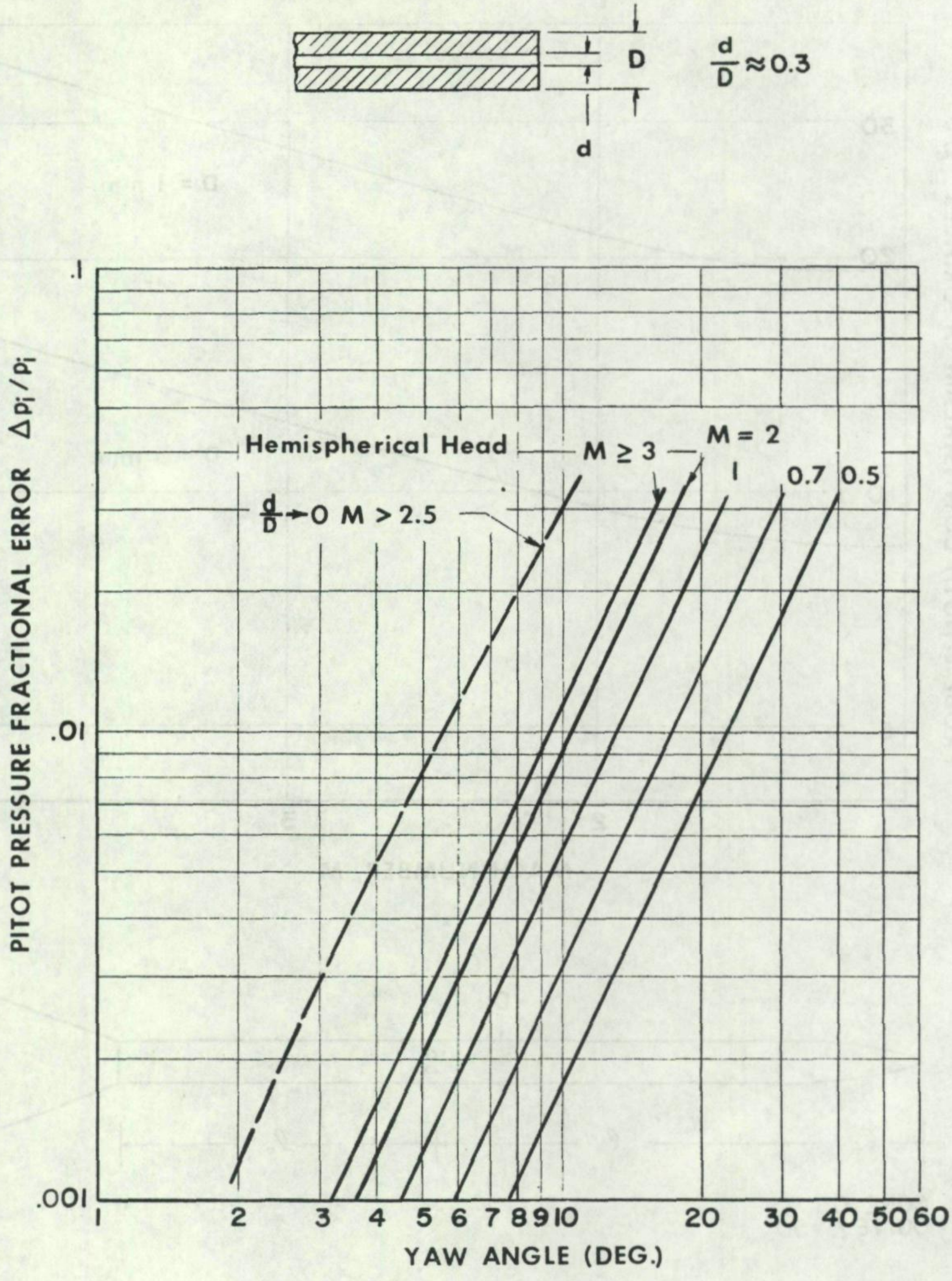

Fig. IV-23. Estimated error due to yaw of conventional pitot tubes.

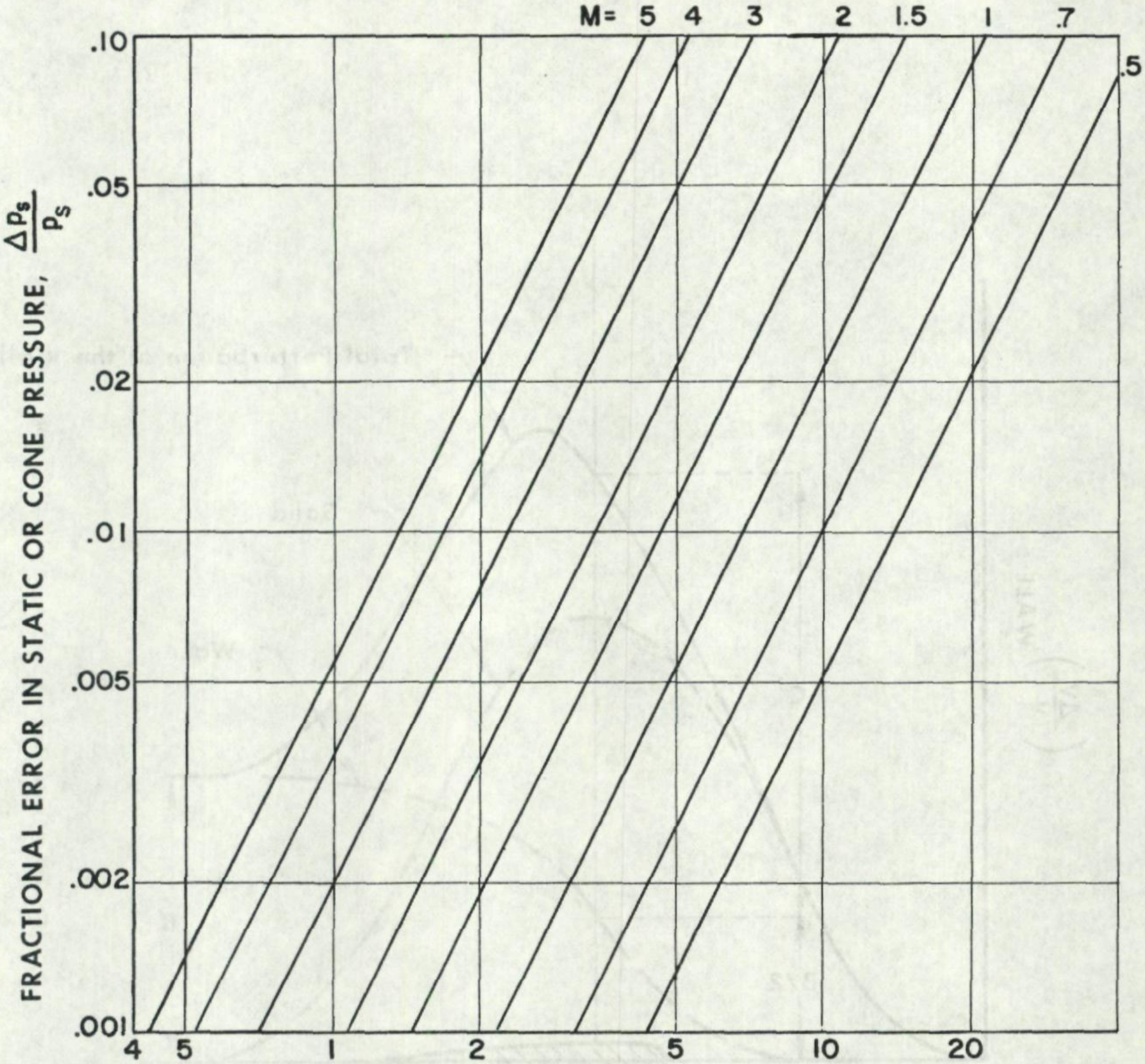

Fig. IV-24. Estimated error due to yaw of static probes and slender cones.

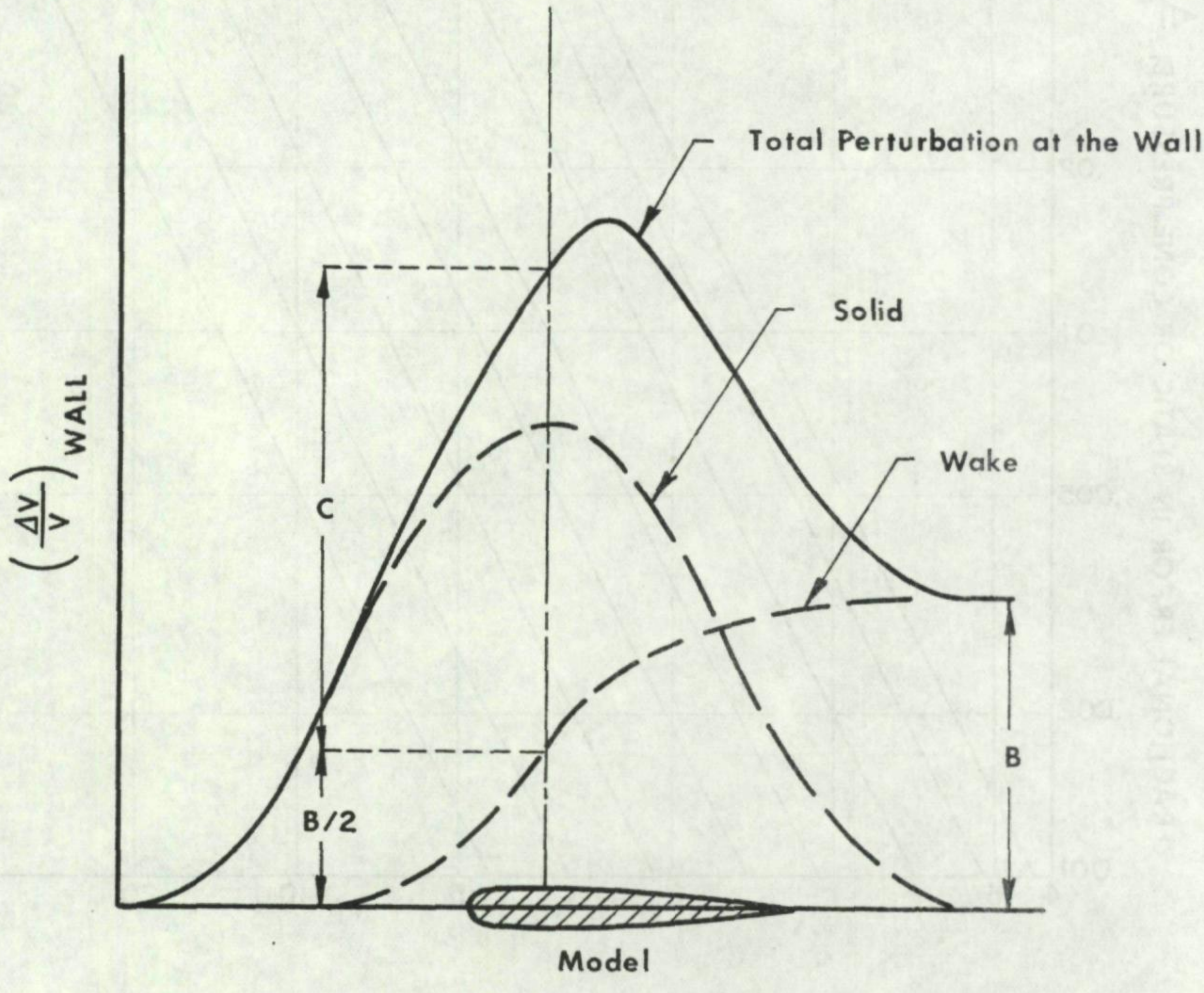

Fig. IV-25. Velocity perturbation at the wall.

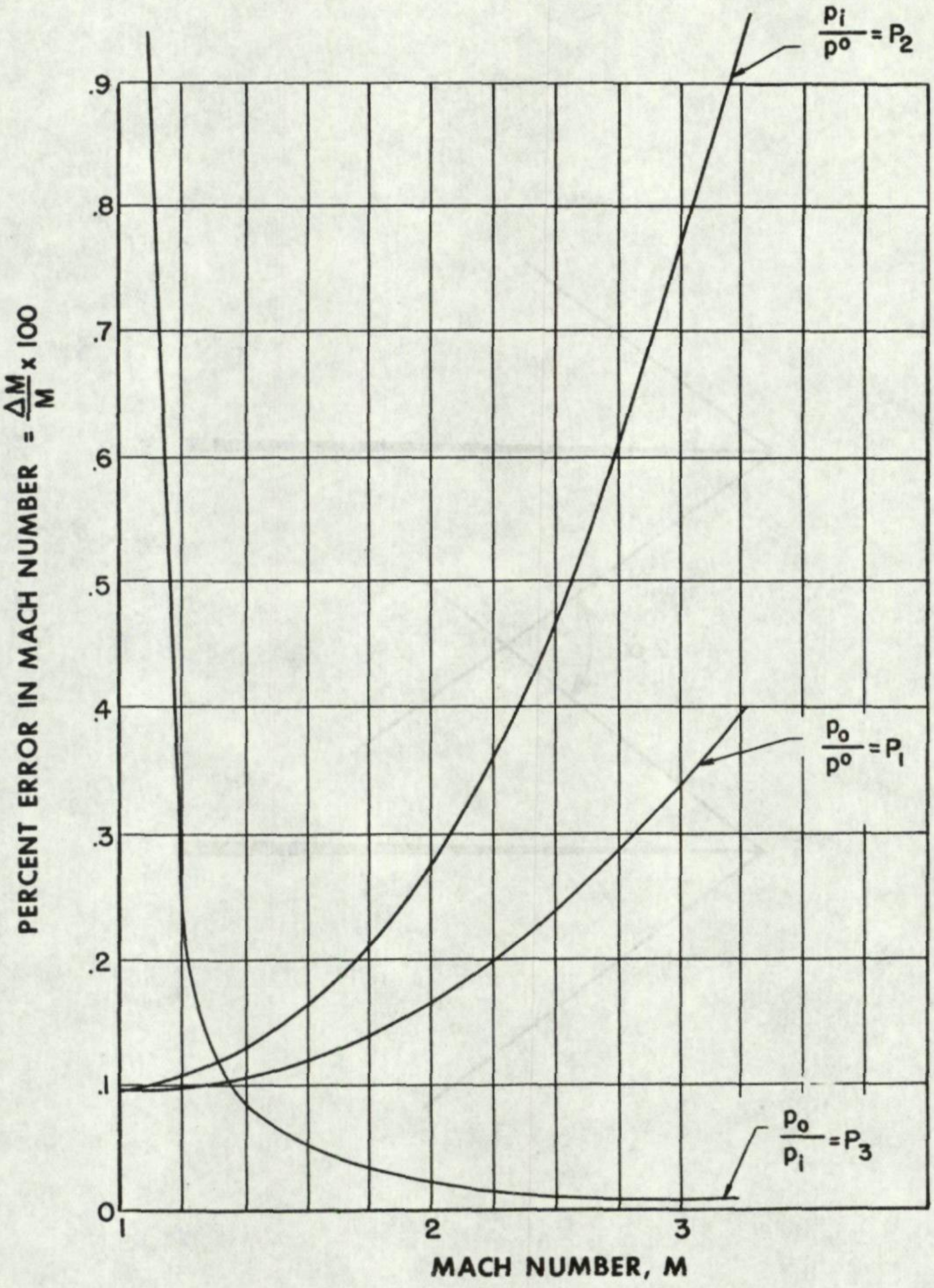

Fig. V-1. Error in Mach number for measuring accuracy giving $\Delta P/P$ = .0003 for each parameter and with boundary layer error on static probe.

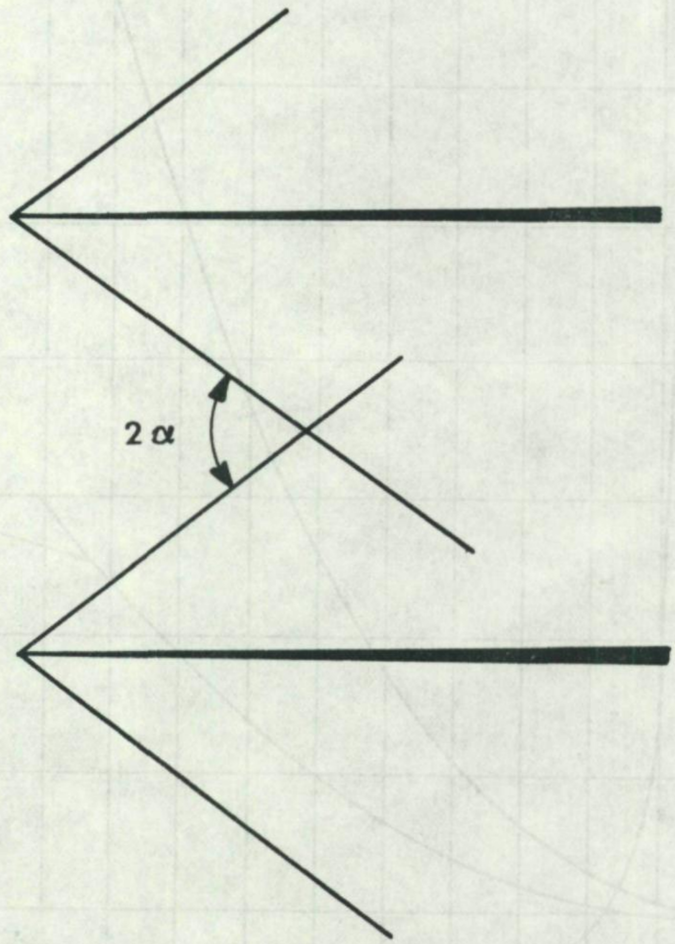

Fig. V-2. Generation of Mach waves.

Table I. Function of Mach Number

Thermo-dynamic Property	Isentropic Flow	Normal Shock (M > 1)	Heat Addition
$\frac{p_2}{p_1}$	$\left[\frac{1+\frac{\gamma-1}{2}M_1^2}{1+\frac{\gamma-1}{2}M_2^2}\right]^{\gamma/(\gamma-1)}$	$\frac{2\gamma M_1^2-(\gamma-1)}{\gamma+1}$	$\frac{1+\gamma M_1^2}{1+\gamma M_2^2}$
$\frac{p_2}{p_1}$	$\left[\frac{1+\frac{\gamma-1}{2}M_1^2}{1+\frac{\gamma-1}{2}M_2^2}\right]^{\frac{1}{\gamma-1}}$	$\frac{(\gamma+1)M_1^2}{2+(\gamma-1)M_1^2}$	$\frac{M_1^2}{M_2^2}\,\frac{(1+\gamma M_2^2)}{(1+\gamma M_1^2)}$
$\frac{T_2}{T_1}$	$\frac{1+\frac{\gamma-1}{2}M_1^2}{1+\frac{\gamma-1}{2}M_2^2}$	$\frac{\left[2+(\gamma-1)M_1^2\right]\left[2\gamma M_1^2-(\gamma-1)\right]}{(\gamma+1)^2M_1^2}$	$\frac{M_2^2}{M_1^2}\left[\frac{1+\gamma M_1^2}{1+\gamma M_2^2}\right]^2$
$\frac{a_2}{a_1}$	$\sqrt{\frac{1+\frac{\gamma-1}{2}M_1^2}{1+\frac{\gamma-1}{2}M_2^2}}$	$\frac{\sqrt{\left[2+(\gamma-1)M_1^2\right]\left[2\gamma M_1^2-(\gamma-1)\right]}}{(\gamma+1)M_1}$	$\frac{M_2}{M_1}\,\frac{(1+\gamma M_1^2)}{(1+\gamma M_2^2)}$
$\frac{V_2}{V_1}$	$\frac{M_2}{M_1}\sqrt{\frac{1+\frac{\gamma-1}{2}M_1^2}{1+\frac{\gamma-1}{2}M_2^2}}$	$\frac{2+(\gamma-1)_1^2}{(\gamma+1)M_1^2}$	$\frac{M_2^2}{M_1^2}\,\frac{(1+\gamma M_1^2)}{(1+\gamma M_2^2)}$
$\frac{A_2}{A_1}$	$\frac{M_1}{M_2}\left[\frac{1+\frac{\gamma-1}{2}M_2^2}{1+\frac{\gamma-1}{2}M_1^2}\right]^{\frac{\gamma+1}{2(\gamma-1)}}$	1	1
$\frac{M_2^2}{M_1^2}$	$\frac{M_2^2}{M_1^2}$	$\frac{1}{M_1^2}\,\frac{1+\frac{\gamma-1}{2}M_1^2}{\gamma M_1^2-\frac{\gamma-1}{2}}$	$\frac{1+\gamma M_1^4-2\gamma M_1^2C\pm(1+\gamma M_1^2)\sqrt{(M_1^2-1)^2-2(\gamma+1)M_1^2C}}{M_1^2\left[2\gamma M_1^2+2\gamma^2M_1^2C-\gamma+1\right]}$*

*C equals q/C_pT_1 where q equals heat added equals $c_p(T_{0_2} - T_{0_1})$, negative square root equals heat addition plus normal shock; positive square root equals heat addition only.

Table II. Pressure Ratio Parameter

1.	Static and stagnation	P_1	=	p_o/p^o
2.	Static and pitot	P_2	=	p_i/p^o
3.	Stagnation and pitot	P_3	=	p_o/p_i
4.	Static and wedge static	P_4	=	p^o/p_w
5.	Static and cone static	P_5	=	p^o/p_c
6.	Stagnation and wedge static	P_6	=	p_o/p_w
7.	Stagnation and cone static	P_7	=	p_o/p_c
8.	Pitot and wedge static	P_8	=	p_i/p_w
9.	Pitot and cone static	P_9	=	p_i/p_c
10.	Pitot behind oblique shock and pitot	P_{10}	=	p_i/p_{i_w}
11.	Pitot behind oblique shock and wedge static	P_{11}	=	p_{i_w}/p_w

Table III. Pressure Sensitivities

$$P_1 = \frac{p_o}{p^o} = \left[1 + \frac{\gamma - 1}{2} M^2\right]^{\frac{\gamma}{\gamma - 1}}$$

$$S_1 = \frac{1 + \frac{\gamma - 1}{2} M^2}{\gamma M^2}$$

$$P_2 = \frac{p^o}{p_i} = \left[\frac{2\gamma M^2 - (\gamma - 1)}{(\gamma + 1)\left(\frac{\gamma + 1}{2} M^2\right)^{\gamma}}\right]^{\frac{1}{\gamma - 1}}$$

$$S_2 = \frac{1 + \gamma(2M^2 - 1)}{2\gamma(1 - 2M^2)}$$

$$P_3 = \frac{p_o}{p_i} = \left[\frac{2\gamma M^2 - \gamma + 1}{(\gamma + 1)}\right]^{\frac{1}{\gamma - 1}} \left[\frac{2 + (\gamma - 1)M^2}{(\gamma + 1)M^2}\right]^{\frac{\gamma}{\gamma - 1}}$$

$$S_3 = \frac{\left[2\gamma M^2 - \gamma + 1\right]\left[(\gamma - 1)M^2 + 2\right]}{4\gamma(M^2 - 1)^2}$$

$$P_4 = \frac{p_w}{p^o} = \frac{2\gamma(M \sin\beta)^2 - \gamma + 1}{(\gamma + 1)}$$

$$S_4 = \frac{\dfrac{2\gamma(M \sin\beta)^2 - \gamma + 1}{4\gamma}}{\left[M^2 \sin^2\beta + \left(\dfrac{(\gamma + 1)\tan\delta}{2\sin^2\beta(\cos\beta + \sin\beta\tan\delta)^2} - 1\right)^{-1}\right]}$$

$$P_5 = \frac{p_c}{p^o}$$

S_5 = computed from Tables in Ref. 16

$$P_6 = \frac{p_w}{p_o} = \frac{p_w}{p^o} \cdot \frac{p^o}{p} = P_4 P_1^{-1}$$

$$S_6 = \frac{S_4 S_1}{S_1 - S_4}$$

$$P_7 = \frac{p_c}{p_o} = \frac{p_c}{p^o} \cdot \frac{p^o}{p_o} = P_5 P_1^{-1}$$

$$S_7 = \frac{S_5 S_1}{S_1 - S_5}$$

$$P_8 = \frac{p_w}{p_i} = \frac{p_w}{p^o} \cdot \frac{p^o}{p_i} = P_4 P_2$$

$$S_8 = \frac{S_2 S_4}{S_2 + S_4}$$

$$P_9 = \frac{p_c}{p_i} = \frac{p_c}{p^o} \cdot \frac{p^o}{p_i} = P_5 P_2$$

$$S_9 = \frac{S_2 S_5}{S_2 + S_5}$$

$$P_{10} = \frac{p_{i_w}}{p_i} = \frac{p_{i_w}}{p_w} \cdot \frac{p_w}{p^o} \cdot \frac{p^o}{p_i} = \frac{P_4 P_2}{P_{2_w}}$$

$$S_{10} = \left[\frac{1}{S_2(M)} + \frac{1}{S_4} - \frac{1}{S_2(M_w)}\left(\frac{M}{M_w}\right)\left(\frac{\partial M_w}{\partial M}\right)\right]^{-1}$$

$$P_{11} = \frac{p_w}{p_{i_w}} = \frac{p_w}{p_i} \cdot \frac{p_i}{p_{i_w}} = P_8 P_{10}^{-1}$$

$$S_{11} = \frac{P_8 P_{10}}{P_{10} - P_8}$$

Table IV. Isentropic Expansion from 4 atm. to 0.01 atm. with $T_0 \cong 334°K$

	$\gamma = 1.4$	Real Air	Error (percent)
Mach Number	4.764	4.769	-0.1
Velocity (m/sec)	742.7	740.6	+0.3
Sound Speed (m/sec)	155.9	155.3	+0.4
Dynamic Pressure (kg/cm^2)	0.1642	0.1646	-0.3
Stagnation Temperature Rise $T_0 - T^0$, (°K)	273.8	274.1	-0.1

Table V. Isentropic Expansion from 40 atm. to 0.1 atm. with $T_0 \cong 447^\circ K$

	$\gamma = 1.4$	Real Air	Error (percent)
Mach Number	4.764	4.782	-0.4
Velocity (m/sec)	874.9	856.2	+ 2.2
Sound Speed (m/sec)	183.7	179.0	+ 2.6
Dynamic Pressure (kg/cm^2)	1.642	1.655	-0.8
Stagnation Temperature Rise $T_0 - T^0$, ($^\circ K$)	366.5	367.2	-0.2

Table VI. Isentropic Expansion from 40 atm. to 0.1 atm. with $T_0 \cong 1111^\circ K$

	$\gamma = 1.4$	Thermally Perfect, Calorically Imperfect	Error (percent)	Real Air	Additional Error (percent)
Mach Number	4.764	4.705	+ 1.3	4.718	-0.3
Velocity (m/sec)	1335.	1385.	-3.6	1387.	-0.2
Sound Speed (m/sec)	280.1	294.3	-4.8	294.0	+ 0.1
Dynamic Pressure (kg/cm^2)	1.642	1.603	+2.5	1.611	-0.5
Stagnation Temperature Rise $T_0 - T^\circ$, ($^\circ K$)	910.5	895.8	+1.6	896.1	0.0

Table VII. Recommended Measurement Parameters

Mach Number Range	Application	Recommended Parameter
Subsonic $M < .8$	Test Section Calibration	$P_1 = p_o / p^o$
	Nonuniform Flow	$P_1 = p_o / p^o$
Transonic $.8 \leqq M \leqq 1.4$	Test Section Calibration	$P_1 = p_o / p^o$
	Nonuniform Flow	$P_2 = p_i / p^o$
Supersonic and Hypersonic $1.4 < M$	Test Section Calibration	$P_3 = p_o / p_i$
	Nonuniform Flow	$P_9 = p_i / p_c$

DISTRIBUTION

Copies of AGARD Publications May be Obtained in the Various Countries
at the Addresses Given Herewith

BELGIUM
Centre National d'Etudes et de
Recherches Aéronautiques
11, rue d'Egmont
Bruxelles, Belgique

CANADA
Director of Scientific Information Service
Defence Research Board
Department of National Defence
"A" Building
Ottawa, Ontario, Canada

DENMARK
Military Research Board
Defence Staff
Kastellet, Copenhagen Ø, Denmark

FRANCE
ONERA (Direction)
25, avenue de la Division-Leclerc
Châtillon-sous-Bagneux, Seine, France

GERMANY
Wissenschaftliche Gesselschaft für
Luftfahrt
Zentralstelle der Luftfahrtdokumentation
München 64, Flughafen, Germany
Attn: Dr. Ing. H. J. Rautenberg

GREECE
Greek Nat. Def. Gen. Staff
B. MEO
Athens, Greece

ICELAND
Iceland Delegation to NATO
Palais de Chaillot
Paris 16, France

ITALY
Centro Consultivo Studi e Ricerche
Ministero Difesa Aeronautica
Via Salaria 336, Roma, Italy

LUXEMBOURG

NETHERLANDS
Netherlands Delegation to AGARD
Kanaalstraat 10
Delft, Holland

NORWAY
Chief Engineering Division
Royal Norwegian Air Force
Deputy Chief of Staff/Materiel
Myntgaten 2, Oslo, Norway
Attn: Lt. Col. S. Heglund

PORTUGAL
Subsecretariado da Estado da Aeronautica
Av. da Liberdade 252
Lisbon, Portugal
Attn: Lt. Col. Jose Pereira do Nascimento

TURKEY
M. M. Vekaleti
Erkaniharbiyei Umumiye Riyaseti
Ilmi Istisare Kurulu Mudurlugu
Ankara, Turkey
Attn: Colonel Fuat Ulug

UNITED KINGDOM
Ministry of Supply
T.I.L., Room 009A
First Avenue House
High Holborn
London W.C.1, England

UNITED STATES
National Advisory Committee for
Aeronautics
1512 H Street, N.W.
Washington 25, D.C., U.S.A.

AGL (1) 3-57-2000-57092

DISTRIBUTION

Copies of AGARD publications May be Obtained in the Various Countries at the Addresses Given Below

BELGIUM
Centre National d'Etudes et de Recherches Aéronautiques
11, rue d'Egmont
Bruxelles, Belgique

CANADA
Director of Scientific Information Service
Defence Research Board
Department of National Defence
"A" Building
Ottawa, Ontario, Canada

DENMARK
Military Research Board
Defence Staff
Kastellet, Copenhagen Ø, Denmark

FRANCE
O.N.E.R.A. (Direction)
25, avenue de la Division-Leclerc
Châtillon-sous-Bagneux, Seine, France

GERMANY
Wissenschaftliche Gesellschaft für Luftfahrt
Zentralstelle der Luftfahrtdokumentation
München 64, Flughafen, Germany
Attn: Dr. Ing. H. J. Rautenberg

GREECE
Greek National Def. Gen. Staff
B. MEO
Athens, Greece

ICELAND
Iceland Delegation to NATO
Palais de Chaillot
Paris 16, France

ITALY
Centro Consultivo Studi e Ricerche
Ministero Difesa-Aeronautica
Via Salaria 336, Rome, Italy

LUXEMBOURG

NETHERLANDS
Netherlands Delegation to AGARD
Kanaalweg 10
Delft, Holland

NORWAY
Chief Engineering Division
Royal Norwegian Air Force
Deputy Chief of Staff/Materiel
Myntgaten 2, Oslo, Norway
Attn: Lt. Col. S. Engesbak

PORTUGAL
Subsecretário do Estado da Aeronáutica
Av. da Liberdade 252
Lisbon, Portugal
Attn: Lt. Col. José Pereira do Nascimento

TURKEY
M. M. Vekâleti
Hava Müsteşarlığı
Ankara, Turkey
Attn: Colonel Fuat Ulug

UNITED KINGDOM
Ministry of Supply
T.I.L., Room 009A
First Avenue House
High Holborn
London W.C.1, England

UNITED STATES
National Aeronautics and Space Administration
1520 H Street, N.W.
Washington 25, D.C., U.S.A.